

Contrails



WADC TECHNICAL REPORT 55-12

(Title--UNCLASSIFIED)
EXPERIMENTAL INVESTIGATION OF A METHOD OF INTERFERENCE
DRAG REDUCTION OF A SWEEP WING AIRCRAFT BY
MEANS OF FUSELAGE INDENTATION

M. Degen
Brown University

MAY 24 1956

MARCH 1956

ENGINEERING DEPT. LIBRARY
CHANCE VOUGHT AIRCRAFT
INCORPORATED
DALLAS, TEXAS

Aeronautical Research Laboratory
Contract No. AF 33(616)-2319
Task No. 70113
Project No. 1366

Wright Air Development Center
Air Research and Development Command
United States Air Force
Wright-Patterson Air Force Base, Ohio



55WCRR-3786



FOREWORD

This report was prepared by the Division of Engineering of Brown University, Providence, Rhode Island on Air Force Contract No. AF 33(616)-2319 under Project No. 1366 "External and Internal Aerodynamics". The work was initiated under Task No. 70113 by Mr. Fred L. Daum, Wright Air Development Center.

The investigation was carried out under the direction of Professor P. F. Maeder with Mr. M. Degen acting as project engineer.

This document, excepting the title is classified **CONFIDENTIAL** in its entirety because of the nature of, and potential military application of, the research work and data described herein.

WADC TR-55-12





ABSTRACT

Preliminary investigations, performed on a body of revolution with the same cross-section area distribution as a model of the F-86 E, failed to establish similarity in the drag increase due to compressibility. Further tests, carried out on a body of revolution with a parabolic area distribution, showed a remarkable drag reduction compared to the body with the same distribution and the same thickness ratio as the F-86 E model and thus verified the importance of having a smooth area distribution.

Three component force measurements and a pressure survey on the isolated F-86 E wing, together with previously obtained data for the entire model, gave qualitative information about the interference drag and made possible the determination of the sweep of the lines of constant pressure above the wing.

A modified model with a fuselage indentation designed for $M = 1.00$ proved to have higher drag than the original F-86 E model, due to the increased drag of its thicker fuselage. The interference drag of this model, however, was decreased, and the reduction of the shock intensity on the wing improved the behavior of the pitching moment.

A second redesigned model with a shaped fuselage of circular cross-section, designed for $M = 0.95$, was found to have a drag which was 14 to 20 per cent lower than that of the original F-86 E model, even at supersonic speeds, although it exhibited higher isolated fuselage drag.

PUBLICATION REVIEW

This report has been reviewed and is approved.

FOR THE COMMANDER

ALDRO LINGARD, Colonel, USAF
Chief, Aeronautical Research Laboratory
Directorate of Research





TABLE OF CONTENTS

	Page
LIST OF ILLUSTRATIONS	v
LIST OF TABLES	x
SYMBOLS.....	xi
INTRODUCTION.....	1
I. APPARATUS AND EQUIPMENT	3
II. PRELIMINARY INVESTIGATION	4
III. THREE COMPONENT FORCE MEASUREMENTS AND THE PRESSURE SURVEY OF THE F-86E WING.....	7
IV. THE MODIFIED MODEL	12
V. REDESIGNED FUSELAGE WITH CIRCULAR CROSS-SECTION	16
VI. TEST RESULTS OF THE REDESIGNED MODEL	19
VII. CONCLUSIONS	22
REFERERENCES	23
TABLE 1	24
TABLE 2	26
TABLE 3	26
ILLUSTRATIONS	27



LIST OF ILLUSTRATIONS

FIGURES:	Page
1. Drag Comparisons of F-86E Model with Two Bodies of Revolution	27
2. A Comparison of Shock Position	28
3. Area Distribution of Two Bodies of Revolution	29
4. Rate of Change of Cross-sectional Area Distribution in x-Direction for F-86E Model	30
5. Radial Thickness Distribution of Two Bodies of Revolution	31
6. Photographs of Bodies of Revolution	32
7. Schlieren Photographs of the Bodies of Revolution	33
8. Schlieren Photographs of the Bodies of Revolution	34
9. F-86E Wing Polar Curves	35
10. Drag Coefficient as a Function of M at $C_L = 0$, & $\alpha_{geo} = 0^\circ$ for F-86E Wing	36
11. Schlieren Photographs of F-86E Wing	37
12. C_L vs. α_{geo} for F-86E Wing	38
13. C_L vs. α_{geo} for F-86E Wing	39
14. C_D vs. α_{geo} for F-86E Wing	40
15. $C_{m_{c.g.}}$ vs. C_L for the F-86E Wing	41
16. $C_{m_{c.g.}}$ vs. C_L for the F-86E Wing	42
17. Pitching Moment Coefficient as a Function of Mach Number at $\alpha_{geo} = 0^\circ$	43
18. Lines of Constant Pressure Coefficient for the Isolated F-86E Wing at M = 0.90, $\alpha_{geo} = 0^\circ$	44
19. Lines of Constant Pressure Coefficient for the Isolated F-86E Wing at M = 0.95, $\alpha_{geo} = 0^\circ$	45

Contracts



FIGURES:	Page
20. Lines of Constant Pressure Coefficient for the Isolated F-86E Wing at $M = 1.00$, $\alpha_{geo} = 0^\circ$	46
21. Lines of Constant Pressure Coefficient for the Isolated F-86E Wing at $M = 1.05$, $\alpha_{geo} = 0^\circ$	47
22. Chordwise Pressure Distribution Above the Center of the Isolated F-86E Wing $\alpha_{geo} = 0^\circ$ $M = .90$	48
23. Chordwise Pressure Distribution Above the Center of the Isolated F-86E Wing $\alpha_{geo} = 0^\circ$ $M = .95$	49
24. Chordwise Pressure Distribution Above the Center of the Isolated F-86E Wing $\alpha_{geo} = 0^\circ$ $M = 1.00$	50
25. Chordwise Pressure Distribution Above the Center of the Isolated F-86E Wing $\alpha_{geo} = 0^\circ$ $M = 1.05$	51
26. Chordwise Pressure Distribution, $M = .90$, 1 Inch off Center, 1/2 Inch Above T.E. for $\alpha_{geo} = 0^\circ$	52
27. Chordwise Pressure Distribution, $M = .95$, 1 Inch off Center, 1/2 Inch Above T.E. for $\alpha_{geo} = 0^\circ$	53
28. Chordwise Pressure Distribution, $M = 1.00$, 1 Inch off Center, 1/2 Inch Above T.E. for $\alpha_{geo} = 0^\circ$	54
29. Chordwise Pressure Distribution, $M = 1.05$, 1 Inch off Center, 1/2 Inch Above T.E. for $\alpha_{geo} = 0^\circ$	55
30. Chordwise Pressure Distribution, $M = .90$, 2 1/8 Inches off Center, 1/2 Inch Above T.E. for $\alpha_{geo} = 0^\circ$	56
31. Chordwise Pressure Distribution, $M = .95$, 2 1/8 Inches off Center, 1/2 Inch Above T.E. for $\alpha_{geo} = 0^\circ$	57
32. Chordwise Pressure Distribution, $M = 1.00$, 2 1/8 Inches off Center, 1/2 Inch Above T.E. for $\alpha_{geo} = 0^\circ$	58
33. Chordwise Pressure Distribution, $M = 1.05$, 2 1/8 Inches off Center, 1/2 Inch Above T.E. for $\alpha_{geo} = 0^\circ$	59





FIGURES:	Page
34. Chordwise Pressure Distribution, $M = .90$, 2.42 Inches off Center, 1/2 Inch Above T.E. for $\alpha_{geo} = 0^\circ$	60
35. Chordwise Pressure Distribution, $M = .95$, 2.42 Inches off Center, 1/2 Inch Above T.E. for $\alpha_{geo} = 0^\circ$	61
36. Chordwise Pressure Distribution, $M = 1.00$, 2.42 Inches off Center, 1/2 Inch Above T.E. for $\alpha_{geo} = 0^\circ$	62
37. Chordwise Pressure Distribution, $M = 1.05$, 2.42 Inches off Center, 1/2 Inch Above T.E. for $\alpha_{geo} = 0^\circ$	63
38. Chordwise Pressure Distribution, $M = .90$, 2.98 Inches off Center, 1/2 Inch Above T.E. for $\alpha_{geo} = 0^\circ$	64
39. Chordwise Pressure Distribution, $M = .95$, 2.98 Inches off Center, 1/2 Inch Above T.E. for $\alpha_{geo} = 0^\circ$	65
40. Chordwise Pressure Distribution, $M = 1.00$, 2.98 Inches off Center, 1/2 Inch Above T.E. for $\alpha_{geo} = 0^\circ$	66
41. Chordwise Pressure Distribution, $M = 1.05$, 2.98 Inches off Center, 1/2 Inch Above T.E. for $\alpha_{geo} = 0^\circ$	67
42. Spanwise Distribution of Minimum Pressure Coefficient for Isolated F-86E Wing	68
43. Diagram of Frontal Area Distribution of a Swept Wing	69
44. A Comparison of the Sum of the Wing + Fuselage Drag and Total Model Drag of the F-86E at $C_L = 0$	70
45. Area Distribution of F-86E Wing Profile Referred to Chord = Unity	71
46. Correction Factor for Area Indentation	72
47. Area Distribution of the Modified Fuselage	73
48. Photographs of Modified F-86E Model	74
49. Photographs of Original F-86E Model	75



Contrails



FIGURES	Page
50. A Comparison of Fuselage and Total Model Drags of the F-86E and Modified Models at $C_L = 0$	76
51. A Comparison of the Sum of Wing and Fuselage Drag and Total Model Drag of the Modified Model at $C_L = 0$	77
52. Reduction of Interference Drag by Indentation of the Modified Model (with Respect to the F-86E Model) at $C_L = 0$	78
53A. Schlieren Photographs of the Three Models	79
53B. Schlieren Photographs of the Three Models	80
54. Pitching Moment Versus Lift Coefficient for the Modified Model	81
55. Pitching Moment Versus Lift Coefficient for the Modified Model	82
56. Pitching Moment Versus Lift Coefficient for the Modified Model	83
57. Polar Curves of the Modified Model	84
58. Lift Coefficient as a Function of α_{geo} and M for the Modified Model, $M = 0.70-0.75$	85
59. Lift Coefficient as a Function of α_{geo} and M for the Modified Model, $M = 0.80-0.90$	86
60. Lift Coefficient as a Function of α_{geo} and M for the Modified Model, $M = 0.95-1.05$	87
61. Area Distribution of Original and Redesigned Fuselages	88
62. Area Distribution as a Function of Length for the Three Fuselages	89
63. Drag Coefficients of the Redesigned and F-86E Fuselages as a Function of M	90
64. Schlieren Photographs of the Redesigned Model with and without the Wing	91






FIGURES:

65.	Drag Coefficients of the Redesigned and F-86E Models as a Function of M	92
66.	Drag Coefficients of the Redesigned and F-86E Models as a Function of M	93
67.	Drag Reduction of the Redesigned Model with Respect to the F-86E Model	94
68.	A Comparison of the Sum of Wing + Fuselage Drag and Total Model Drag of the Redesigned Model at $\alpha_{geo} = 0^\circ$	95
69.	Polar Curve Comparison between the F-86E and Redesigned Models	96
70.	Photographs of F-86E with Redesigned Fuselage	97
71.	Photograph of F-86E Wing on Struts	98






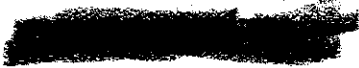
LIST OF TABLES

TABLE		PAGE
I	RADIAL CO-ORDINATES OF THE TWO BODIES OF REVOLUTION	24
II	A COMPARISON OF THE DIMENSIONS OF THE F-86E, THE MODIFIED, AND REDESIGNED FUSELAGES	26
III	RADIAL CO-ORDINATES OF THE REDESIGNED CIRCULAR FUSELAGE	26

WADC-TR-55-12



Contrails



SYMBOLS

A	Cross-section area
ΔA	Area removed from fuselage cross-section for purposes of indentation.
b	Ratio of wing span to chord
c	Wing chord
c_D	Drag coefficient
c_L	Lift coefficient
$c_{mC.G.}$	Pitching moment coefficient referred to center of gravity.
Δc_D	Difference in drag coefficient
$\Delta p/g$	Pressure coefficient
L/D	Slenderness ratio = fuselage length/maximum diameter.
M	Free stream Mach number
R_e	Reynolds number
r	Radial co-ordinate of circular fuselage
S_o	Area of airfoil section of unit chord
S(x)	Area of airfoil section included between leading edge and co-ordinate x.
T. E.	Trailing edge of wing
t	Maximum wing profile thickness
u'	x component of the perturbation velocity
U_∞	Free stream velocity
x	Co-ordinate along or parallel to axis of symmetry of the fuselage or the wing.
α_{geo}	Geometrical angle of attack

WADC TR-55-12



Contrails



SYMBOLS

- β Prandtl-Glauert factor ($\sqrt{1-M^2}$)
- γ Isentropic coefficient
- Λ Angle of sweep of the $c/4$ line
- φ Angle of sweep of the isobaric lines
- τ Thickness ratio of wing (t/c).

WADC-TR-55-12





INTRODUCTION

It is well known that the finite swept wing is less effective than the infinite swept wing in reducing drag in the transonic speed range, since the approaching air is not sufficiently forewarned to permit the streamlines to conform to a subsonic flow pattern at the center section of the wing. The outer portions of the wing, being further removed from the initial Mach cone, experience to a larger degree the benefit of the sweep at transonic speeds.

It can also be deduced that, by reason of the symmetry and continuity of the isobaric lines, the Mach number component normal to these lines at the center sections, must be nearly the free stream Mach number. Local transonic effects will, therefore, show up in this region at free stream velocities well below the speed of sound.

The presence of a conventional fuselage will in no way improve the flow pattern at the wing root. On the contrary, since the highest perturbation velocities of a body of revolution are shifted downstream from its position of maximum cross-section area with increasing Mach number, the fuselage will reduce the angle of sweep of the lines of constant pressure, and thus increase the wave drag near the root.

Similar effects will result if conventional engine nacelles and/or wing tip tanks are mounted on the wing. If, on the other hand, the fuselage (or nacelle) is given a shape which creates a flow pattern on the wing similar to that found on an infinite wing, a reduction of the wave drag is possible.

NOTE - This report was released by the author for publication in December 1954.

WADC TR - 55-12



55WCRR-3786

Contrails



This method of shaping the fuselage (or engine nacelle) to obtain a subsonic flow pattern on the wing (Ref. 1) must clearly be distinguished from the method of indenting the fuselage to reduce the perturbation velocities, which are locally increased by the presence of the fuselage. The former method can only be applied to a swept wing-body combination. The latter may be applied to any wing-body configuration. The present investigation has been restricted to modifying the fuselage so as to obtain the subsonic flow pattern of the infinite wing. If the tail surfaces are swept, a wave drag reduction can also be expected by properly shaping the fuselage near the tail section.

It should be noted that the importance of reducing the shock intensity on the wing and on the tail is actually twofold, as not only will the drag be reduced, but the stability and control of the aircraft will probably be improved also.





I. APPARATUS AND EQUIPMENT

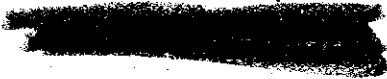
The tests were carried out in a 9 by 9 inch transonic wind tunnel with a slotted test section. Detailed information of the equipment used is contained in the technical reports WT-2 (Ref. 2) and WT-16 (Ref. 3).

A model of the F-86 E was manufactured from brass. The redesigned versions and the wing were fabricated from aluminum. The dimensions are as follows:

Span:		6.363 in.
Maximum chord of wing:		1.767 in.
Minimum	" " "	0.907 in.
Mean chord	" "	1.330 in.
Wing area	" "	8.46 in. ²

These dimensions correspond to a scale of 1/70 of the actual size. The nose of the original F-86 E model was redesigned according to the area rule as no air inlet was provided (Ref. 7). Thus the cross-sectional area was reduced locally by the amount of the duct area. By this, the length of the model from nose to the tail pipe was increased to 6.007 inches (420.5 in. for the full-size plane as compared with the actual length of 410 in.).

The aircraft models and the bodies of revolution were connected to the balance by a single strut. For the wing, a swept double strut was used. (See Fig. 71). It was necessary to restrict the values of the lift coefficient to 0.5 since for higher values of C_L the forces on the model would have been sufficient to break the connection between the strut and the model.





II. PRELIMINARY INVESTIGATION

It has been shown in Ref. 4, 5, etc. that under certain conditions the wave drag of a wing-body combination is equal to that of a body of revolution possessing the same cross-sectional area distribution, the condition being that

$$\beta^2 b^2 (1 - \ln b) + \gamma^2 \tau b^3 (1 + \ln b)^2 < 1$$

If the wing-body combination is investigated at $M = 1$, this term reduces to

$$\gamma^2 \tau b^3 (1 + \ln b)^2 < 1$$

The critical parameters are the ratio b of wing span to chord and, to a lesser degree, the wing thickness ratio τ . Using the dimensions of the original F-86E model ($b = 4.78$ and $\tau = 0.09$) a value of 77.8 is obtained, which clearly shows that the present model, by far, does not fulfill the necessary condition to apply this rule.

Drag measurements at zero angle of attack as a function of the Mach number are presented in Fig. (1), which show that the compressible drag increase of the F-86E model is considerably greater than that of its corresponding body of revolution. A comparison of the Schlieren pictures at $M = 0.95$ and 1.00 , however, shows a similarity of shock position (See Fig. 2). It must be concluded, therefore, that the shock intensity of the wing-body combination is considerably higher than that of the body of revolution.

The cross-sectional area distribution of the F-86E model is plotted in Fig. (3).





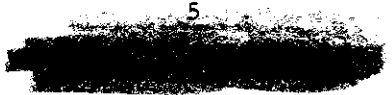
The expression for the perturbation velocities for a slender body of revolution in the transonic speed range is given by Oswatitsch's Rule (Ref. 5):

$$\left(\frac{u'}{U_\infty}\right)_{\text{compr}} = \left(\frac{u'}{U_\infty}\right)_{\text{incompr}} + \frac{1}{2\pi} \ln \beta \frac{d^2A}{dx^2}$$

Since the value of $\ln \beta$ is always negative, the largest increments of the perturbation velocity due to compressibility must occur at positions of the body where the term $\frac{d^2A}{dx^2}$ exhibits high negative values.

The change of cross-sectional area in the axial direction is presented in Fig. (4). There are three regions where the slope of this curve is negative. The first is near the nose of the body of revolution. The second between stations 1.4 and 1.6 is due to cockpit influence (See Fig. 3). The third region of negative slope is located approximately 2.9 inches from the nose near the position of maximum cross-sectional area. Since the incompressible perturbation velocity near the nose opposes the free stream velocity, the critical speed is apparently first reached near stations 2.9 and 1.4. The Schlieren picture taken at $M = 0.90$, as seen in Fig. (7), shows, in fact, that at station 1.4 the sonic speed has just been reached, whereas the stronger shock which appears earlier near the position of maximum thickness has already been shifted downstream to station 3.2. A close examination of this Schlieren picture reveals that the weaker shock extending from station 1.4 to 1.56 coincides surprisingly well with the range of the negative slope of $\frac{dA}{dx}$ seen in Fig. (4).

The preliminary investigation was therefore extended to investigate the effect of area distribution on the drag of a body of revolution. It was assumed
WADC-TR-55-12





that it should be possible to eliminate the forward shock by a modification of the area distribution and thus decrease the drag within the transonic range.

A second body of revolution with a parabolic area distribution (elliptic thickness distribution), as shown in Figs. (3, 5, and 6) was constructed.

Applying the Oswatitsch Rule to the body of revolution with parabolic cross-sectional area distribution, a constant negative value is obtained for $\frac{d^2A}{dx^2}$.

The body with the parabolic area distribution has a considerably lower drag than the body with the area distribution of the F-86 E. At Mach number 1, Body No. 2 (with parabolic area distribution in front half) exhibits only 66% of the drag experienced by Body No. 1 (F-86 E area distribution) (See Fig. 1).

The Schlieren pictures substantiate this decrease of drag. The first shock was completely eliminated and the intensity of the second shock (downstream from the position of maximum thickness) was substantially decreased, as shown in Figs. (7 and 8).

Thus it may be concluded that, although no wave drag similarity exists between the F-86 E model and its corresponding body of revolution, a smooth area distribution is important. A similar improvement could probably be achieved through the use of an area distribution such as that of a Sears-Haak body etc., as long as the value of $\frac{dA}{dx}$ is steady. The table in Appendix I gives the radial coordinates of both bodies of revolution.





III. THREE COMPONENT FORCE MEASUREMENTS AND THE PRESSURE SURVEY OF THE F-86 E WING.

Tests on the isolated F-86 E wing were carried out for two reasons:

- (1) To obtain information about the drag and the pitching moment.
- (2) To determine the flow behavior around the wing.

The first will give some information about the interference drag through a comparison with the drag of the entire F-86 E model, which was previously tested, and a modified version of the F-86 E, the results of which will be presented later. The latter will provide information concerning the general behavior of the flow around the wing. The configuration of the isobars will be very helpful in determining the effect of the indented fuselage of the modified version.

The isolated wing was connected to the balance by two swept back struts. The pitching moment was referred to the position of the center of gravity of the F-86 E aircraft, which is located above the wing and slightly in front of the C/4 point of the mean aerodynamic chord. The polar curves are presented in Fig. (9) and the drag coefficient at $\alpha_{geo} = 0$ and $C_L = 0$ is plotted as a function of M in Fig. (10).

A rapid increase in drag occurs for $M > 0.90$ due to the appearance of shock waves, as can be observed from the Schlieren pictures (Fig. 11). The lift coefficients are an almost linear function of α_{geo} , and the slope $\frac{dC_L}{d\alpha_{geo}}$ experiences an increase up to $M = 1$, beyond which, it remains almost constant (Figs. 12 and 13).

WADC-TR-55-12





The pitching moment at low Mach numbers is stable in the range of small lift coefficients. See Figs. (15-17). It becomes indifferent at higher angles of attack and unstable as the flow starts to separate at the outer portions of the wing. The stability of the wing increases with increasing Mach number. This effect is more pronounced at the lower values of lift coefficient. The isolated wing becomes very stable at sonic and supersonic speeds as the aerodynamic center moves backwards to the $C/2$ line of the mean aerodynamic chord. The variation of the pitching moment at $C_L = 0$ with Mach number is small.

The pressure coefficients $\frac{\Delta P}{q}$ were measured in a horizontal plane 1/2 inch above the trailing edge at different spanwise locations, for zero geometrical angle of attack. This permitted the plotting of the isobaric lines above the entire upper surface of the wing.

Chordwise traverses were made at the following sections of the wing:

- At the center
- 1 inch off center
- 2.125 inches off center
- 2.42 inches off center
- 2.98 inches off center

The lines of constant pressure above the isolated F-86E wing for different Mach numbers at zero angle of attack are shown in Figs. (18-21). They clearly show that the point of minimum pressure is shifted back at the center of the wing, whereas at the outer portions the largest perturbation velocities occur near or even in front of the point of maximum thickness of the airfoil section.



Contrails



With increasing Mach number the point of minimum pressure is shifted further backwards at the center as well as at the outer sections of the wing. This effect has two consequences:

(1) The local drag coefficient, even at subsonic speeds, is increased in the center section of the wing because the suction effect at the front of the airfoil sections is decreased and at the rear it is increased.

(2) At higher speeds the local Mach number of the component of the flow normal to the isobars is much higher near the center of the wing than at the outer sections, where the flow experiences a substantial benefit from the sweep. At $M = 0.90$, isobars near the tip of the wing are swept about 30 degrees. This explains why the increase in critical Mach number due to the sweep-back of the wing is actually less than that of a swept infinite wing for which the critical Mach number is proportional to $\frac{1}{\cos\psi}$.

Available systematic drag measurements comparing straight and swept wings, for $\Lambda = 35$ degrees, show that this gain in critical Mach number is of the order of 0.07 - 0.08 for an airfoil of $\tau = 0.09$, which means that the effective average angle of sweep is of the order of 24 to 25 degrees. This compares favorably with the results of the pressure survey.

The pressure distribution above the wing in the direction of the chord at different span sections is plotted in Figs. (21-41) for various Mach numbers. For reasons of comparison, the corresponding pressure distributions measured on the original F-86 E model and the modified model have been included.

The results of these tests will be discussed later.

WADC-TR-55-12





Since the minimum pressure coefficient at $M = 0.90$ is definitely at the kink (Fig. 42), the critical speed appears to be first reached at the center-section at a Mach number slightly below 0.90. It has been observed that for an untwisted swept wing with constant thickness, the highest perturbation velocities in the transonic speed range occur at the intersection of the line of maximum profile thickness and the plane of maximum cross-section area distribution of the wing (See Fig. 43) and not at the center-section of the wing. It is believed that the twist of the F-86 E wing, which has an angle of attack at the center-section of one degree positive and at the tip one degree negative, results in this effect being somewhat delayed, so that it occurs at higher Mach numbers. This can be observed for $M = 1.00$ and 1.05 in Fig. (42), which shows that the position of the minimum pressure coefficient is gradually shifted towards the outer portions of the F-86 E wing for increasing Mach numbers.

In order to calculate the interference drag, it is necessary to reduce the drag coefficient of the wing, since part of its center-section is covered by the fuselage and is not exposed to the airstream. This, however, could only be done if the local drag coefficients at the center-section were known for all Mach numbers. A determination of these values would require a separate report. However, some idea of the relative sizes of the interference drags of the original and modified models may be had from a comparison of the model drag with the sum of the isolated wing drag plus the isolated fuselage drag for the two models.

In Fig. (44), the sum of the drags of the wing and the separately measured fuselage, as well as the drag of the entire original F-86 E model are plotted.

WADC-TR-55-12





It is seen that the sum of the separate drags is only slightly greater than the drag values of the model within the entire speed range.

Comparing the results of the pressure measurements of the isolated wing with a similar pressure survey for the entire F-86 E model, it is seen that the presence of the fuselage shifts the lines of constant pressure downstream near the root (Figs. 26-33). Thus, the sweep of the isobaric lines is less than that of the isolated wing, which accounts for the comparatively high interference drag. It can thus be concluded, that the maximum thickness of the fuselage should be shifted forward in order to change the pressure distribution in such a way as to increase the sweep of the isobaric lines. The reduced sweep of these lines, caused by the fuselage, can be noticed at a considerable spanwise distance from the root as seen in Figs. (30-36). The magnitude of the largest perturbation velocities is practically unchanged by the presence of the fuselage.





IV. THE MODIFIED MODEL

The angle of the isobars near the root of the wing may be changed by methods other than fuselage indentation. In Ref. (6), Kuechemann proposes that a displacement of the maximum thickness of the airfoil at the root section towards the leading edge would create the same effect as an indentation of the fuselage. Such a change in airfoil is undesirable, since it would not only decrease the torsional and lateral stiffness of the wing, but might also involve serious changes in stalling characteristics.

The present investigation was restricted to fuselage modifications. In Ref. (1), dealing with body indentation for swept wing aircraft, a theory has been developed. It seems necessary to mention that this theory assumes that the perturbation velocities of the fuselage are negligible, which is definitely not the case at high subsonic speeds unless the fuselage is extremely slender. The fuselage was indented by the amount

$$\Delta A = \frac{\sin \Lambda \cos \Lambda}{1 - M^2 \cos^2 \Lambda} \begin{cases} S_0 & x = 0 \\ S_0 - 2S(x) & 0 < x < 1 \\ -S_0 & x = 1 \end{cases} \quad \text{Ref. (4)}$$

where S_0 represents the area of the airfoil section of unit length and $S(x)$ is the area of the airfoil section included between the leading edge and the chordwise coordinate (See Fig. 45). Λ is angle of sweep of the C/4 line.

The factor $\frac{\sin \Lambda \cos \Lambda}{1 - M^2 \cos^2 \Lambda}$ containing the angle of sweep and the Mach number is plotted in Fig. (46). The condition that the original fuselage must not be undercut made it necessary to build up the portion of the fuselage between the





nose and trailing edge of the wing such that when the cross-section area at the trailing edge was undercut by

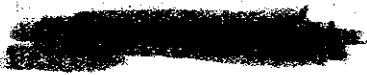
$$\Delta A = \frac{\sin \Lambda \cos \Lambda}{1 - M^2 \cos^2 \Lambda} 2 S_0$$

the area at the trailing edge was not less than that of the F-86 E model. Originally it was planned to design the indentation for a Mach number of 1.10, but it was realized that the change of area would become excessively large, as the term $\frac{\sin \Lambda \cos \Lambda}{1 - M^2 \cos^2 \Lambda}$ rapidly increases with M . Thus, the correction was carried out for $M = 1.00$ with a corresponding factor of 1.428.

Based on the results of the experiments with the bodies of revolution, the area distribution of the built-up fuselage before undercutting was chosen as parabolic. The apex of this parabola reached a maximum value of 1.4 in.² at a distance of 2.55 in. from the nose. Since the chord of the wing near the root is 1.66 in., the area at the trailing edge was undercut by

$$\Delta A = (1.428)(1.66)^2 2 S_0 = (3.93) 2 S_0 = 0.561 \text{ in.}^2$$

a value which represents about 80% of the maximum area of the original F-86 E fuselage. The resulting area distribution of the fuselage after the deduction of the value $(3.93)2S(x)$ representing the section area of the airfoil at the wing root is shown in Fig. (47). The upper contour of the fuselage was not changed, and the lower one was changed only slightly. Thus most of the area had to be added on both sides, and the cross-section became somewhat squared, as can be seen in Figs. (47 and 49).





The maximum frontal area was increased, as shown in Fig. (47), from 0.69 inch² to 1.227 inch². It is obvious that the general effect of an increase in frontal area would be to reduce considerably the critical Mach number of the fuselage and increase the total drag, even though the interference drag may have been reduced.

The choice of a parabolic area distribution, with the maximum cross-section area (prior to undercutting) shifted more towards the rear, would have resulted in an area reduction with corresponding improvement in the drag. However, the condition that the original fuselage area should nowhere be undercut would still have resulted in a bulky and odd shape of the modified fuselage. Referring to Figs. (26-29), where the pressure measurements of the isolated wing, the original F-86 E model, and the modified version have been presented, it can be seen that the point of minimum pressure has been shifted considerably towards the leading edge of the wing near the wing root, as was desired. However, due to the thicker fuselage, the perturbation velocities were also increased, thus reducing the critical Mach number of the fuselage. The influence of this indentation is even felt at a distance of 2.42 inches from the axis of symmetry of the model (See Figs. 30-37).

The drag coefficients of the original and the modified fuselages, as well as the drag coefficients of the original and modified models are plotted in Fig. (50), which shows that the increased thickness of the fuselage is responsible for the increased drag of the modified model. These results also indicate that the interference drag of the modified version has been decreased,





for the difference in drag between the modified and original model is less than the difference between the corresponding fuselages. This is shown again in Figs. (44 and 51), where the model drag and the sum of the isolated wing plus isolated fuselage drags are plotted for the original and the modified models. It is seen that the difference between these two drags is greater for the modified model than for the original model, and thus the interference drag has been decreased due to indentation by an amount ΔC_D shown in Fig. (52). The reduction of interference drag reaches a maximum close to Mach number 1; i. e. the value for which the indentation was calculated.

The fact that a reduction of interference drag has been achieved can also be observed in the schlieren pictures. A comparison, at $M = 0.95$, between schlierens of the modified and original model proves that the shock intensity on the wing has been decreased due to increased sweep of the isobaric lines. The shock strength on the modified fuselage, however, is greater, and the shock extends further (See Fig. 53). The indentation appears to have a favorable effect on the behavior of the pitching moment, which is shown in Figs. (54-56). The moment coefficient not only becomes more nearly linear with the increased angle of attack, but also the variation of the pitching moment coefficient at $C_L = 0$ as a function of the Mach number is smaller (Fig. 17). This is undoubtedly due to the reduction of the shock intensity on the wing.

The modified model does not show any adverse effects in its lift coefficient characteristics with increased angles of attack (Figs. 58-60).





V. REDESIGNED FUSELAGE WITH CIRCULAR CROSS-SECTION

Although an apparent reduction of the interference drag had been accomplished by the indentation of the modified model, the results were not completely satisfactory, as the overall drag of the model still was considerably higher than that of the original F-86 E model. Some valuable information was obtained, however, by comparing the pressure distributions and the schlieren pictures, which confirm the importance and justify the application of the indentation method. Thus it was decided to build and test a redesigned fuselage of circular cross-section, (See Fig. 70), which would be fitted with the cockpit, wing, and tail surfaces of the original model. The circular cross-section was chosen for ease of machining. Based on results of the previous investigation, the following conditions were imposed:

(1) The redesigned fuselage alone was to exhibit a drag which was greater than or equal to that of the original F-86 E fuselage through the entire transonic range. Thus any drag reduction in the redesigned model could be attributed to a reduction in interference drag.

(2) The redesigned fuselage was to have approximately the same volume as the original fuselage.

The indentation method involves a forward displacement of the maximum frontal area. Any shift in this direction must necessarily result in increased perturbation velocities, if the slenderness ratio L/D is to remain the same. Compared with the first modification, four major changes were made on the redesigned fuselage.

WADC-TR-55-12





(1) The condition that the original fuselage could not be undercut was not retained.

(2) The fuselage indentation was designed for a Mach number of 0.95. By so doing, a reduction of the term $\frac{\sin \Lambda \cos \Lambda}{1 - M^2 \cos^2 \Lambda}$ was achieved, (from 1.428 to 1.200), which decreased the indentation ΔA .

(3) The parabolic shape of the area distribution of the front of the fuselage with cockpit before undercutting was retained. The cross-section area reached its maximum at 3.5 inches from the nose and had a value of 0.8 inch². Beyond this, the area distribution was no longer parabolic but was held constant. It was thus possible to reduce the maximum frontal area considerably without undercutting the fuselage excessively.

(4) The overall length of the fuselage was increased from 6 to 7 inches. The wing was displaced one inch further back from the nose, while the position of the cockpit with respect to the nose of the fuselage, remained nearly the same (0.182 inches more toward the rear) in order to maintain similar visibility.

Fig. (61) shows the differences in the area distributions of the F-86 E fuselage and the redesigned version with circular cross-section. It can be seen that the forward portion of the redesigned fuselage is slightly more slender than that of the F-86 E, and the inflection point of the area distribution due to the presence of the cockpit has been completely eliminated by a local indentation of the fuselage.





It is seen that up to a distance of 2 inches from the nose the redesigned fuselage is slightly undercut with respect to the original fuselage, whereas its maximum frontal area has been increased from 0.69 inch² to 0.74 inch². Between stations 2 and 3.5 inches the redesigned fuselage has a greater cross-section area than the original one, and between 3.5 and 4.8 inches it is undercut to compensate for the wing. Beyond 4.8 inches the cross-section area of the redesigned fuselage is greater than that of the original fuselage. The smallest diameter of the redesigned version, which is equivalent to 38 inches in full scale, is at the position of the trailing edge of the wing. The corresponding diameter of a circular fuselage with an area distribution which is the same as the original F-86 E fuselage is 42.8 inches. Table 2 in Appendix II gives the basic dimensions of the three different versions, and the coordinates of the redesigned fuselage are included in Table 3. Fig. (62) shows the cross-section area distribution of the three different fuselage versions.





VI. TEST RESULTS OF THE REDESIGNED MODEL

The first objective of the investigation was to prove that the redesigned fuselage did not exhibit lower drag than the original version. Results of this test are presented in Fig. (63) and show conclusively that the indented circular fuselage, if isolated, exhibits higher drag over the entire transonic range. The largest differences in drag between the two fuselages occur at supersonic speeds due to an increased expansion around the indentation and a increase in pressure drag. At incompressible speeds the flow seems to separate near the position of maximum frontal area, which accounts for the higher drag of the redesigned fuselage in the low speed range.

Conditions are considerably changed by the addition of the wing. Due to the improved area distribution the separation has been completely eliminated. The shock intensity on the fuselage has been decreased by the presence of the wing. This may be verified by comparing the schlieren pictures taken of the isolated redesigned fuselage (Fig. 64), and the redesigned model (Fig. 53). A reduction of the wing drag has also taken place due to the increased sweep of the isobars near the root of the wing. This is again verified by the schlieren pictures of the redesigned model, which show that the wing experiences almost no compressibility effects at $M = 0.95$, thus proving that the local velocity components perpendicular to the isobaric lines have not yet reached sonic speed.

The fuselage indentation was calculated for a Mach number of 0.95, but the improvement in drag is felt to a remarkable degree even at supersonic





speeds, as shown in Figs. (65, 66).

The following table compares values of the drag coefficient of the original F-86 E model and the redesigned version as a function of M at $\alpha_{geo} = 0^\circ$

M	C_D <u>Orig. F-86 E</u>	C_D <u>Redesigned Model</u>	C_D <u>Difference</u>	<u>Percent Relative Reduction of Drag</u>
0.9	0.0332	0.0284	0.0048	14.5
0.95	0.0454	0.0379	0.0075	16.5
1.00	0.0632	0.0545	0.0087	13.7
1.05	0.0760	0.0610	0.0150	19.7

In the subsonic range, the redesigned model shows its greatest relative reduction in drag very close to the design Mach number of 0.95 (Fig. 67).

It is noteworthy to mention that the drag reduction of $C_D = 0.0087$ obtained at $M = 1.00$ for the redesigned model is practically identical with the reduction of interference drag previously evaluated by comparing the original F-86 E model with the modified version (Fig. 52). This is rather surprising, since the modified and redesigned fuselages are entirely different. The large differences between the drag of the isolated redesigned model and the sum of the drags of the isolated redesigned fuselage plus isolated wing for different Mach numbers are shown in Fig. (68), which clearly indicates that the flow patterns around both the wing and the fuselages have been improved by the addition of the wing.

WADC-TR-55-12



Contrails



The drag reduction is not restricted to small angles of attack. This is verified by the polar curves of Fig. (69) comparing the original F-86 E model with the redesigned version, which show that a wave drag reduction is also achieved at higher lift, particularly for supersonic speeds.





VII. CONCLUSIONS

The results of the investigations indicate that an isolated fuselage with low drag at transonic speeds does not necessarily represent a good design when combined with a wing. If the cross-section area of the fuselage near the trailing edge of the wing is determined by the dimensions of the power plant, thus limiting the allowable amount of undercutting, further systematic tests would be needed to determine the most suitable shape of the fuselage. Tests of various fuselage shapes based on different design Mach numbers could be used to find the wing-body combination with the most favorable drag characteristics. In order that the wave drag reduction of the wing is not offset by a reduced critical Mach number of the indented fuselage, it would probably be necessary to lengthen the nose section of the fuselage. Experiments indicate that the fuselage and wing cannot be designed separately as far as minimizing drag is concerned, but must be considered as a unit.





REFERENCES

1. Maeder, P. F. Interference Drag Reduction of Swept Wing-Body Combinations
WADC TR 5A-353
Division of Engineering, Brown University, June 1954
2. Anderson, G. F. The 9 By 9 Inch Transonic Wind Tunnel
Maeder, P. F. Technical Report WT-2
Division of Engineering, Brown University, January 1950
3. Maeder, P. F. Experimental Investigation of Subsonic Wall
Anderson, G. F. Interference in Rectangular Slotted Test
Carroll, J. B. Sections.
Technical Report WT-16
Division of Engineering, Brown University, January 1955
4. Maeder, P. F. Similarity of Slender Bodies and Small
Aspect Ratio Wing-Body Combinations
Technical Report WT-12
Division of Engineering, Brown University, October 1954
5. Oswatitsch, K. The Effect of Compressibility on the Flow
Around Slender Bodies of Revolution
KTH-AERO TN 12
February 1950
6. Kuchemann, D. Wing Junction, Fuselage and Nacelles for
Sweptback Wings
Royal Aircraft Establishment
Report No. AERO 2219
7. Degen, M. Investigation of an F-86 E Model in a
Transonic Wind Tunnel
Technical Report D-1
Division of Engineering, Brown University, October 1953





APPENDIX I.

TABLE I.

x (inches)	BODY NO. 1	BODY NO. 2
	r (inches)	r (inches)
0	0	0
0.2	0.202	0.202
0.4	0.277	0.280
0.6	0.325	0.337
0.8	0.356	0.382
1.0	0.383	0.418
1.2	0.420	0.448
1.4	0.452	0.473
1.6	0.464	0.493
1.8	0.475	0.510
2.0	0.482	0.524
2.2	0.495	0.535
2.4	0.510	0.542
2.6	0.528	0.547
2.8	0.544	0.548
3.0	0.549	0.549
3.2	0.547	0.547
3.4	0.538	0.538
3.6	0.521	0.521
3.8	0.500	0.500

WADC-TR-55-12



Contrails



<u>x (inches)</u>	<u>BODY NO. 1</u> <u>r (inches)</u>	<u>BODY NO. 2</u> <u>r (inches)</u>
4.0	0.471	0.471
4.2	0.436	0.436
4.4	0.392	0.392
4.6	0.356	0.356
4.8	0.331	0.331
5.0	0.312	0.312
5.2	0.298	0.298
5.4	0.288	0.288
6.0	0.275	0.275

WADC-TR-55-12

25





APPENDIX II.

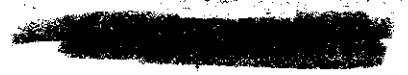
TABLE 2

		<u>Original F-86 E</u> <u>Fuselage</u>	<u>Modified</u> <u>Fuselage</u>	<u>Redesigned</u> <u>Fuselage</u>
Length	(inches)	6.00	6.00	7.00
Max. Diameter'	(inches)	0.937	1.248	0.970
Max. Frontal Area	(inch ²)	0.690	1.223	0.740
Volume	(inch ³)	2.679	3.717	2.890
Slenderness Ratio	L/D _{max}	6.40	4.81	7.21

TABLE 3

Radial Coordinates of Redesigned Circular Fuselage (in inches)

x	r	x	r	x	r
0	0	2.2	0.439	4.4	0.324
0.1	0.118	2.4	0.464	4.6	0.326
0.2	0.167	2.6	0.480	4.8	0.331
0.4	0.234	2.8	0.485	5.0	0.333
0.6	0.282	3.0	0.473	5.2	0.334
0.8	0.321	3.2	0.450	5.5	0.330
1.0	0.353	3.4	0.424	5.75	0.322
1.2	0.370	3.6	0.397	6.0	0.309
1.4	0.382	3.8	0.370	6.25	0.291
1.6	0.390	4.0	0.346	6.5	0.268
1.8	0.397	4.1	0.335	6.75	0.238
2.0	0.415	4.2	0.328	7.0	0.200



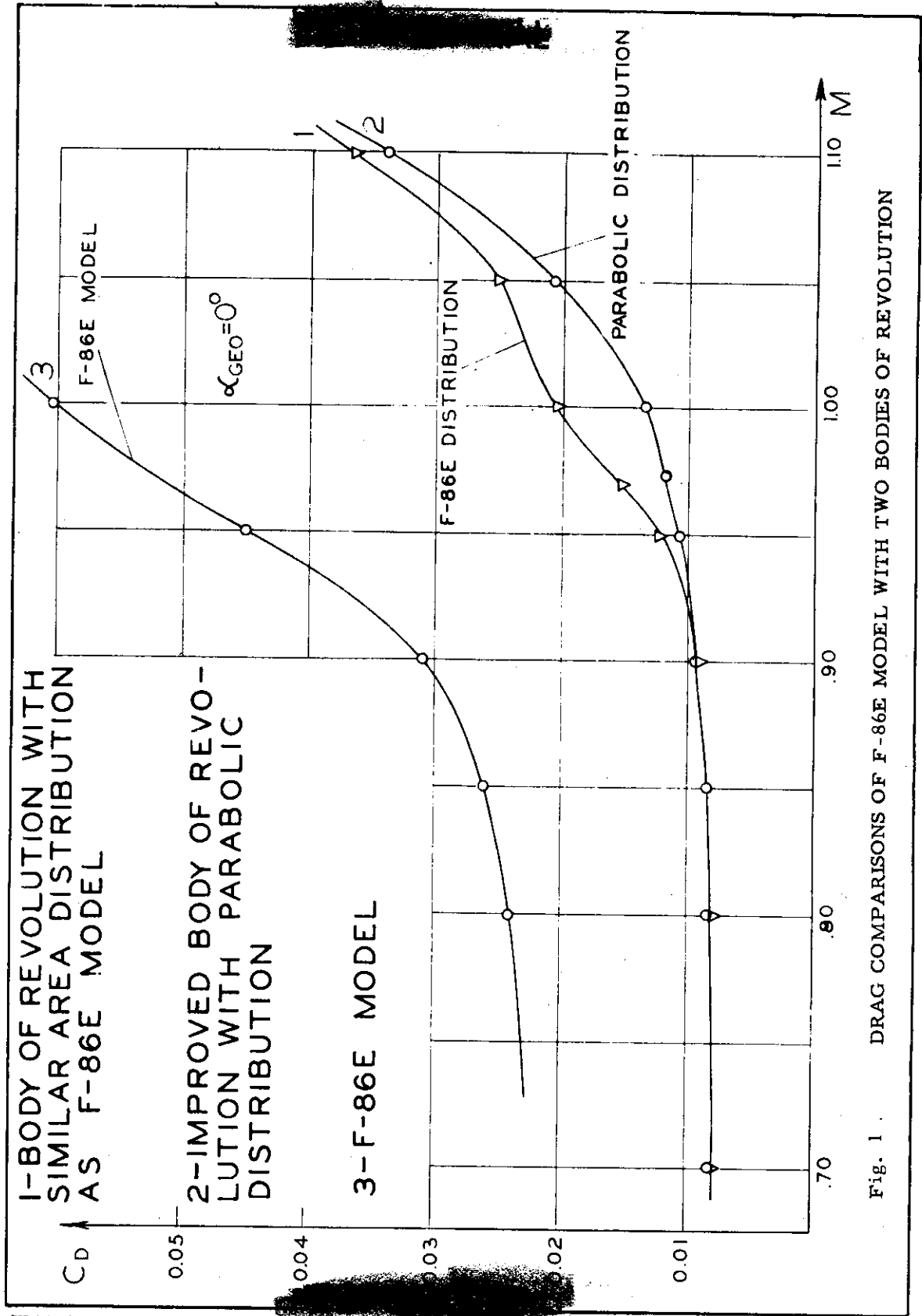


Fig. 1 DRAG COMPARISONS OF F-86E MODEL WITH TWO BODIES OF REVOLUTION

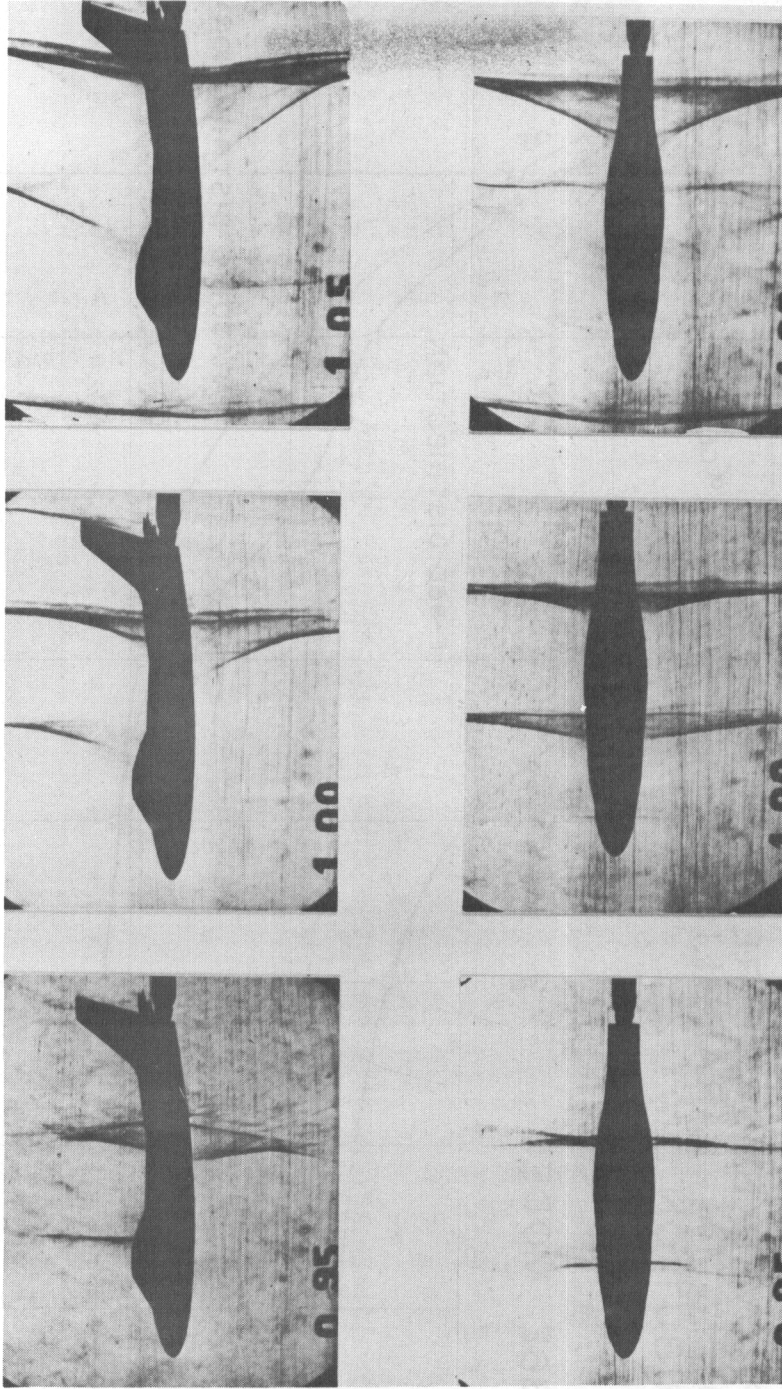
WADC-TR-55-12

A COMPARISON OF SHOCK POSITION

M = 1.05

M = 1.00

M = .95



F-86E MODEL

BODIES OF
REVOLUTION
WITH F-86E
CROSS SECTION
AREA
DISTRIBUTION

Fig. 2 A COMPARISON OF SHOCK POSITION

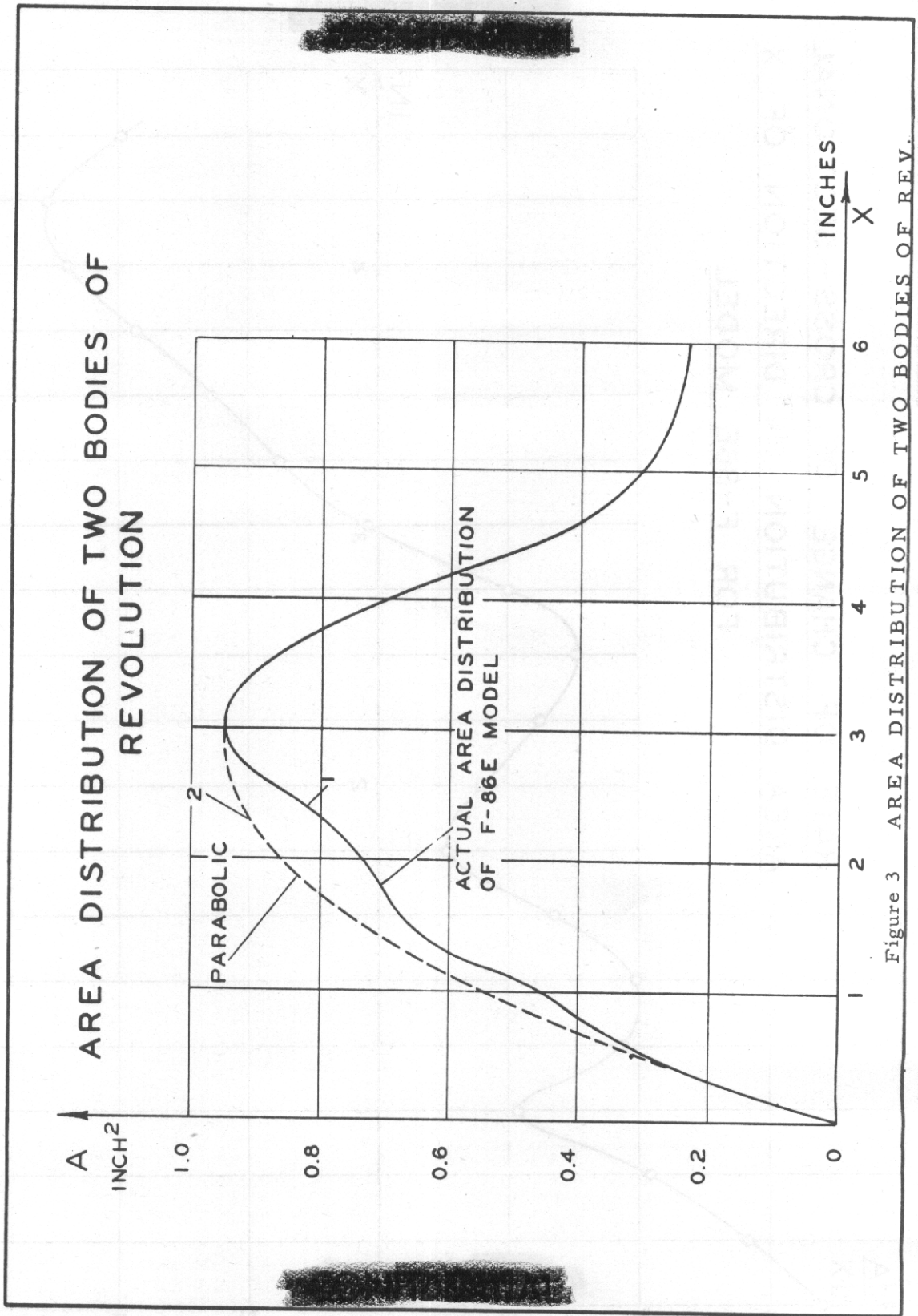


Figure 3 AREA DISTRIBUTION OF TWO BODIES OF REV.

RATE OF CHANGE OF CROSS-SECTIONAL
AREA DISTRIBUTION IN DIRECTION OF X
FOR F-86E MODEL

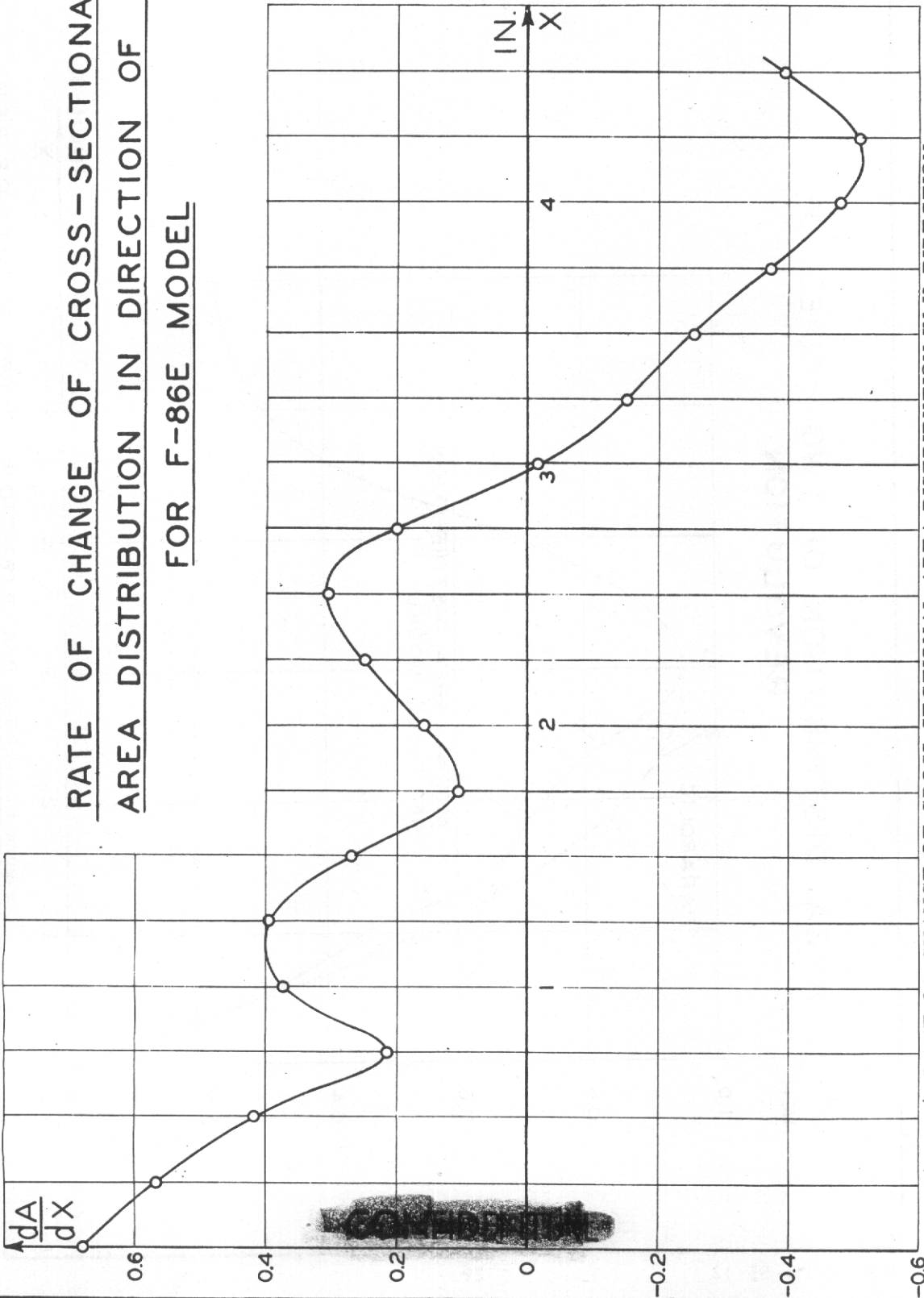


Figure 4 RATE OF CHANGE OF CROSS-SECTIONAL AREA DISTRIBUTION IN X-DIRECTION
FOR F-86E MODEL

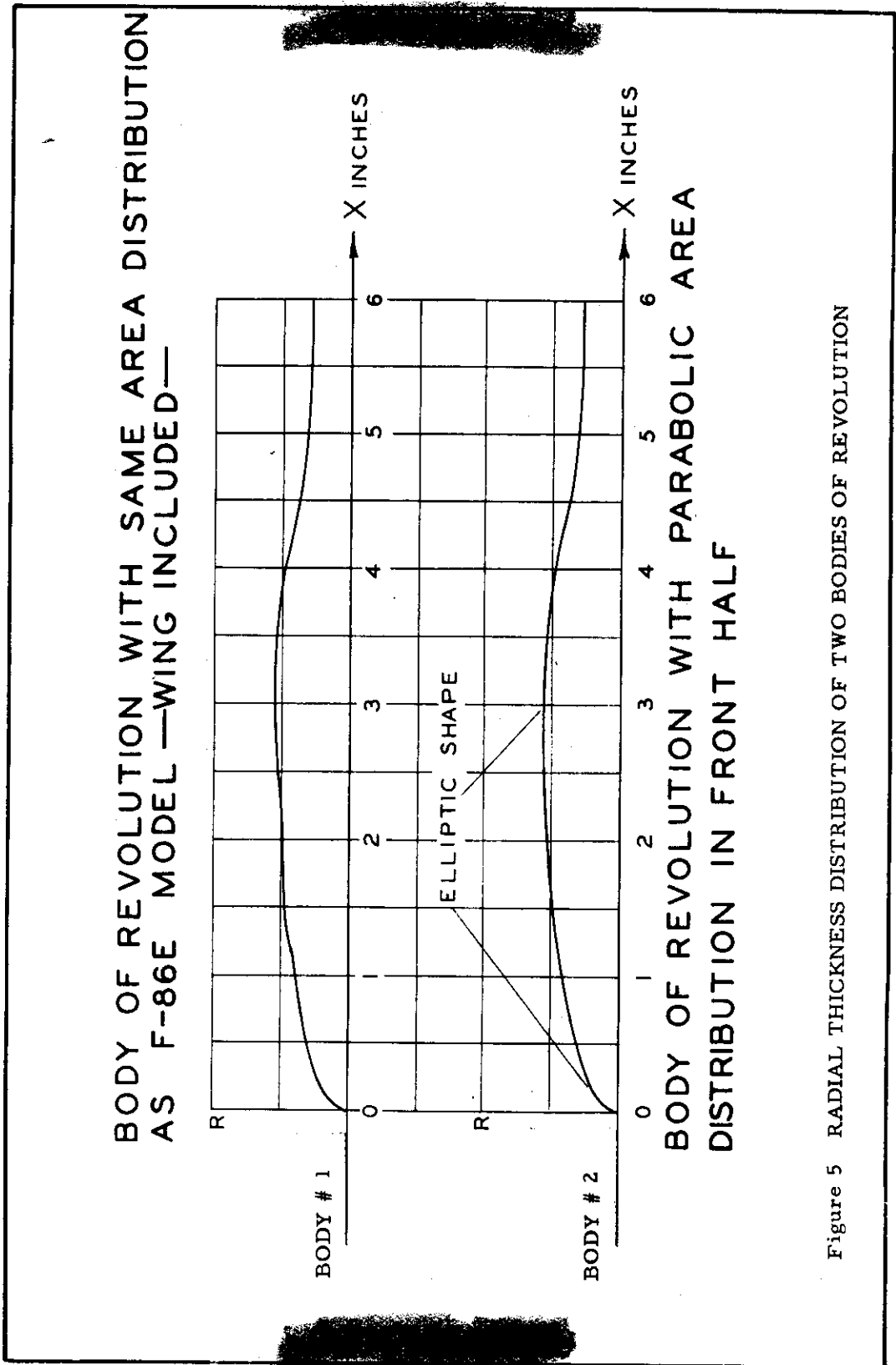
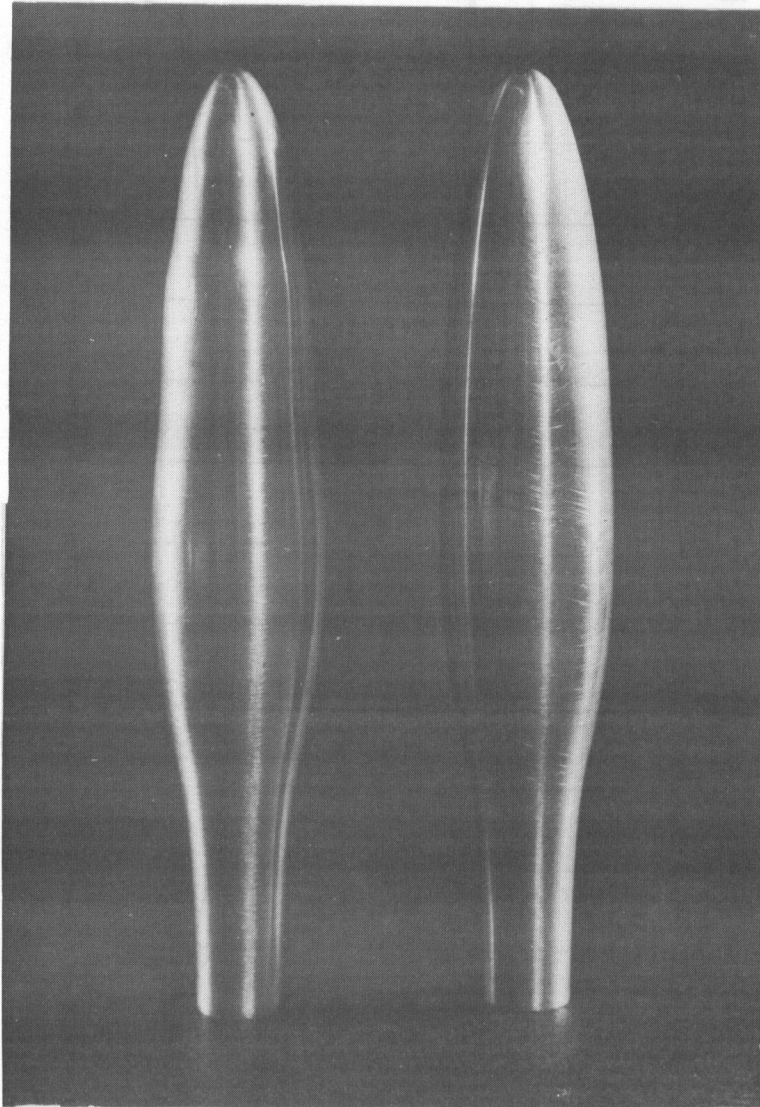


Figure 5 RADIAL THICKNESS DISTRIBUTION OF TWO BODIES OF REVOLUTION

BODIES OF REVOLUTION



BODY #.1

BODY #2

Fig. 6 BODIES OF REVOLUTION

[REDACTED]

SCHLIEREN PHOTOGRAPHS OF THE BODIES OF REVOLUTION

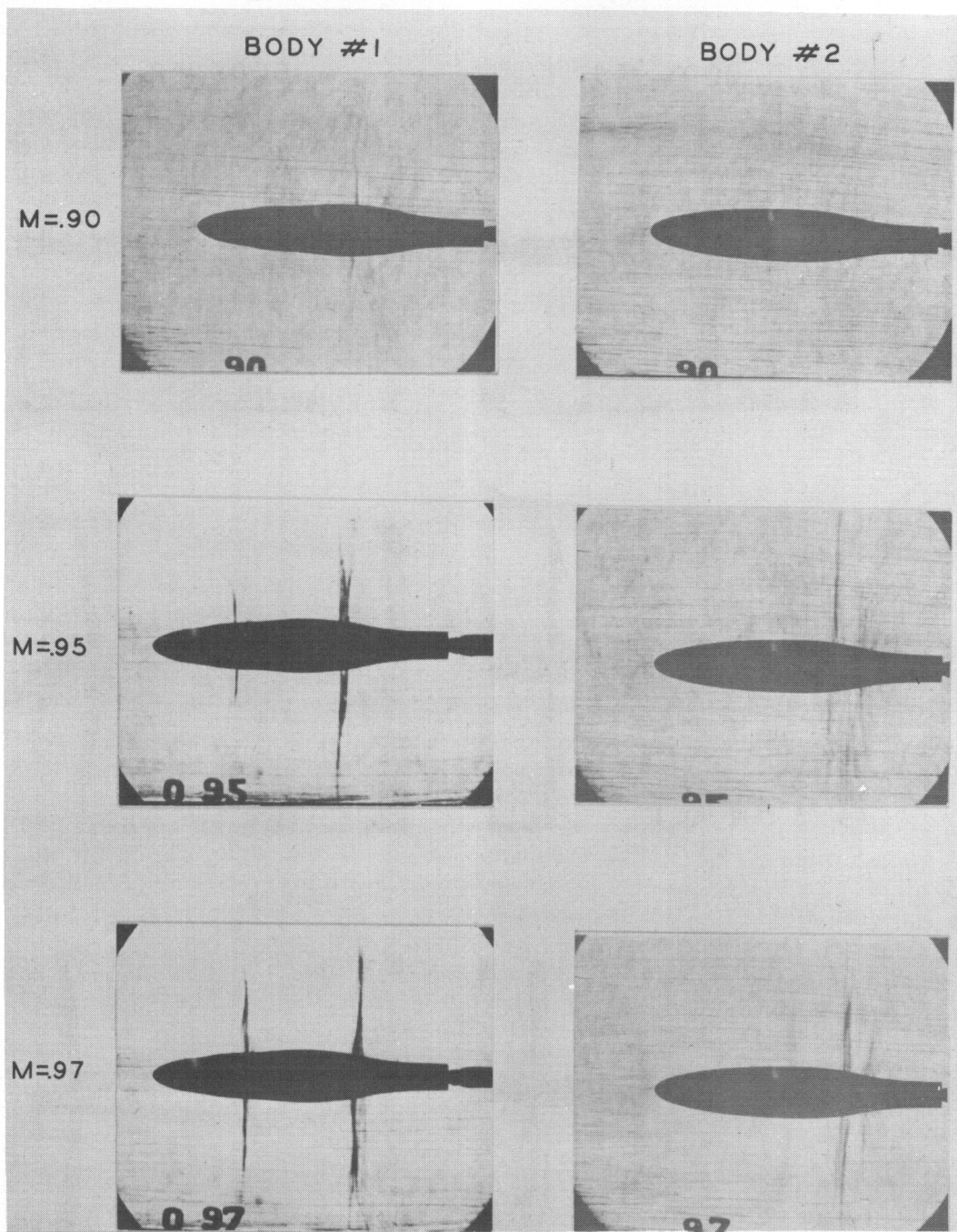
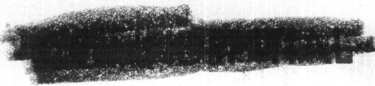


Fig. 7 SCHLIEREN PHOTOGRAPHS OF THE BODIES OF REVOLUTION

[REDACTED]



SCHLIEREN PHOTOGRAPHS OF THE BODIES
OF REVOLUTION

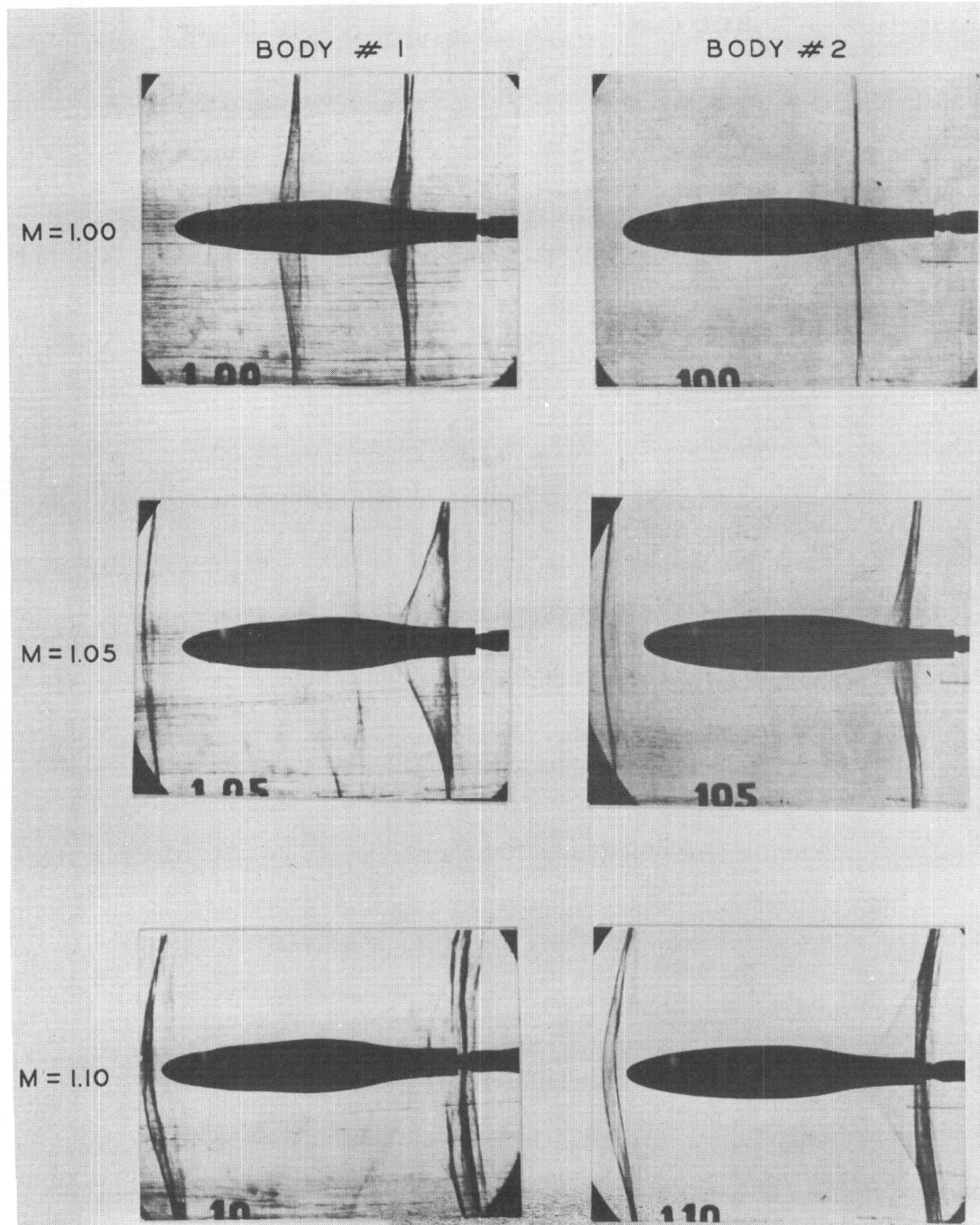
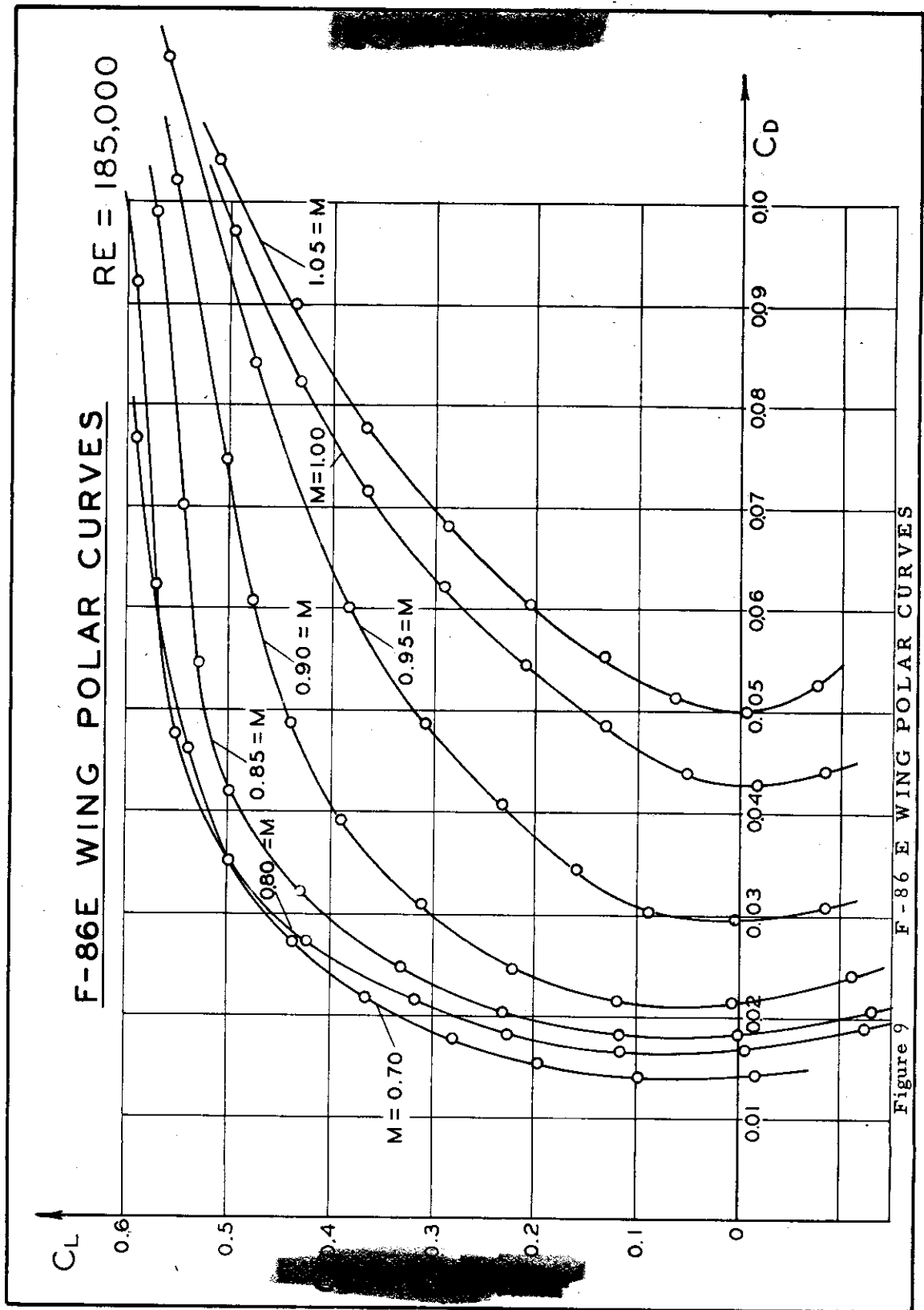


Fig. 8 SCHLIEREN PHOTOGRAPHS OF THE BODIES OF REVOLUTION





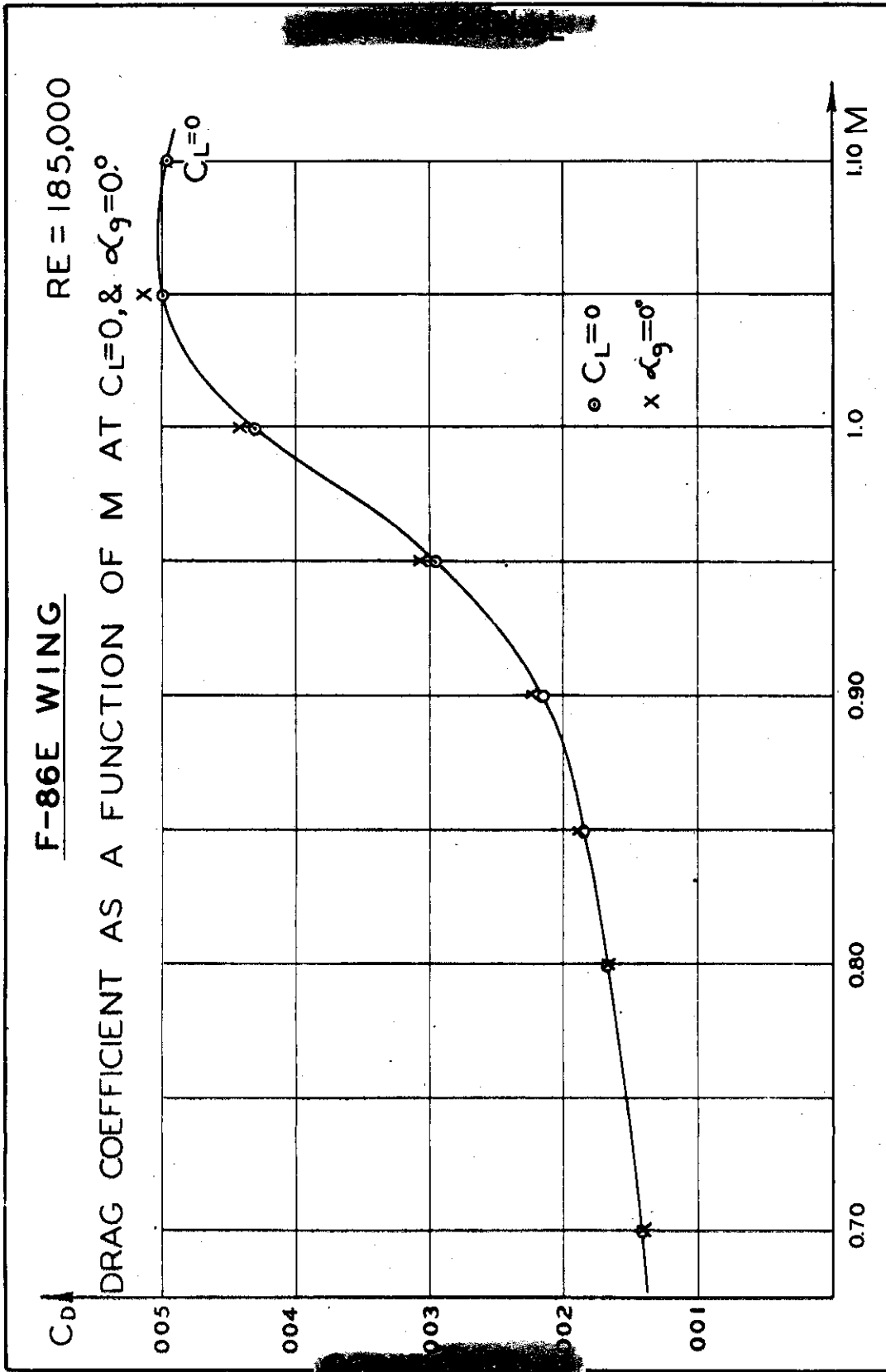


Figure 10 DRAG COEFFICIENT AS A FUNCTION OF M AT $C_L = 0$, & $\alpha_g = 0^\circ$ FOR F-86E WING

Contrails

SCHLIEREN PHOTOGRAPHS OF THE F-86E WING

M = 0.90 $\alpha_{GEO} = 0^\circ$ | M = 0.95 | M = 0.90 $\alpha_{GEO} = 2^\circ$ | M = 0.95

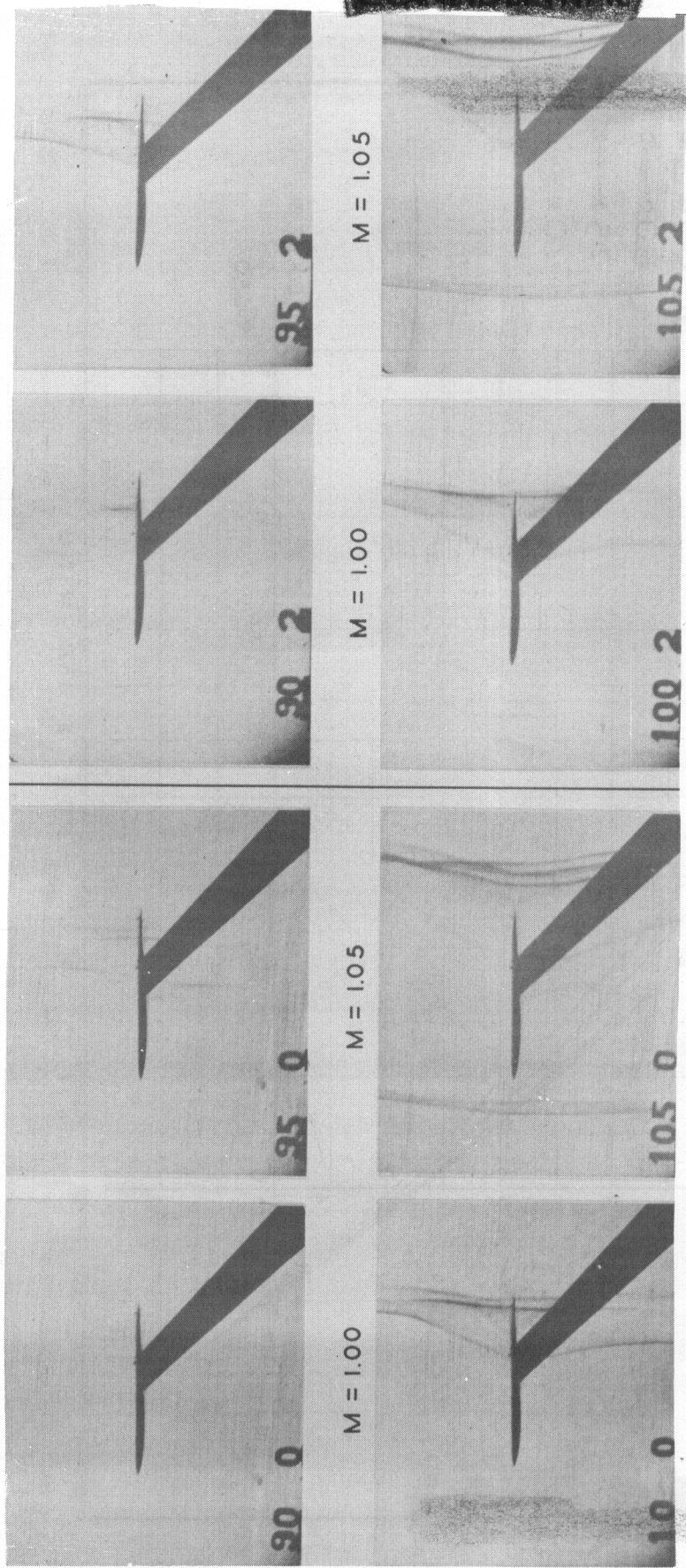


Fig. 11 SCHLIEREN PHOTOGRAPHS OF THE F-86E WING

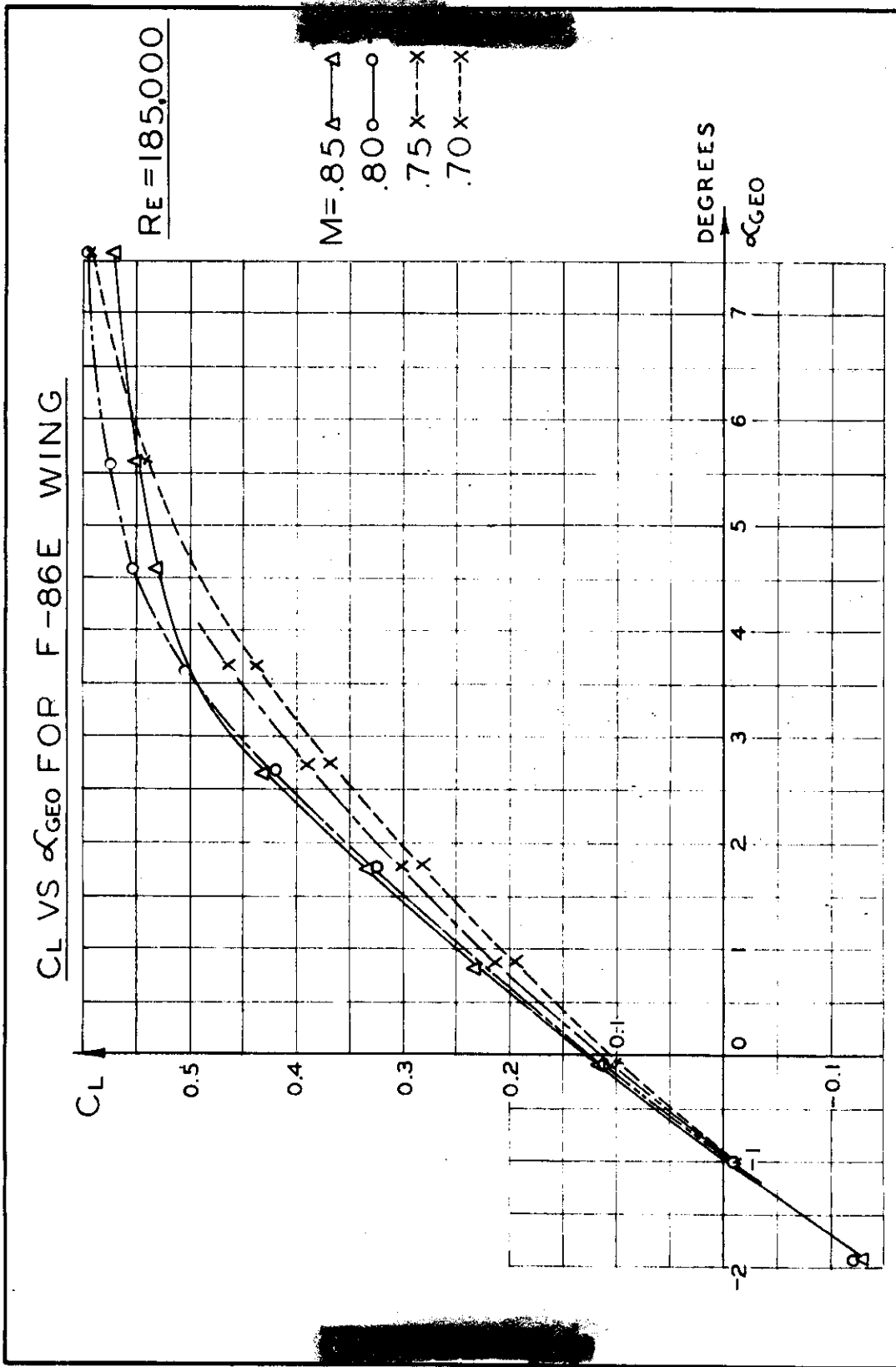


Figure 12 CL VS. α_{geo} FOR F-86E WING

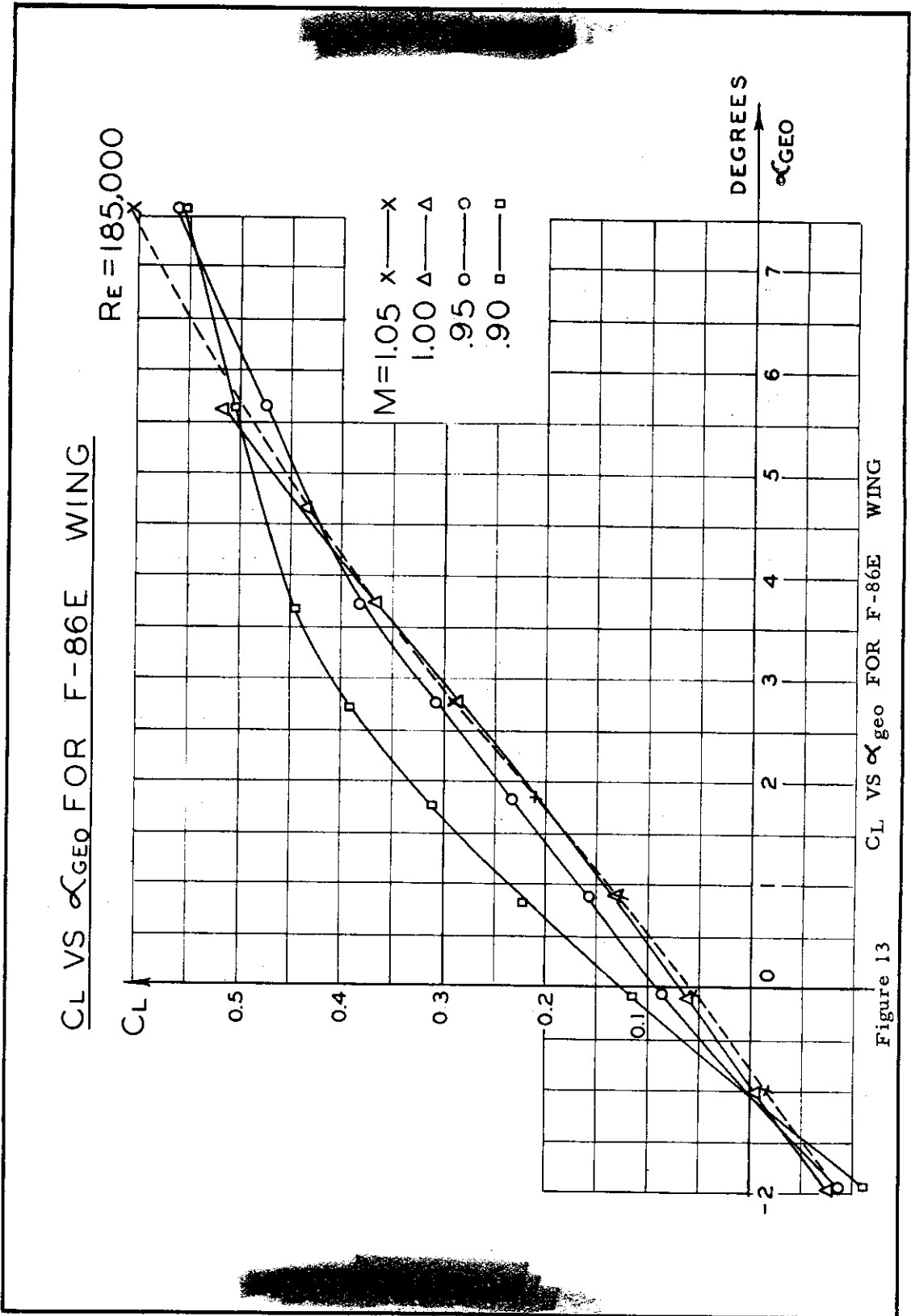


Figure 13

C_D VS α_{GEO} FOR F-86E WING
 $RE=185,000$

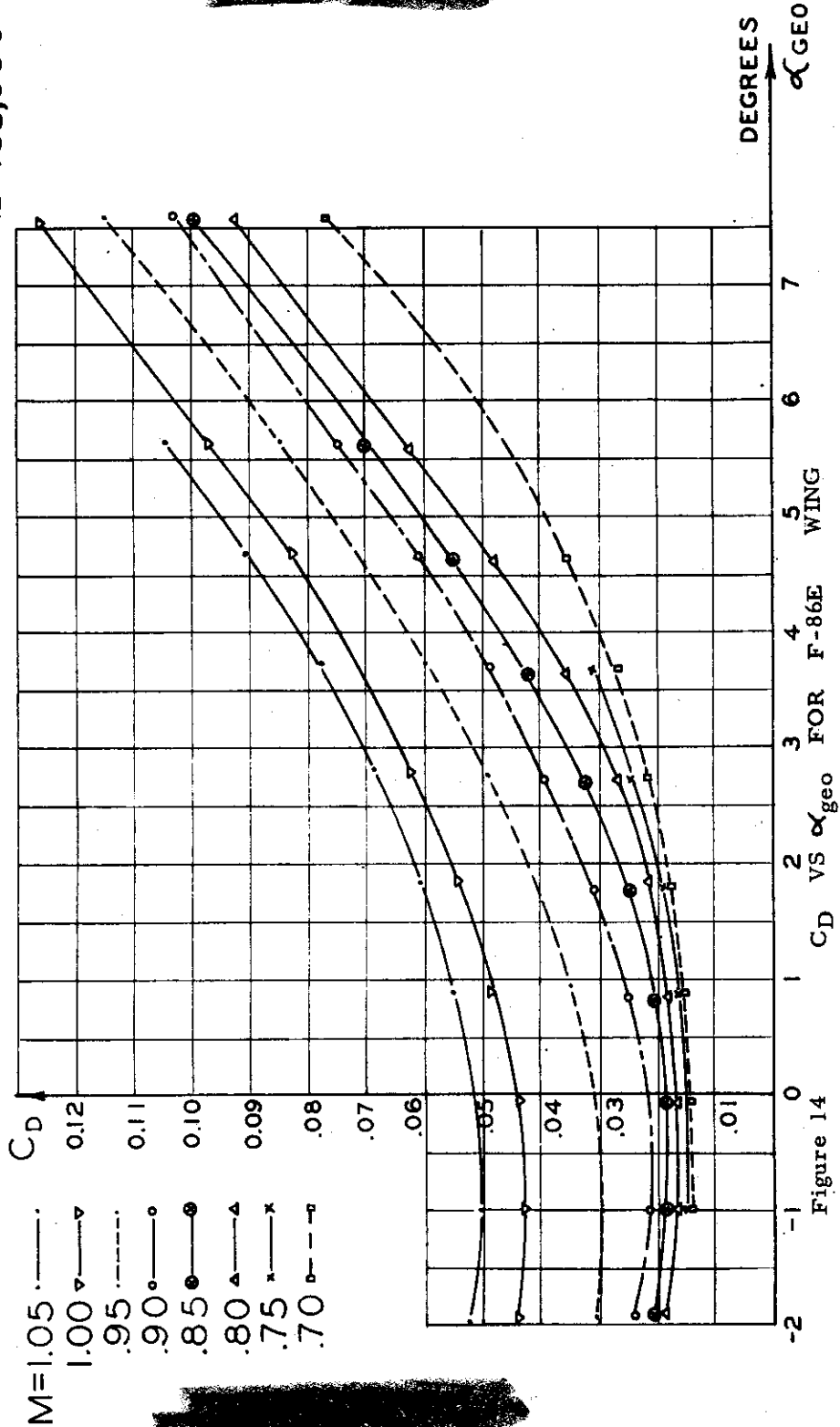


Figure 14

VARIATION OF PITCHING MOMENT
COEFFICIENT WITH LIFT COEFFICIENT
FOR THE F-86E WING

$C_L = f(C_{m_{c.g.}}, M)$ $Re = 185,000$

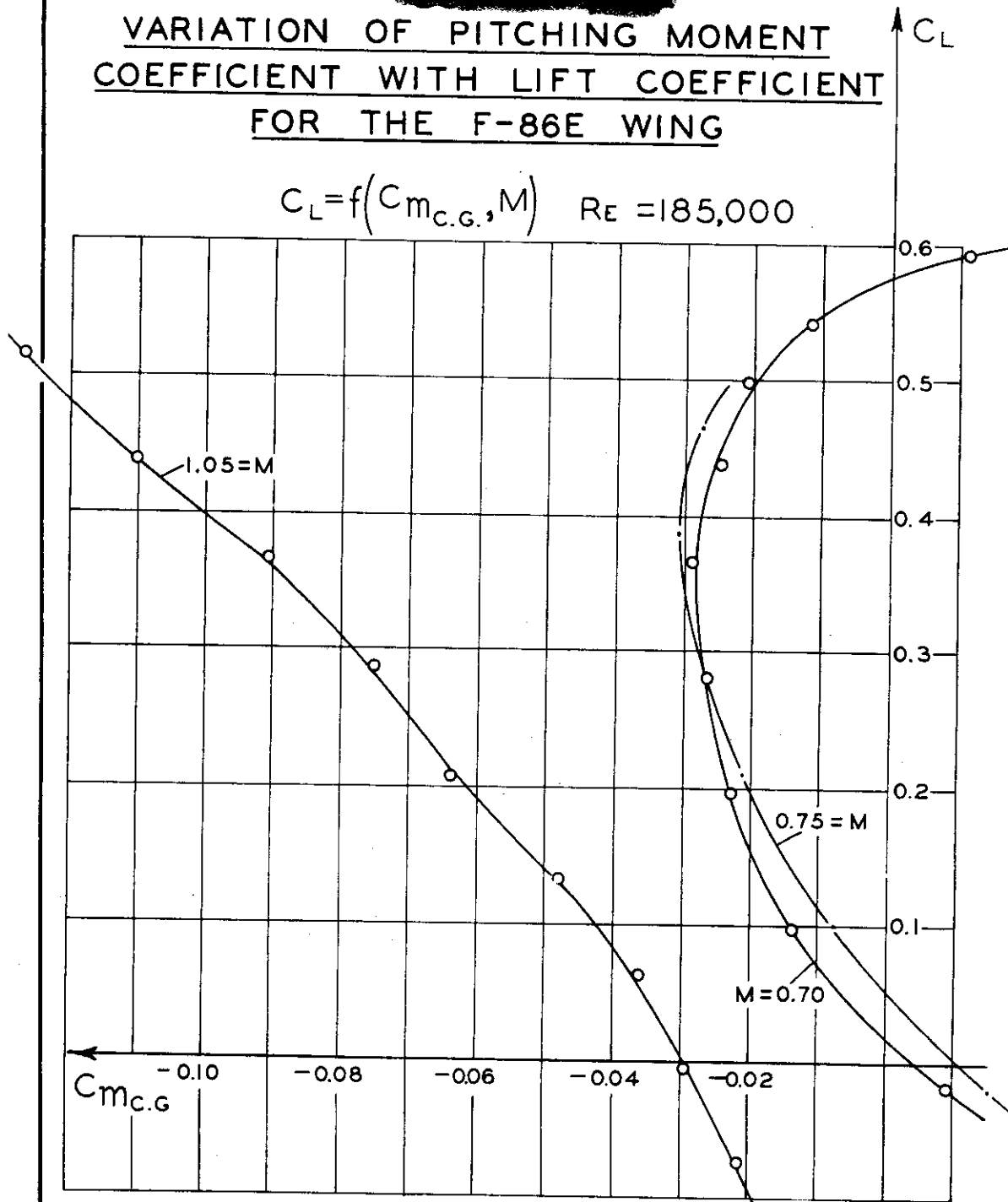


Fig. 15 $C_{m_{c.g.}}$ VERSUS C_L FOR THE F-86E WING

VARIATION OF PITCHING MOMENT
COEFFICIENT WITH LIFT COEFFICIENT
FOR THE F-86E WING

$C_L = f(C_{m_{c.g.}}, M)$
 $Re = 185,000$

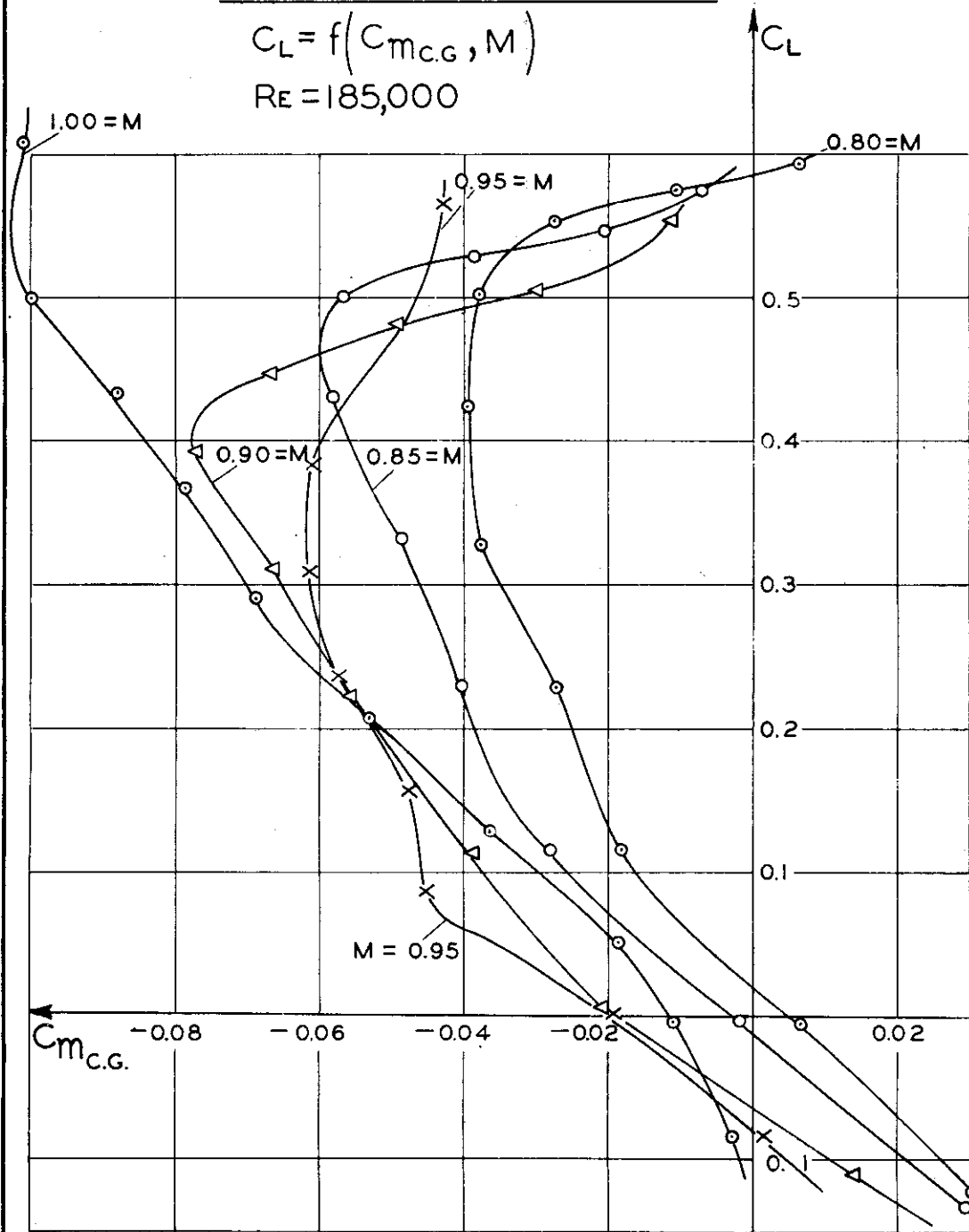


Fig. 16 $C_{M_{c.g.}}$ VERSUS C_L FOR THE F-86E WING

VARIATION OF PITCHING MOMENT AT $\alpha_{GEO} = 0^\circ$
 AS A FUNCTION OF M

$C_{m_{c.g.}}$

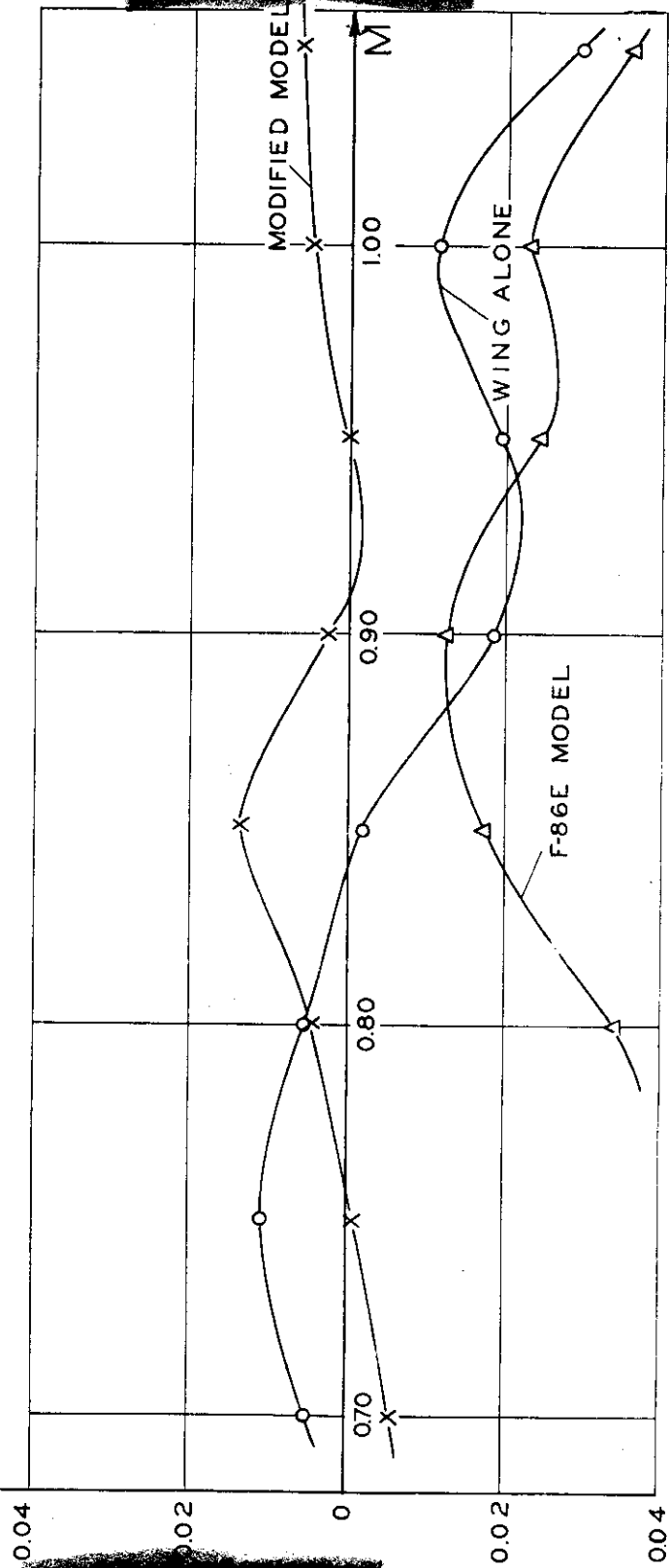
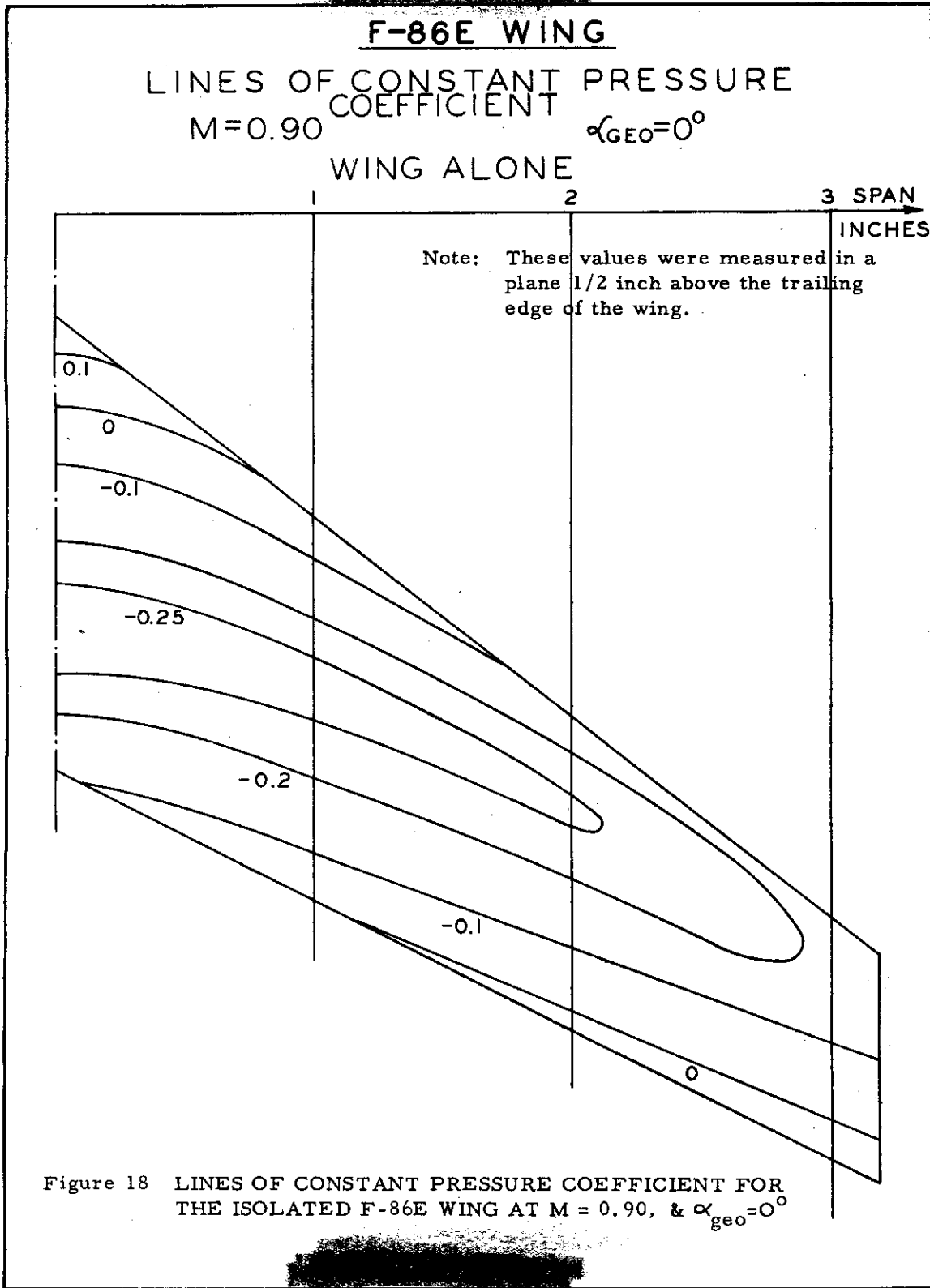


Fig. 17 PITCHING MOMENT COEFFICIENT AS A FUNCTION OF MACH NUMBER AT $\alpha_{GEO} = 0^\circ$



F-86E WING

LINES OF CONSTANT PRESSURE COEFFICIENT

M=0.95

WING ALONE

$\alpha_{GEO} = 0^\circ$

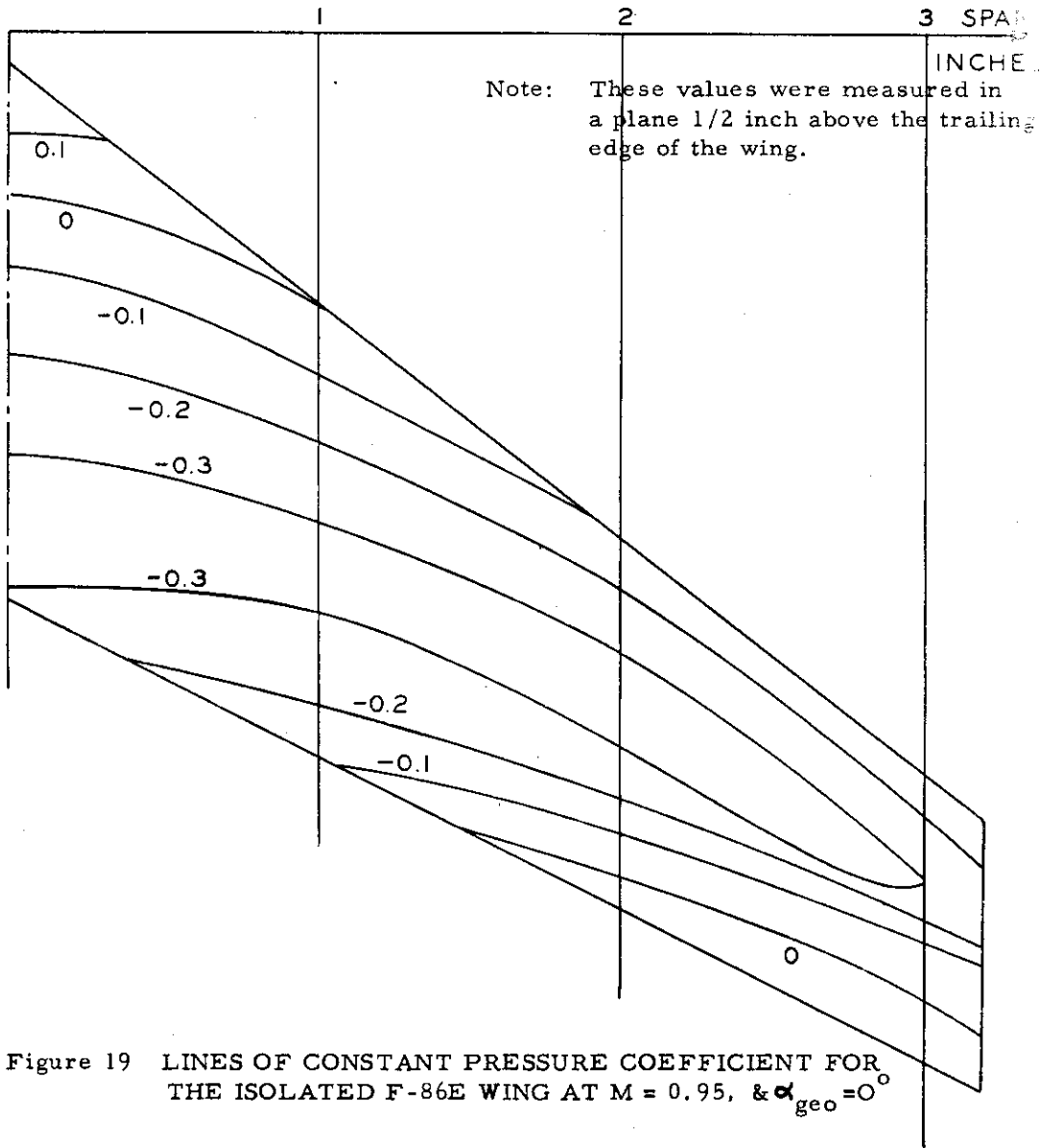


Figure 19 LINES OF CONSTANT PRESSURE COEFFICIENT FOR THE ISOLATED F-86E WING AT M = 0.95, & $\alpha_{geo} = 0^\circ$

F-86E WING

LINES OF CONSTANT PRESSURE COEFFICIENT

M=1.00

$\alpha_{GEO} = 0^\circ$

WING ALONE

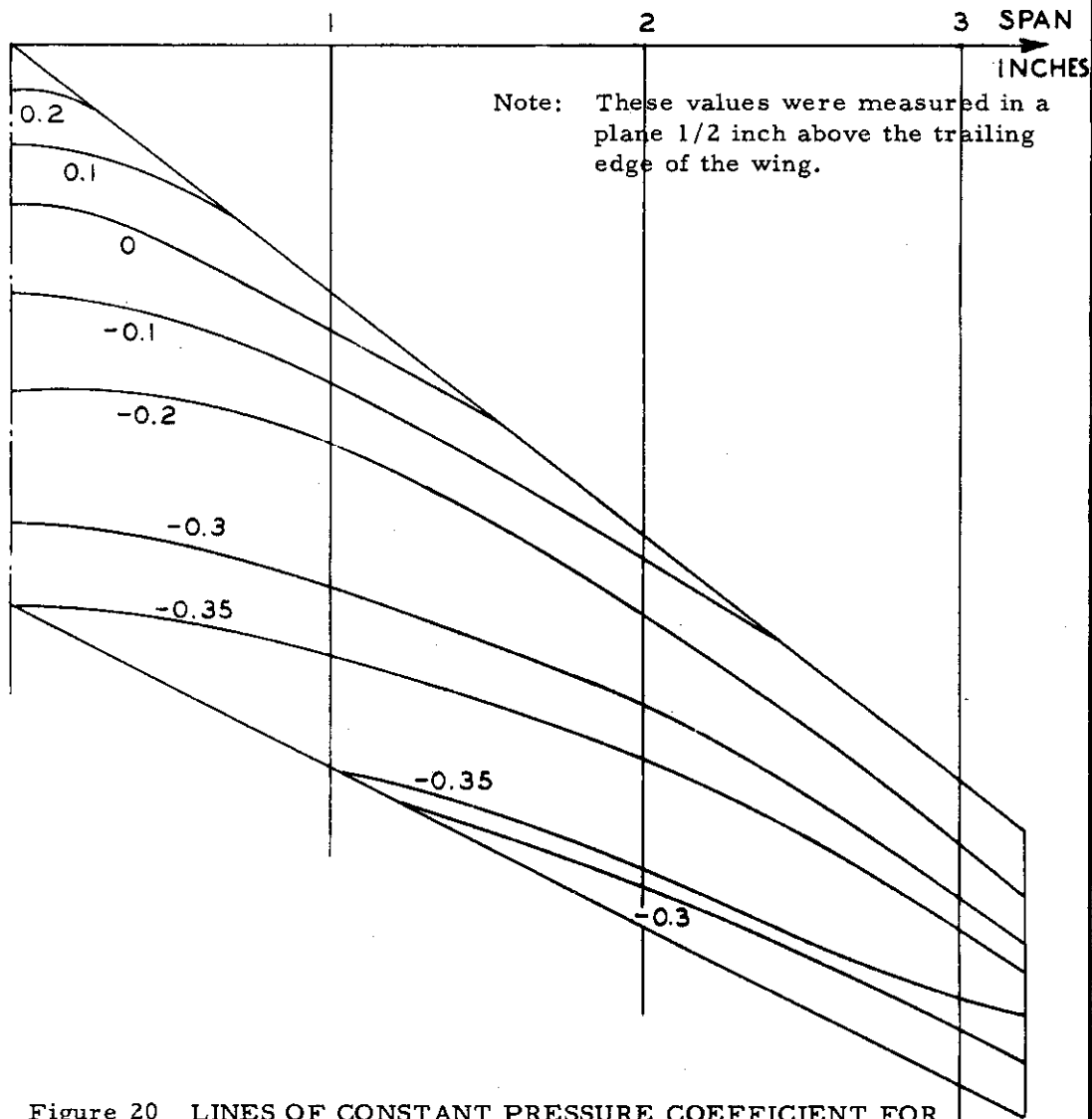


Figure 20 LINES OF CONSTANT PRESSURE COEFFICIENT FOR THE ISOLATED F-86E WING AT M = 1.00, & $\alpha_{geo} = 0^\circ$

F-86E WING

LINES OF CONSTANT PRESSURE
COEFFICIENT

M=1.05

$\alpha_{GEO}=0^\circ$

WING ALONE

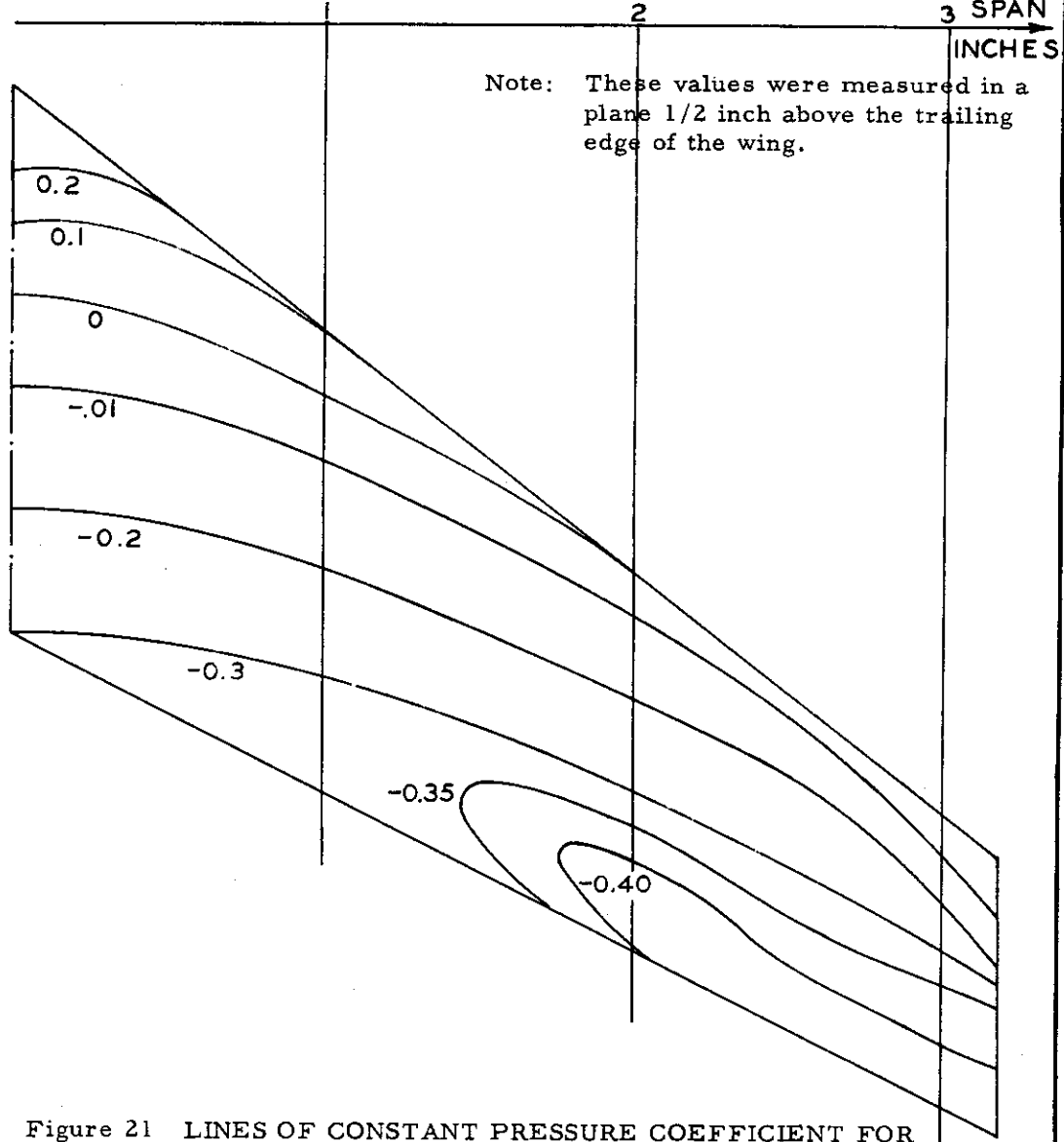
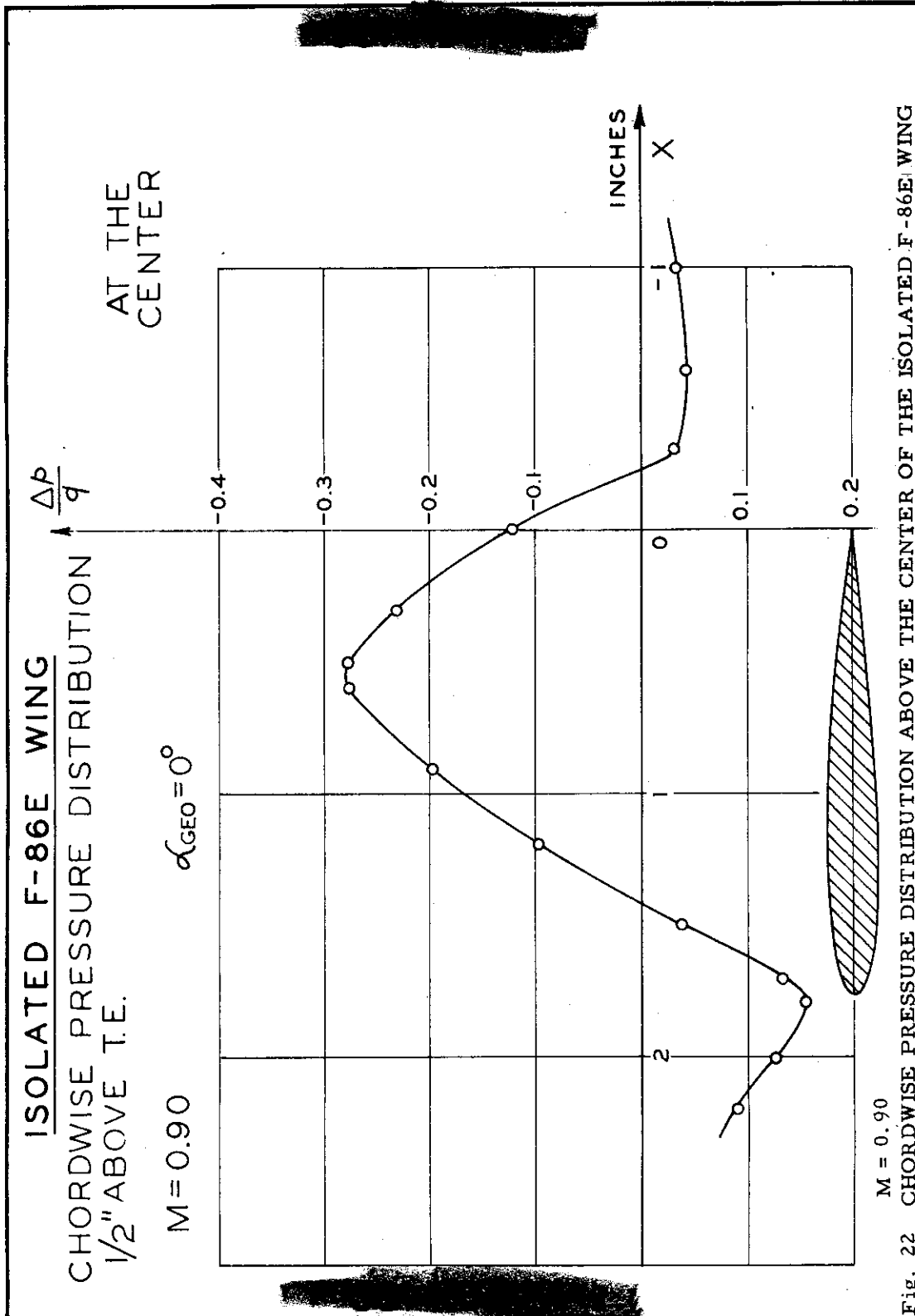


Figure 21 LINES OF CONSTANT PRESSURE COEFFICIENT FOR THE ISOLATED F-86E WING AT M = 1.05, & $\alpha_{geo}=0^\circ$



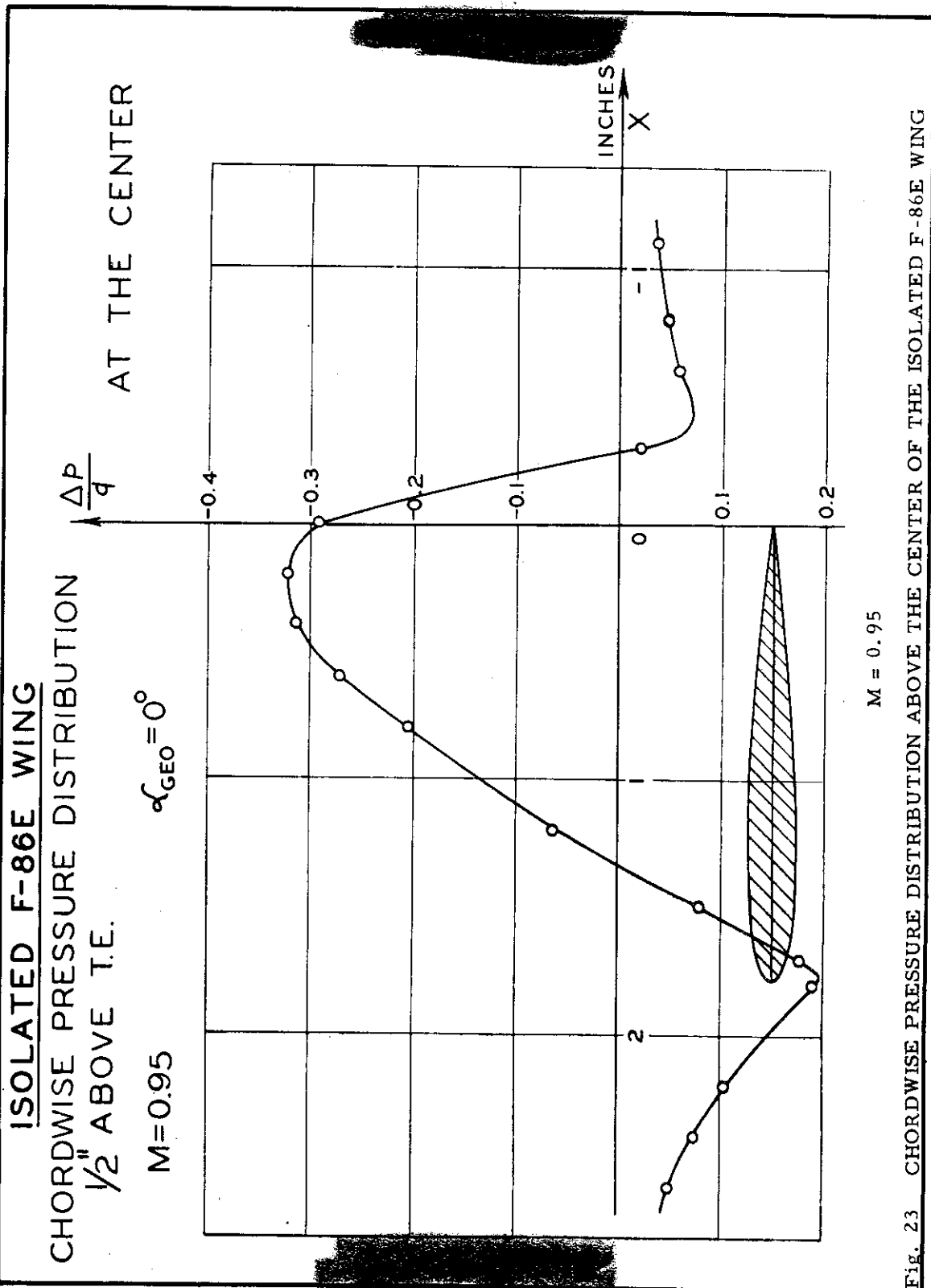


Fig. 23 CHORDWISE PRESSURE DISTRIBUTION ABOVE THE CENTER OF THE ISOLATED F-86E WING

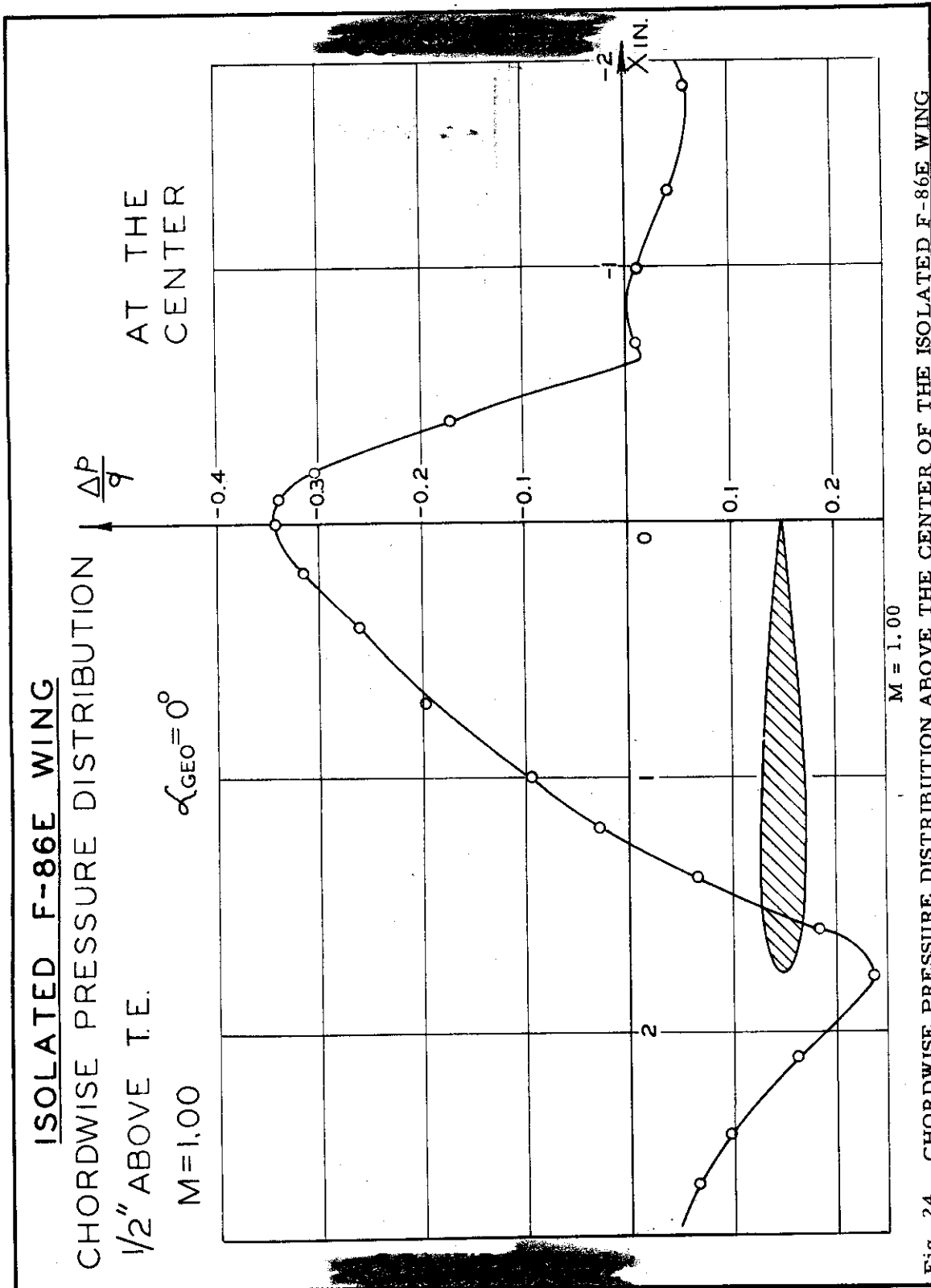


Fig. 24 CHORDWISE PRESSURE DISTRIBUTION ABOVE THE CENTER OF THE ISOLATED F-86E WING

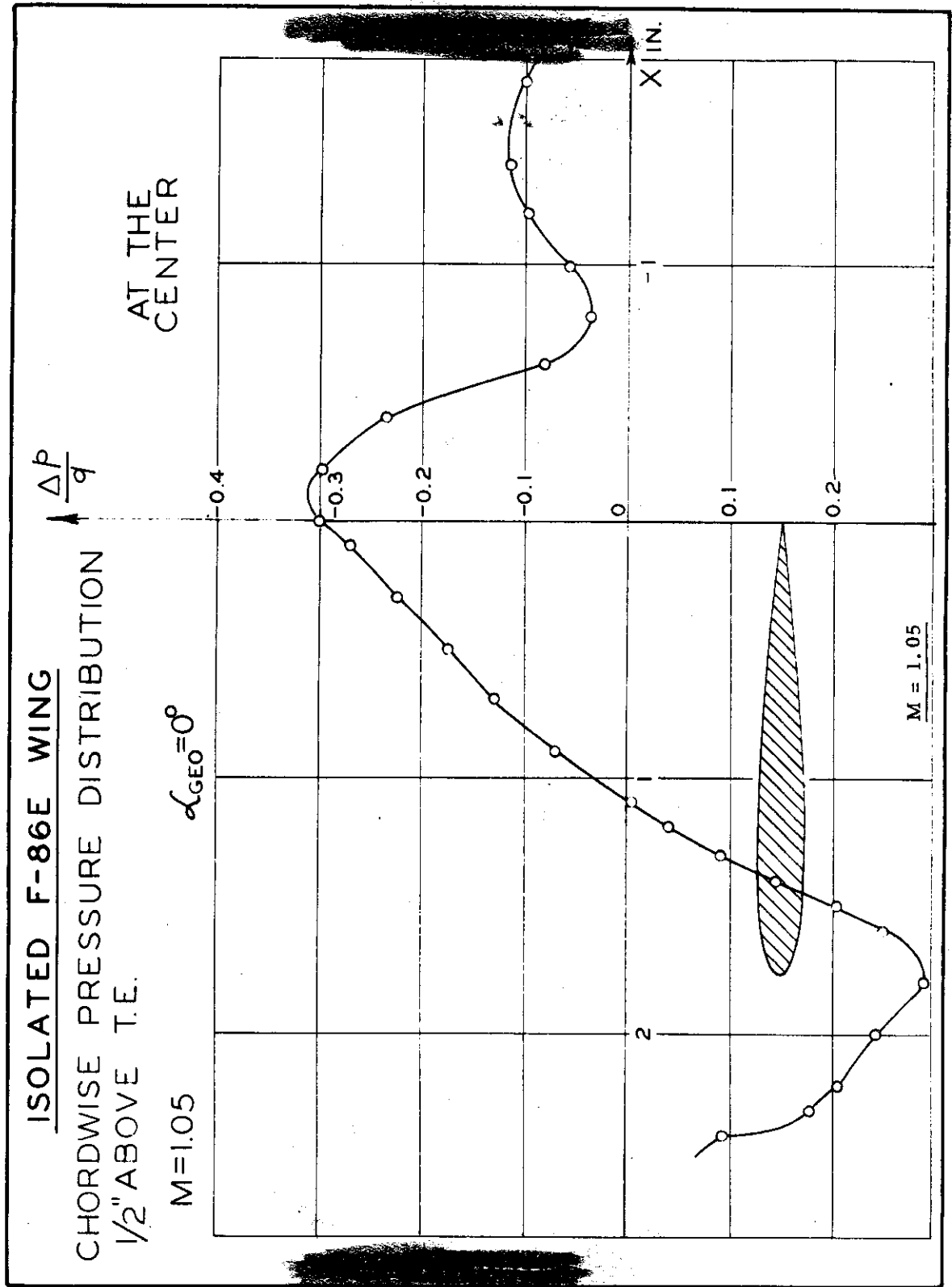


Fig. 25 CHORDWISE PRESSURE DISTRIBUTION ABOVE THE CENTER OF THE ISOLATED F-86E WING

CHORDWISE PRESSURE DISTRIBUTION

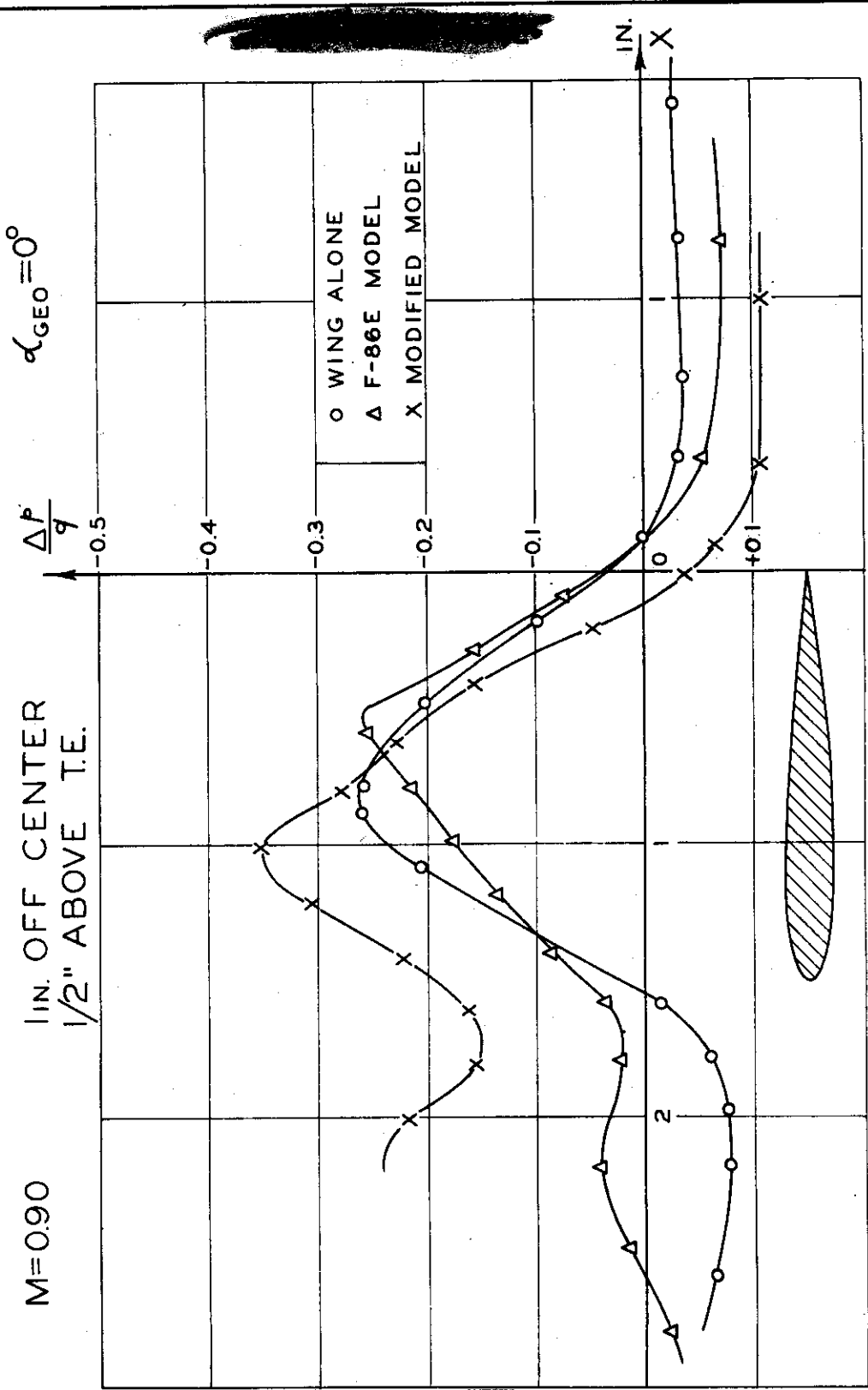


Fig. 26 CHORDWISE PRESSURE DISTRIBUTION $M = 0.90, 1 \text{ " OFF CENTER, } 1/2 \text{ " ABOVE T.E. FOR } \alpha_{\text{geo}} = 0^\circ$

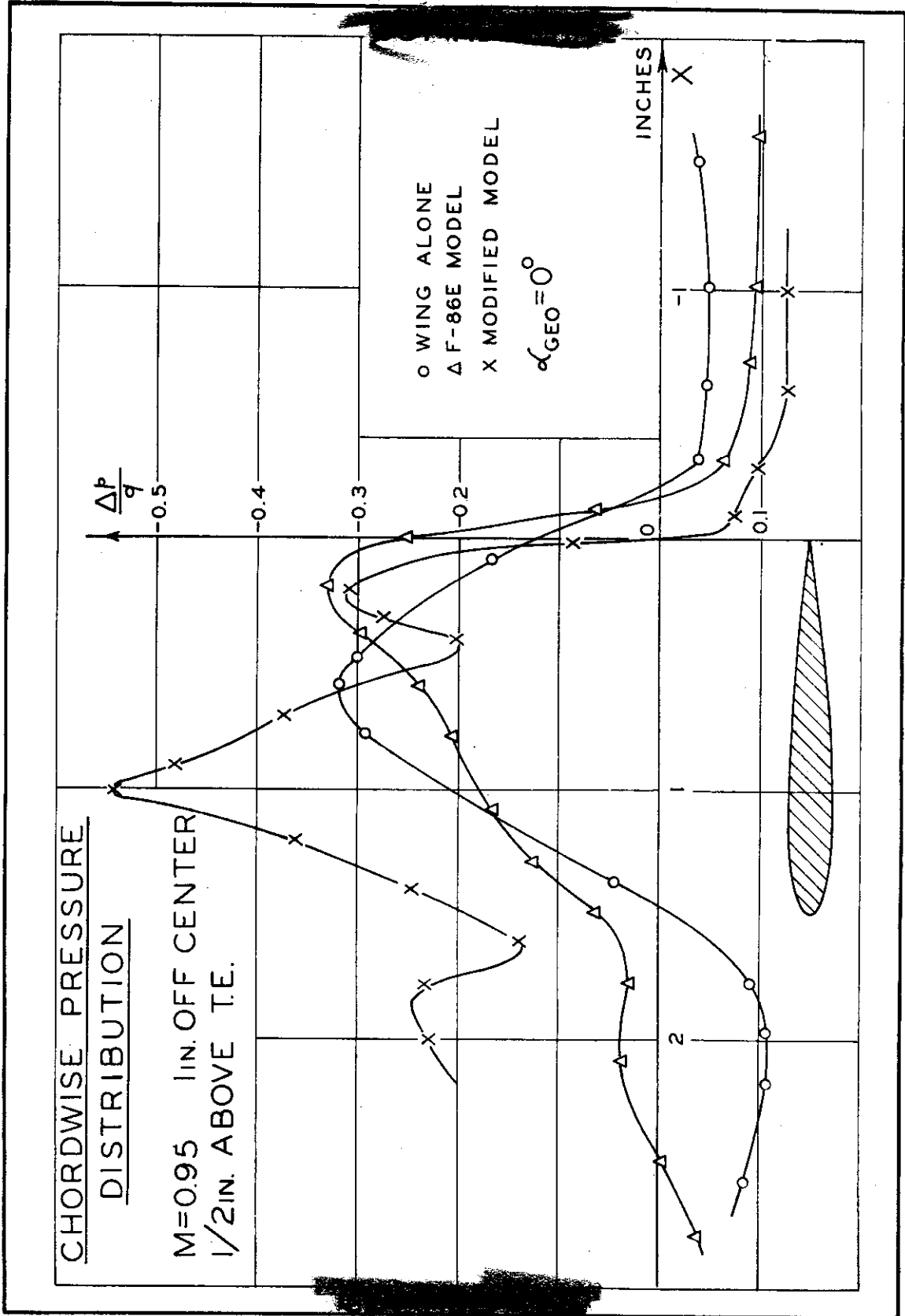


Fig. 27 CHORDWISE PRESSURE DISTRIBUTION M = 0.95, 1" OFF CENTER, 1/2" ABOVE T.E. FOR $\alpha_{geo} = 0^\circ$

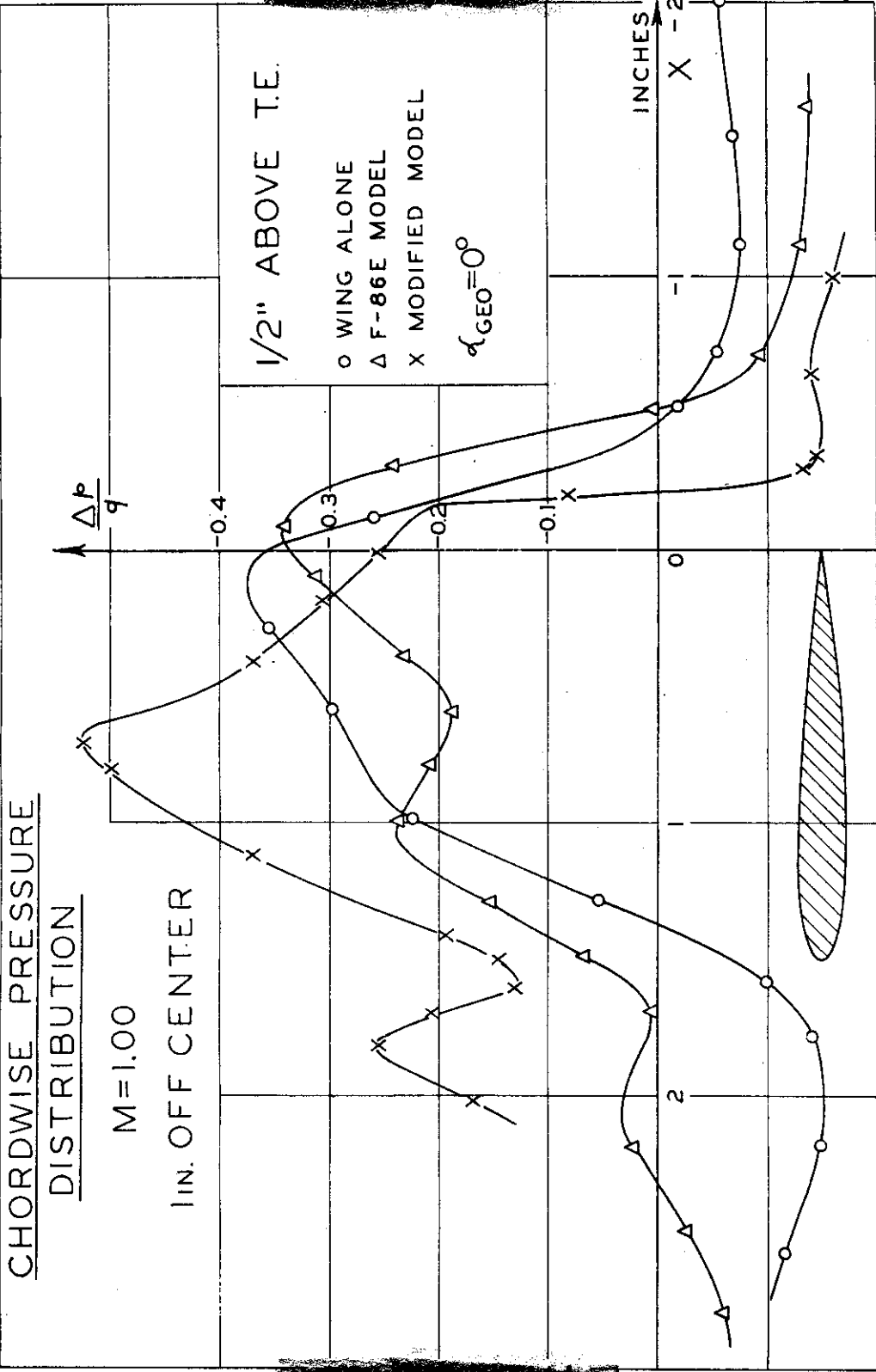


Fig. 28 CHORDWISE PRESSURE DISTRIBUTION M = 1.00, 1" OFF CENTER, 1/2" ABOVE T.E. FOR $\alpha_{geo} = 0^\circ$

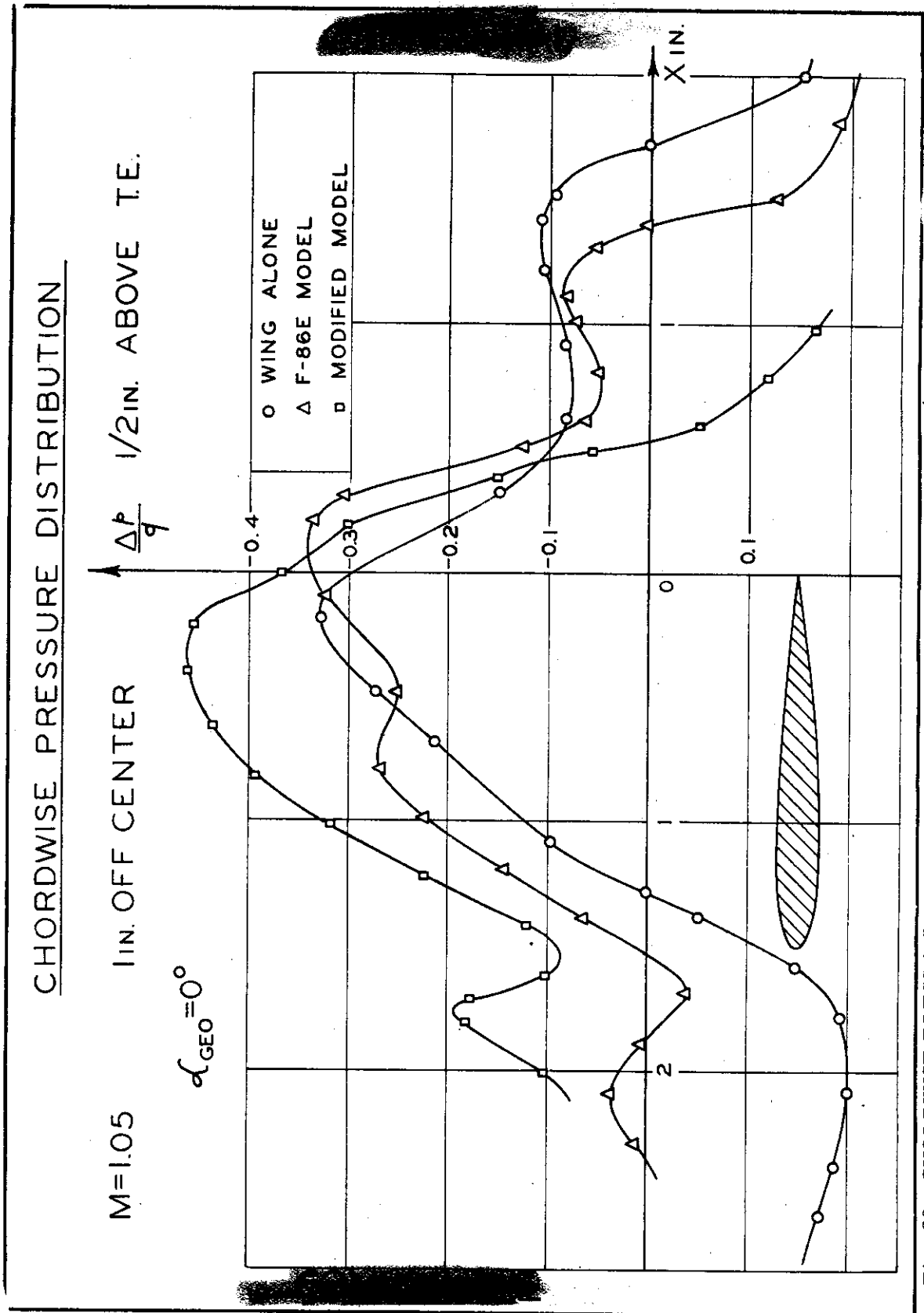


Fig. 29 CHORDWISE PRESSURE DISTRIBUTION $M = 1.05$, 1" OFF CENTER, 1/2" ABOVE T.E. FOR $\alpha_{geo} = 0^\circ$

CHORDWISE PRESSURE DISTRIBUTION

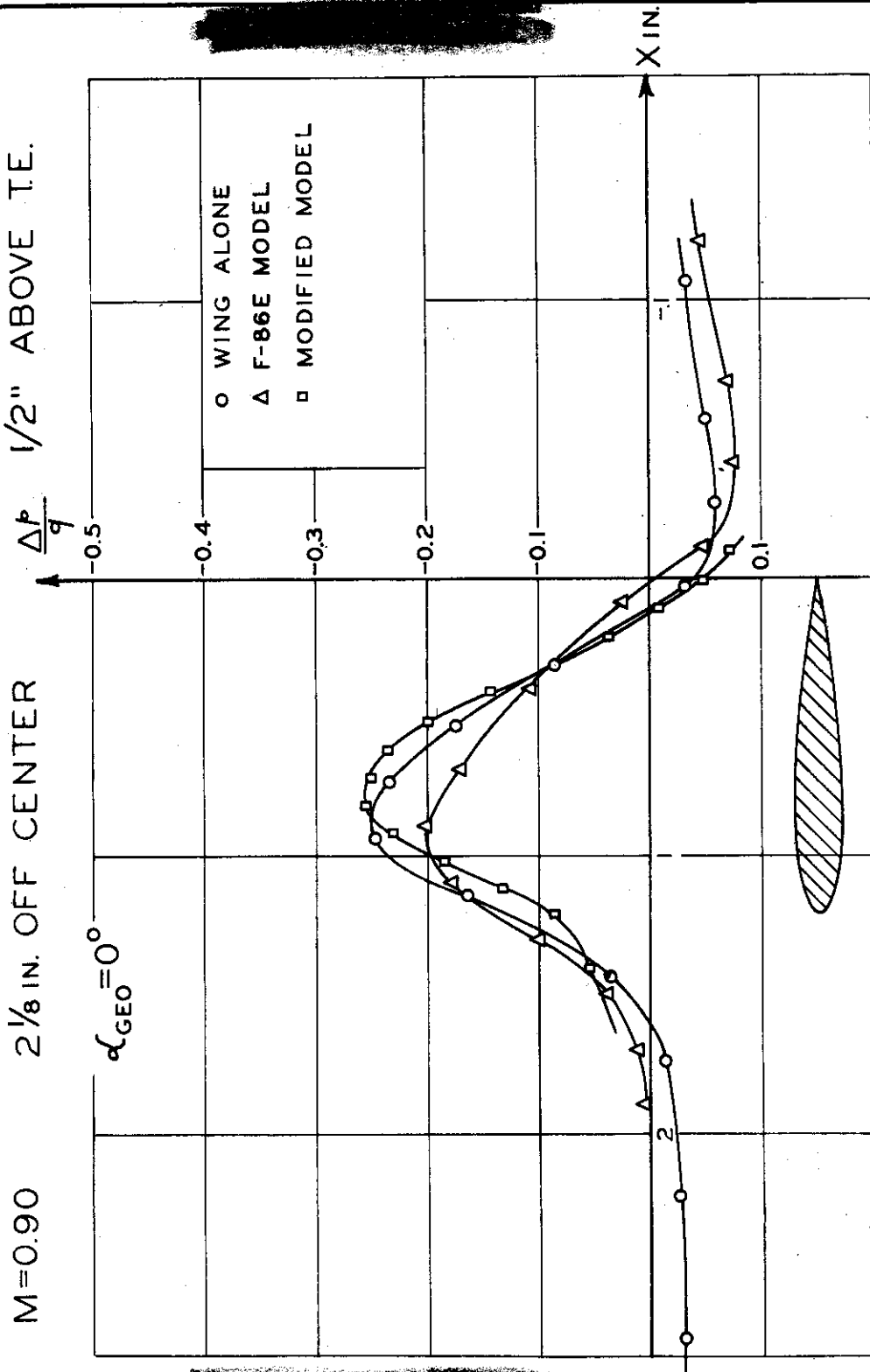


Fig. 30 CHORDWISE PRESSURE DISTRIBUTION M = 0.90, 2 1/8" OFF CENTER, 1/2" ABOVE T.E. FOR $\alpha_{geo} = 0^\circ$

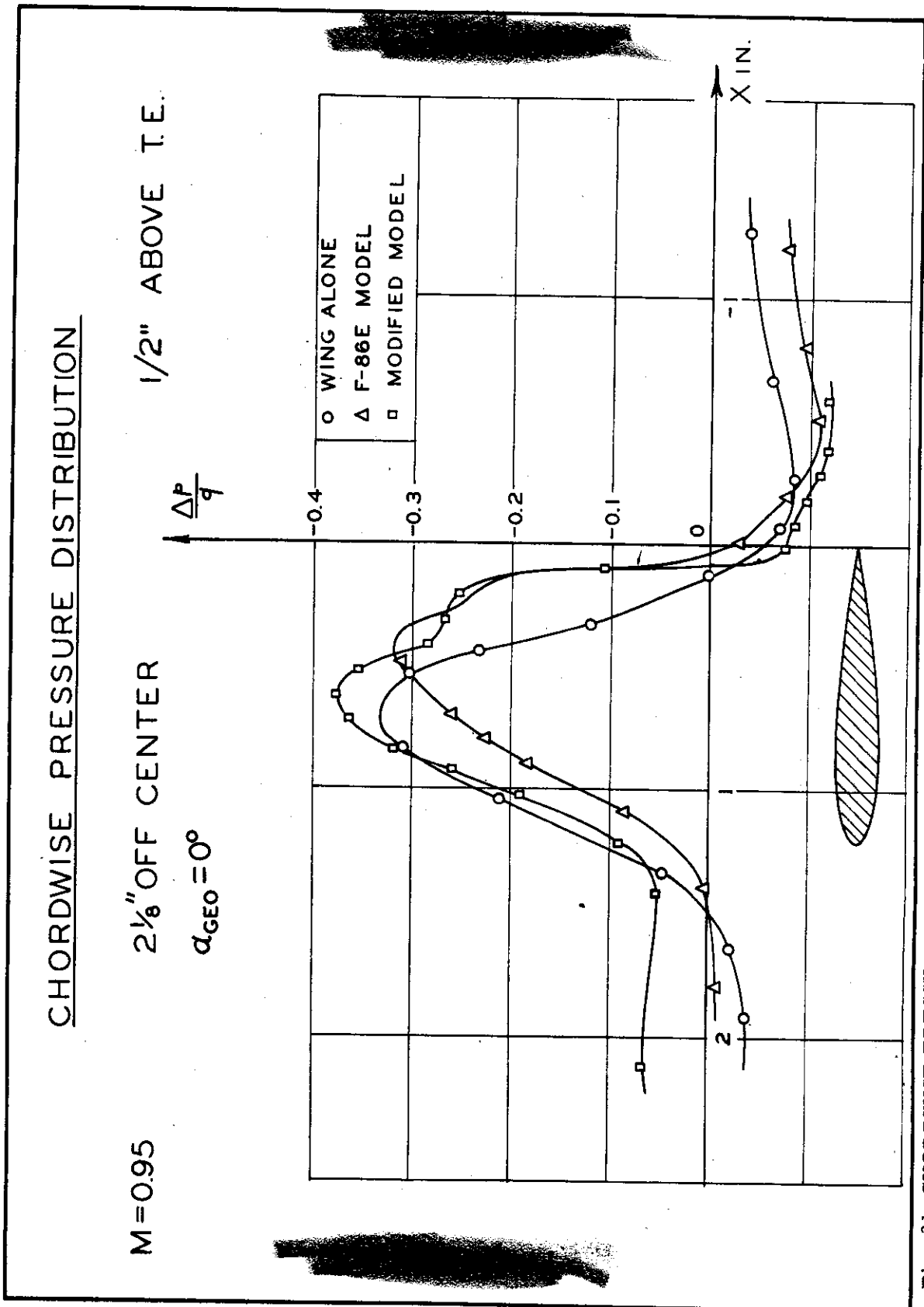


Fig. 31 CHORDWISE PRESSURE DISTRIBUTION M = 0.95, 2 1/8" OFF CENTER, 1/2" ABOVE T.E. FOR $\alpha_{geo} = 0^\circ$

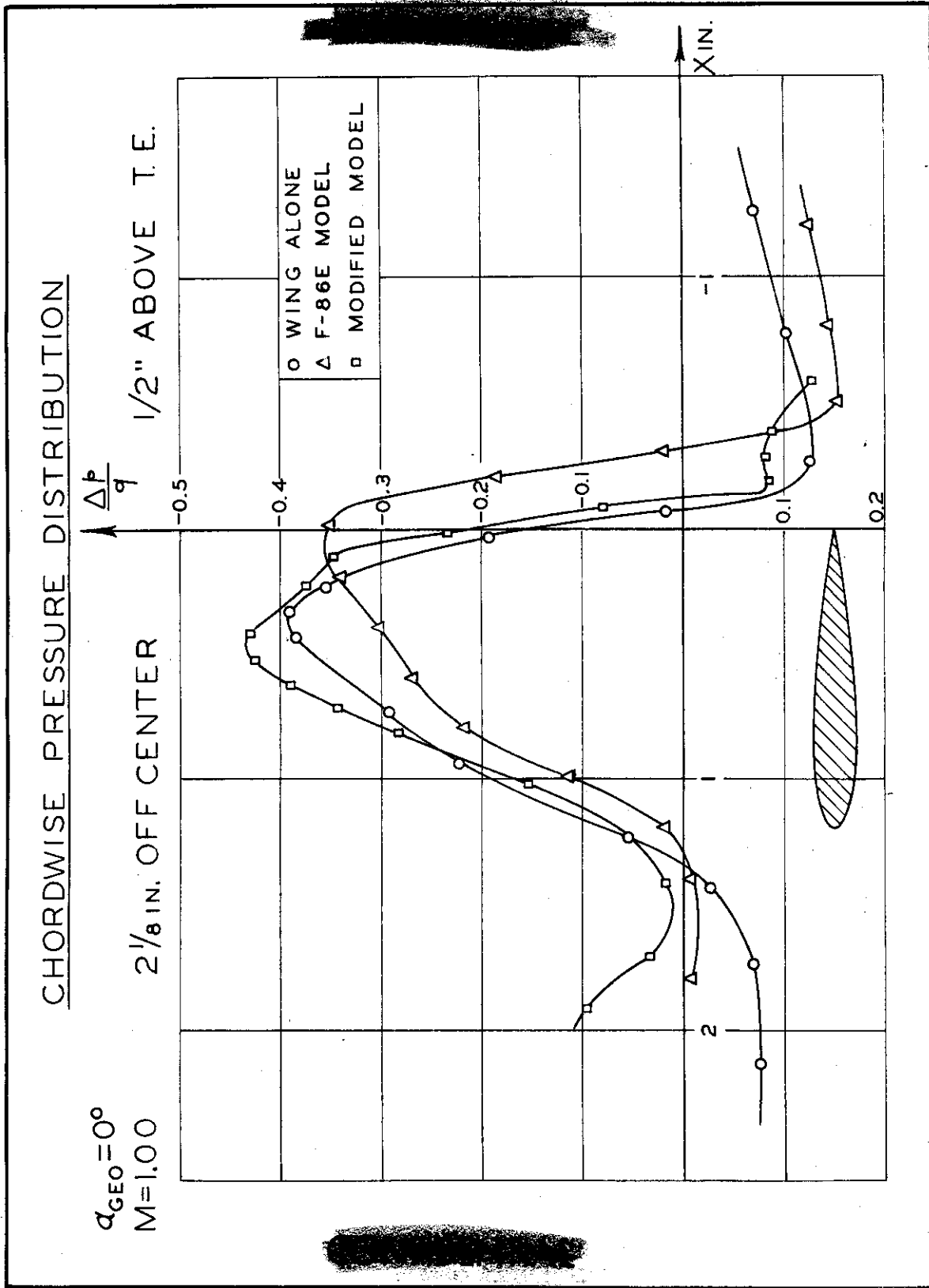


Fig. 32 CHORDWISE PRESSURE DISTRIBUTION $M = 1.00$, 2 1/8 OFF CENTER, 1/2" ABOVE T. E. FOR $\alpha_{geo} = 0^\circ$

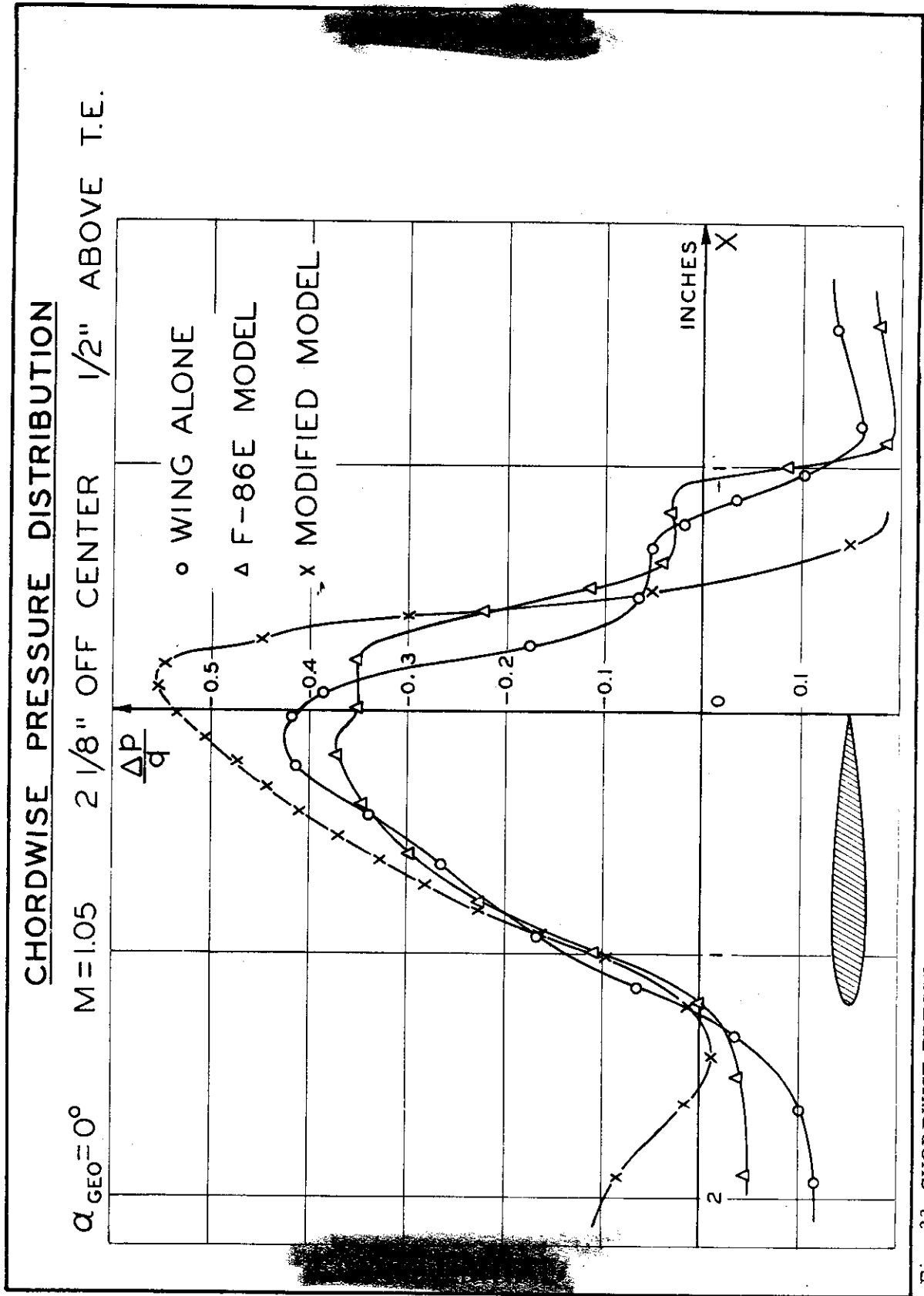


Fig. 33 CHORDWISE PRESSURE DISTRIBUTION $M = 1.05$, $2 \frac{1}{8}"$ OFF CENTER, $1 \frac{1}{2}"$ ABOVE T.E. FOR $\alpha_{GEO} = 0^\circ$

CHORDWISE PRESSURE DISTRIBUTION OF ISOLATED F-86E WING

$\alpha_{geo} = 0^\circ$ $M = 0.90$ $2.42''$ OFF CENTER $1/2''$ ABOVE T.E.

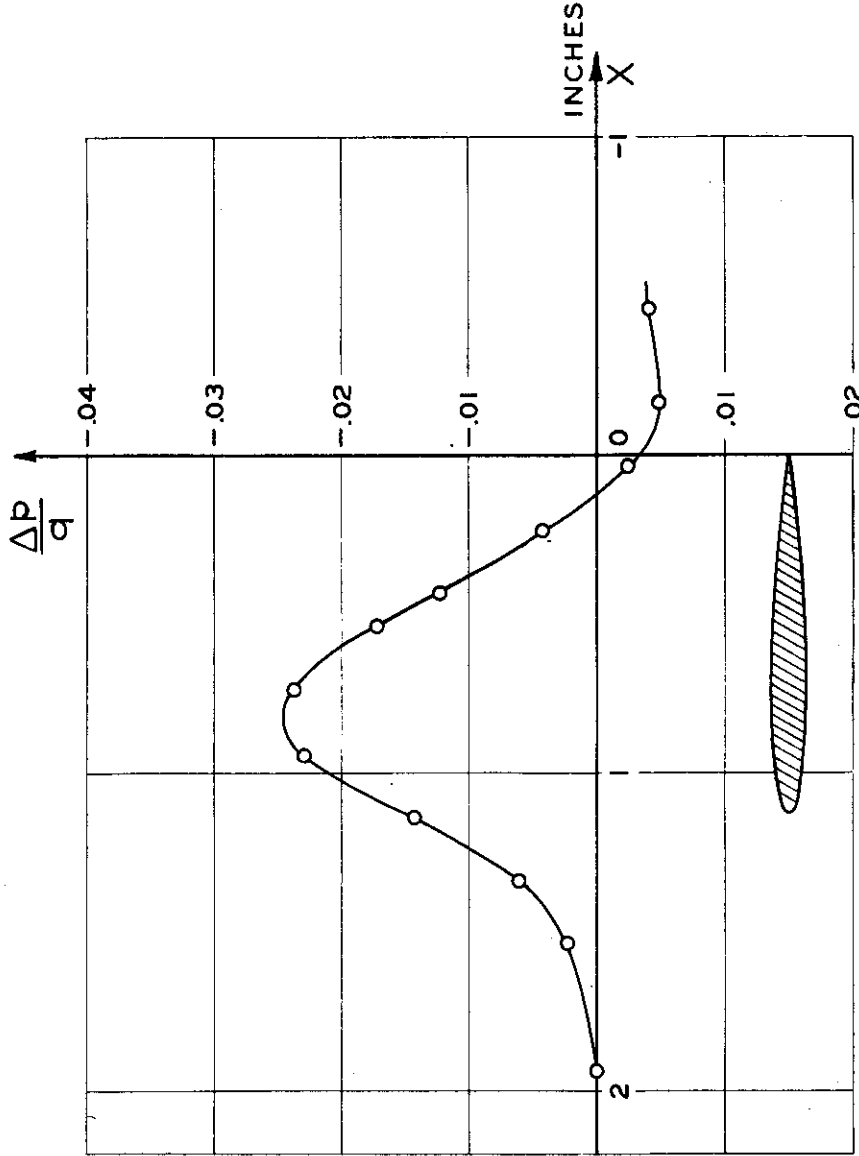


Fig. 34 CHORDWISE PRESSURE DISTRIBUTION $M = 0.90$, $2.42''$ OFF CENTER, $1/2''$ ABOVE T.E. FOR $\alpha_{geo} = 0^\circ$

CHORDWISE PRESSURE DISTRIBUTION

$\alpha_{geo} = 0^\circ$ $M = 0.95$ 2.42" OFF CENTER 1/2" ABOVE T.E.

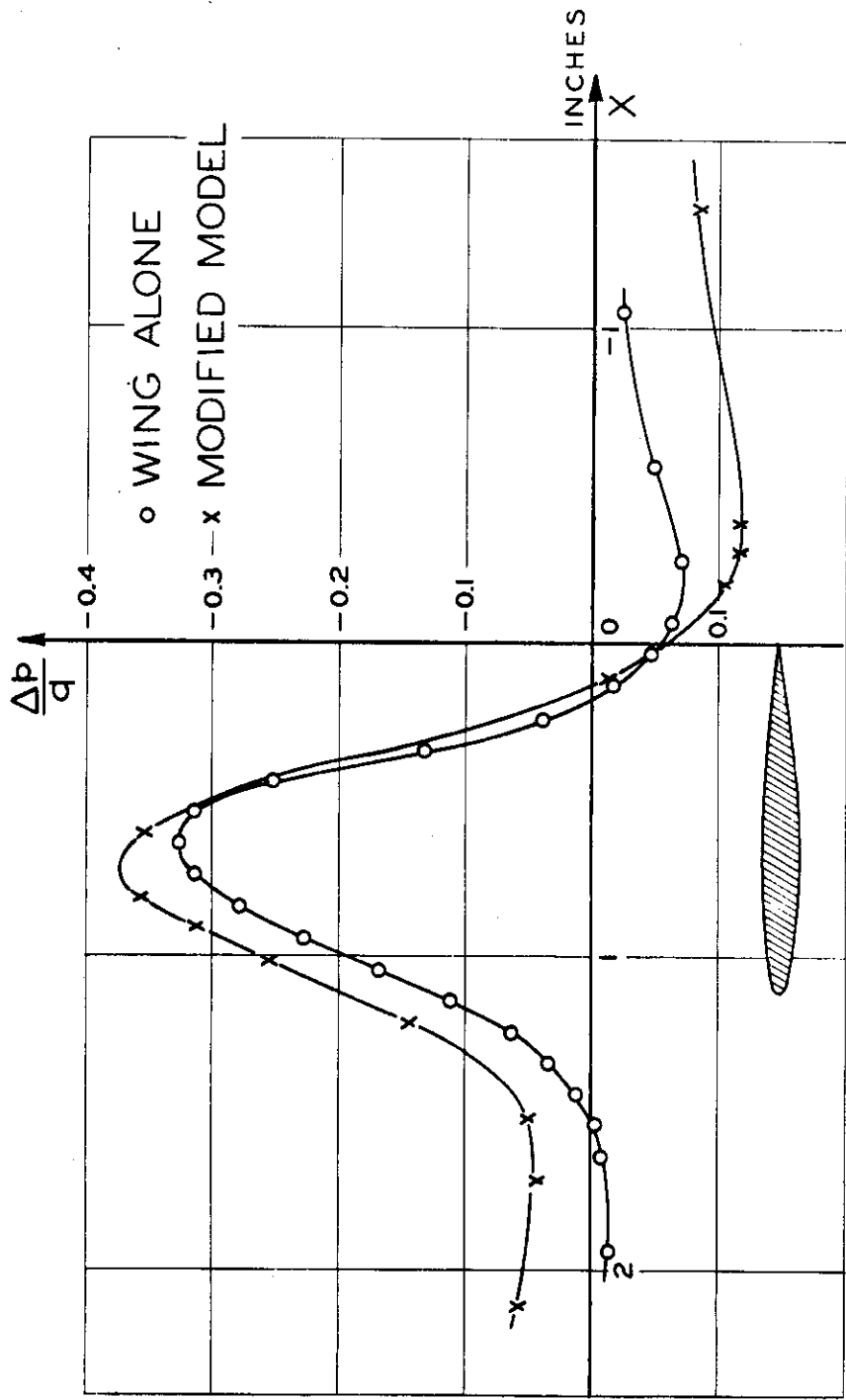


Fig. 35 CHORDWISE PRESSURE DISTRIBUTION $M = 0.95$, 2.42" OFF CENTER, 1/2" ABOVE T.E. FOR $\alpha_{geo} = 0^\circ$

CHORDWISE PRESSURE DISTRIBUTION

$\alpha_{geo} = 0^\circ$ $M = 1.00$ 2.42" OFF CENTER 1/2" ABOVE T.E.

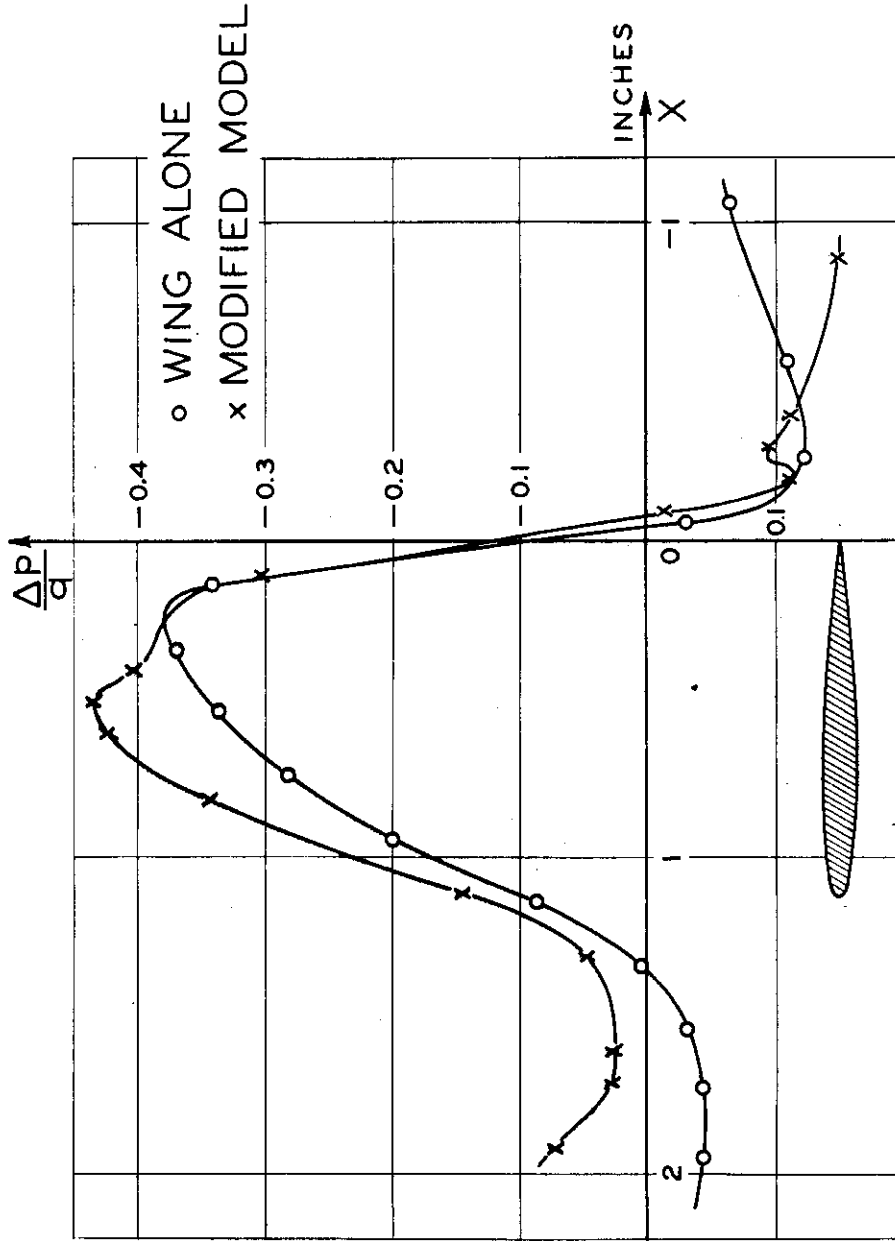


Fig. 36 CHORDWISE PRESSURE DISTRIBUTION $M = 1.00$, 2.42" OFF CENTER, 1/2" ABOVE T.E. FOR $\alpha_{geo} = 0^\circ$

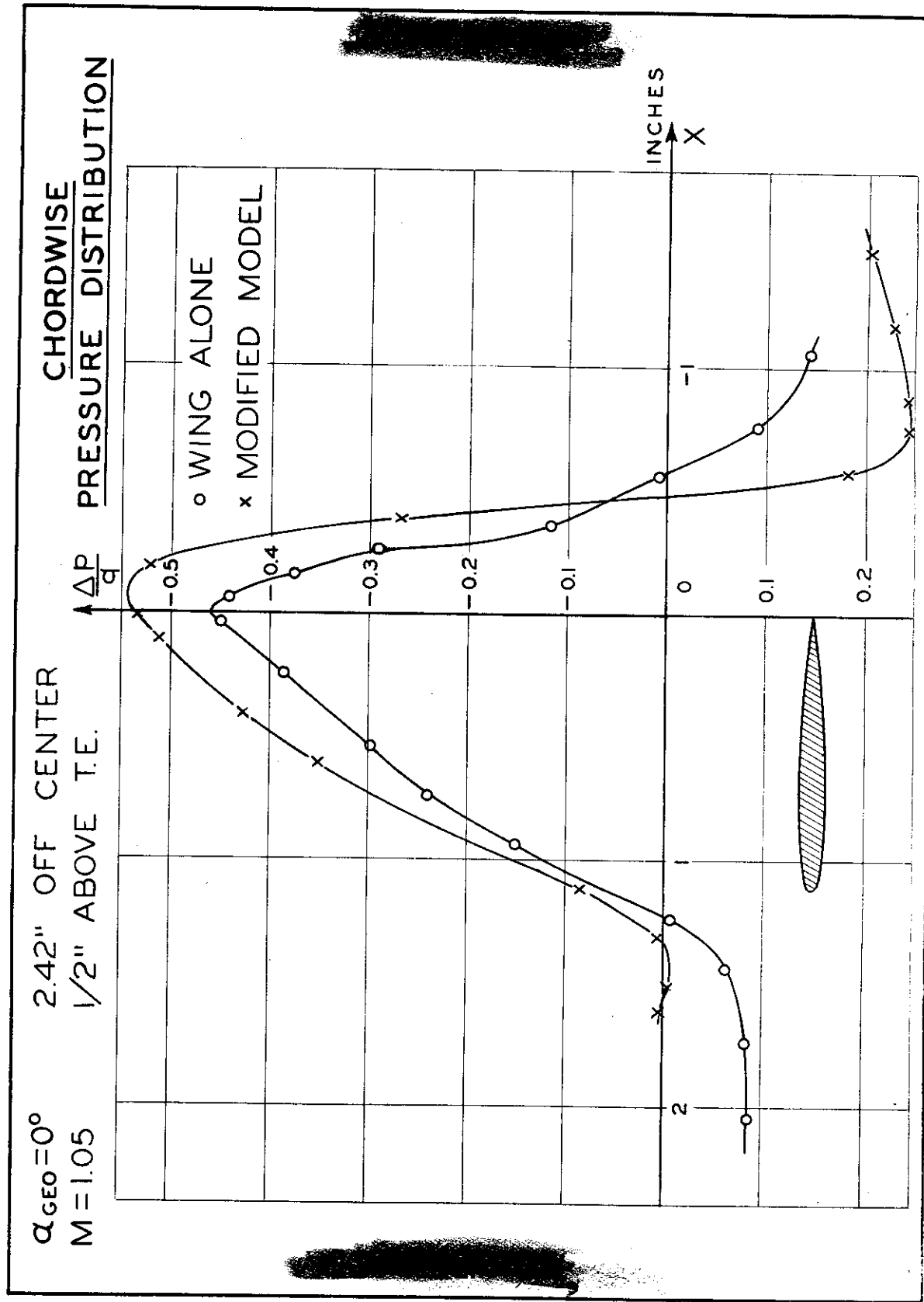


Fig. 37 CHORDWISE PRESSURE DISTRIBUTION $M = 1.05$, 2.42" OFF CENTER, 1/2" ABOVE T.E. FOR $\alpha_{geo} = 0^\circ$

CHORDWISE PRESSURE DISTRIBUTION

$\alpha_{GEO} = 0^\circ$ $M = 0.90$ $2.98''$ OFF CENTER $1/2''$ ABOVE T.E.

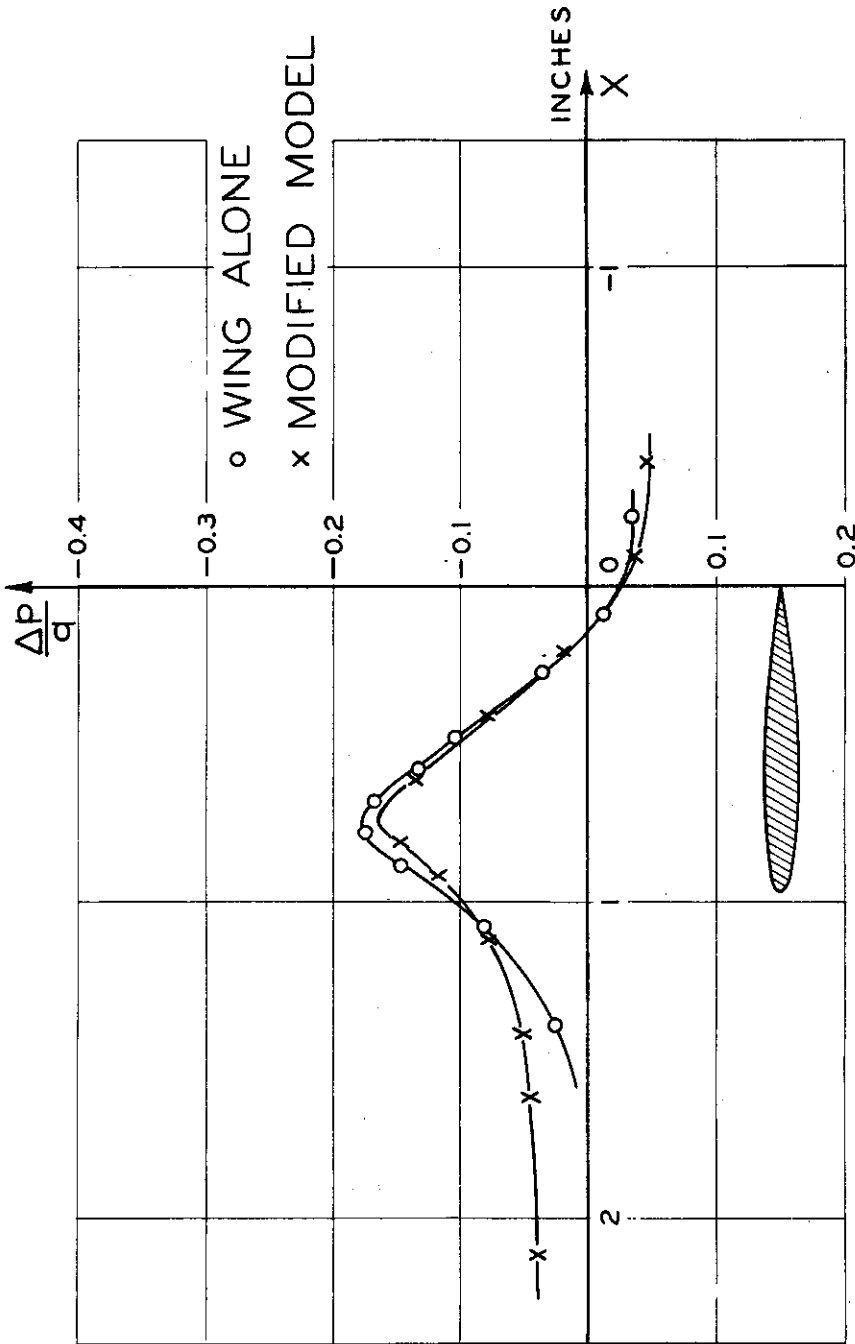


Fig. 38 CHORDWISE PRESSURE DISTRIBUTION $M = 0.90$, $2.98''$ OFF CENTER, $1/2''$ ABOVE T.E. FOR $\alpha_{GEO} = 0^\circ$

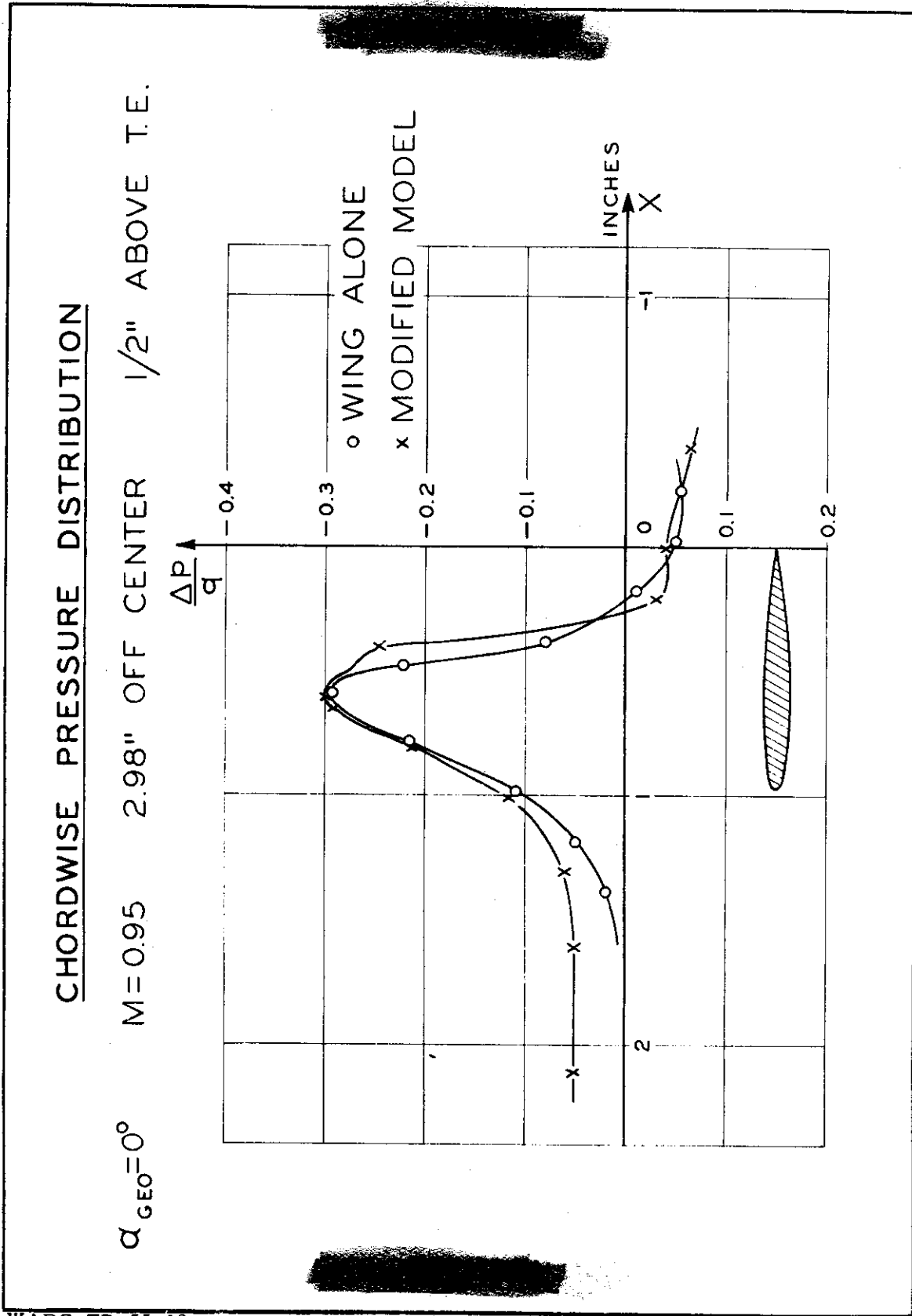


Fig. 39 CHORDWISE PRESSURE DISTRIBUTION $M = 0.95$, $2.98''$ OFF CENTER, $1/2''$ ABOVE T.E. FOR $\alpha_{geo} = 0^\circ$

CHORDWISE PRESSURE DISTRIBUTION

$\alpha_{GEO} = 0^\circ$ $M = 1.00$ $2.98''$ OFF CENTER $1/2''$ ABOVE T.E.

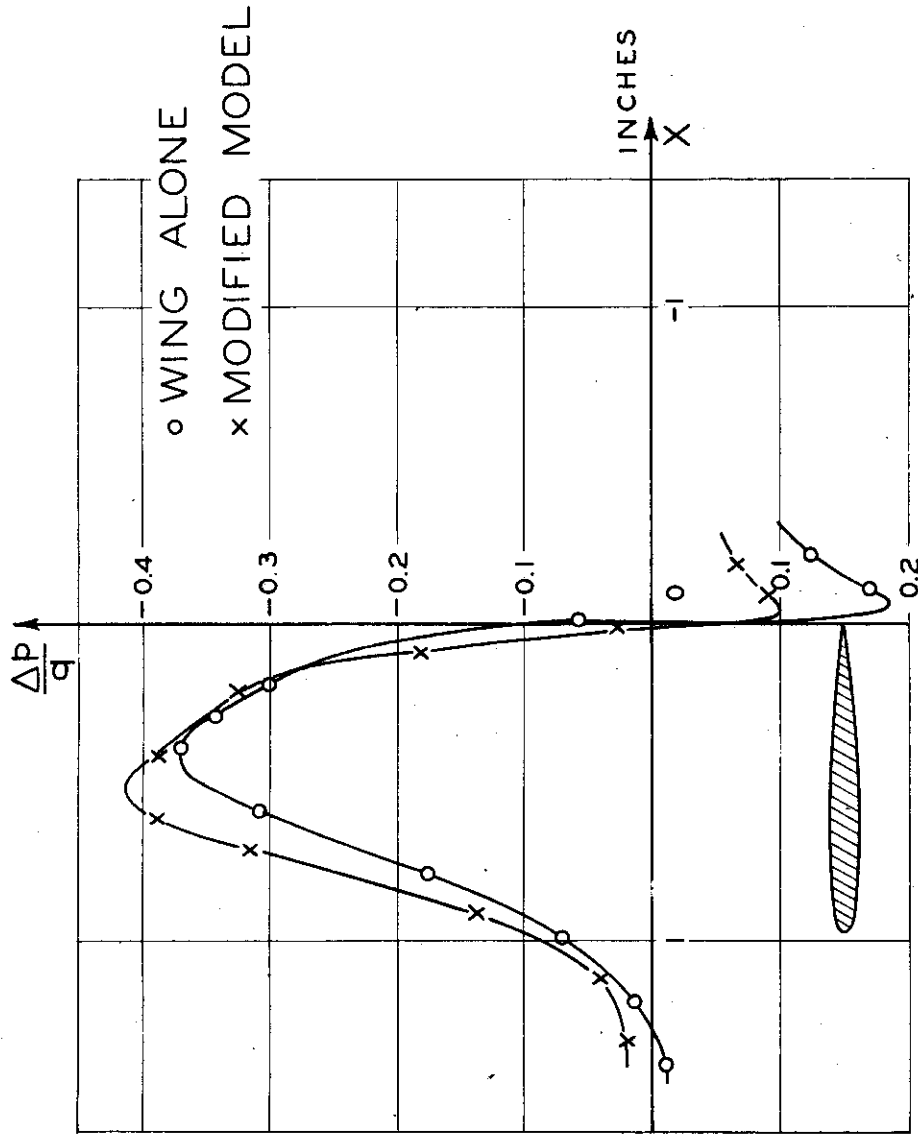


Fig. 40 CHORDWISE PRESSURE DISTRIBUTION $M = 1.00$, $2.98''$ OFF CENTER, $1/2''$ ABOVE T.E. FOR $\alpha_{geo} = 0^\circ$

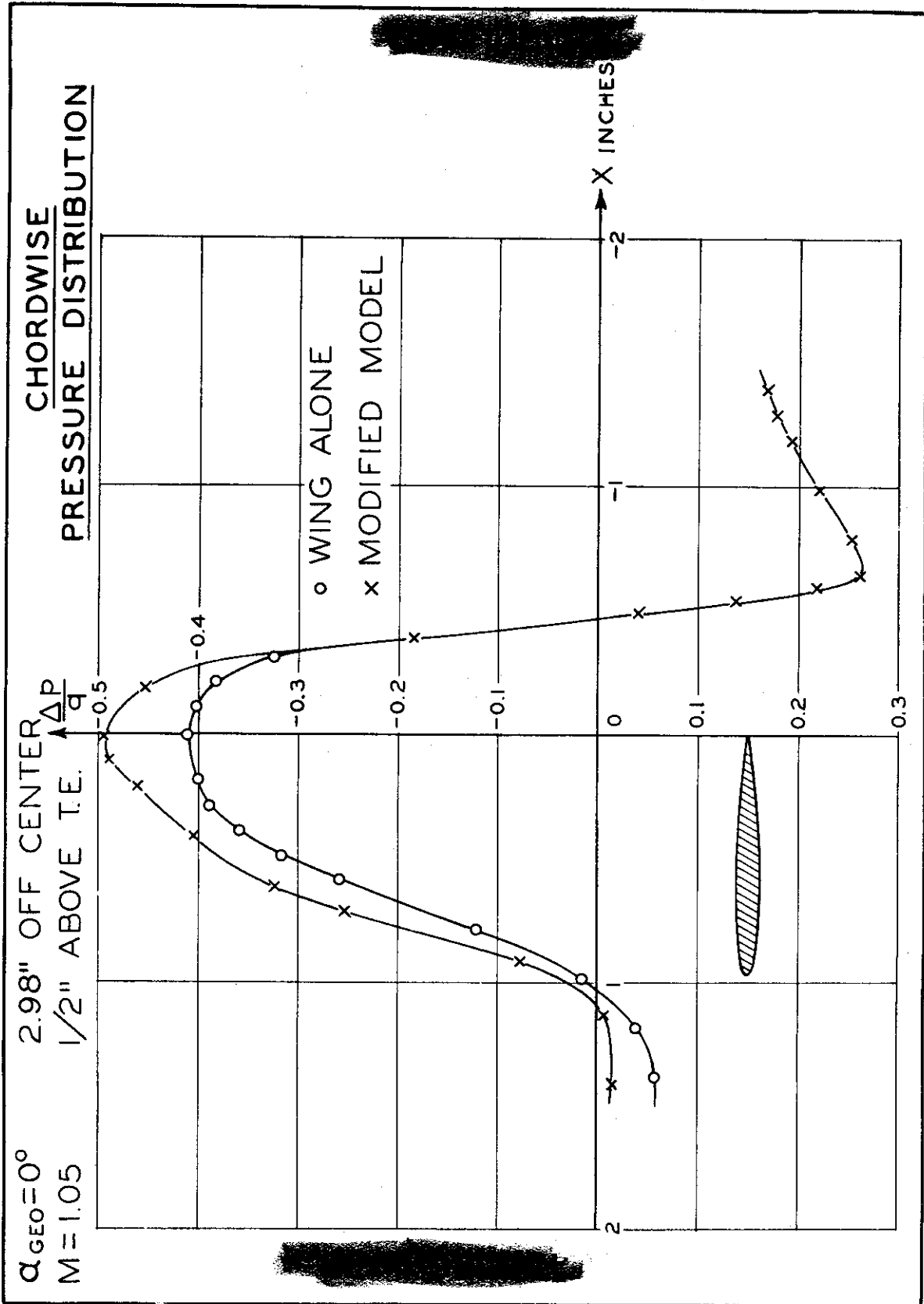


Fig. 41 CHORDWISE PRESSURE DISTRIBUTION M = 1.05, 2.98" OFF CENTER, 1/2" ABOVE T.E. FOR $\alpha_{geo} = 0^\circ$

SPANWISE DISTRIBUTION OF MINIMUM PRESSURE COEFFICIENT

$Re = 185,000$

M

- o = 0.90
- Δ = 0.95
- x = 1.00
- = 1.05

F-86E WING ALONE

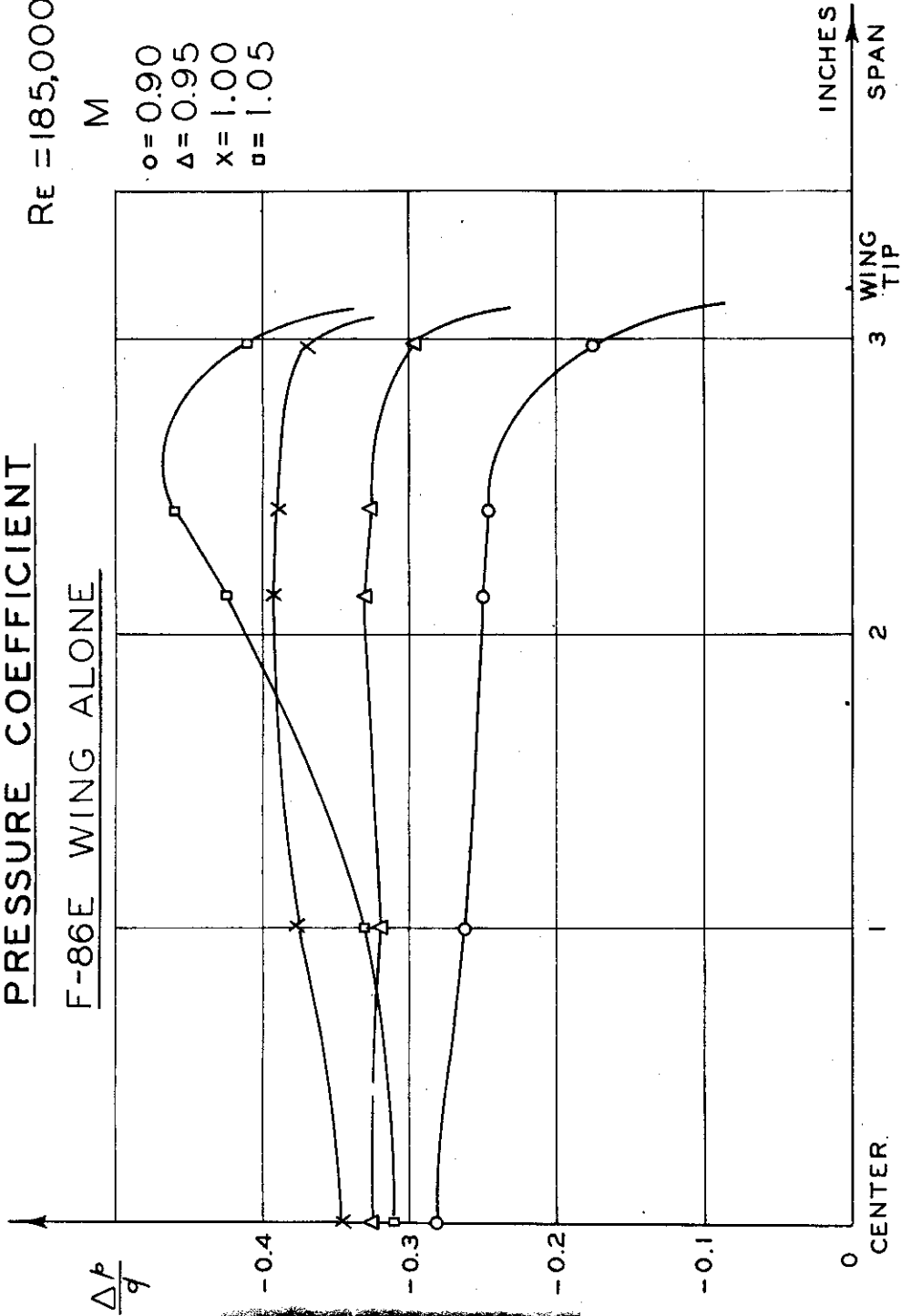


Fig. 42 SPANWISE DISTRIBUTION OF MINIMUM PRESSURE COEFFICIENT FOR ISOLATED F-86E WING

SCHEMATIC DIAGRAM OF FRONTAL AREA DISTRIBUTION OF A SWEEPED WING

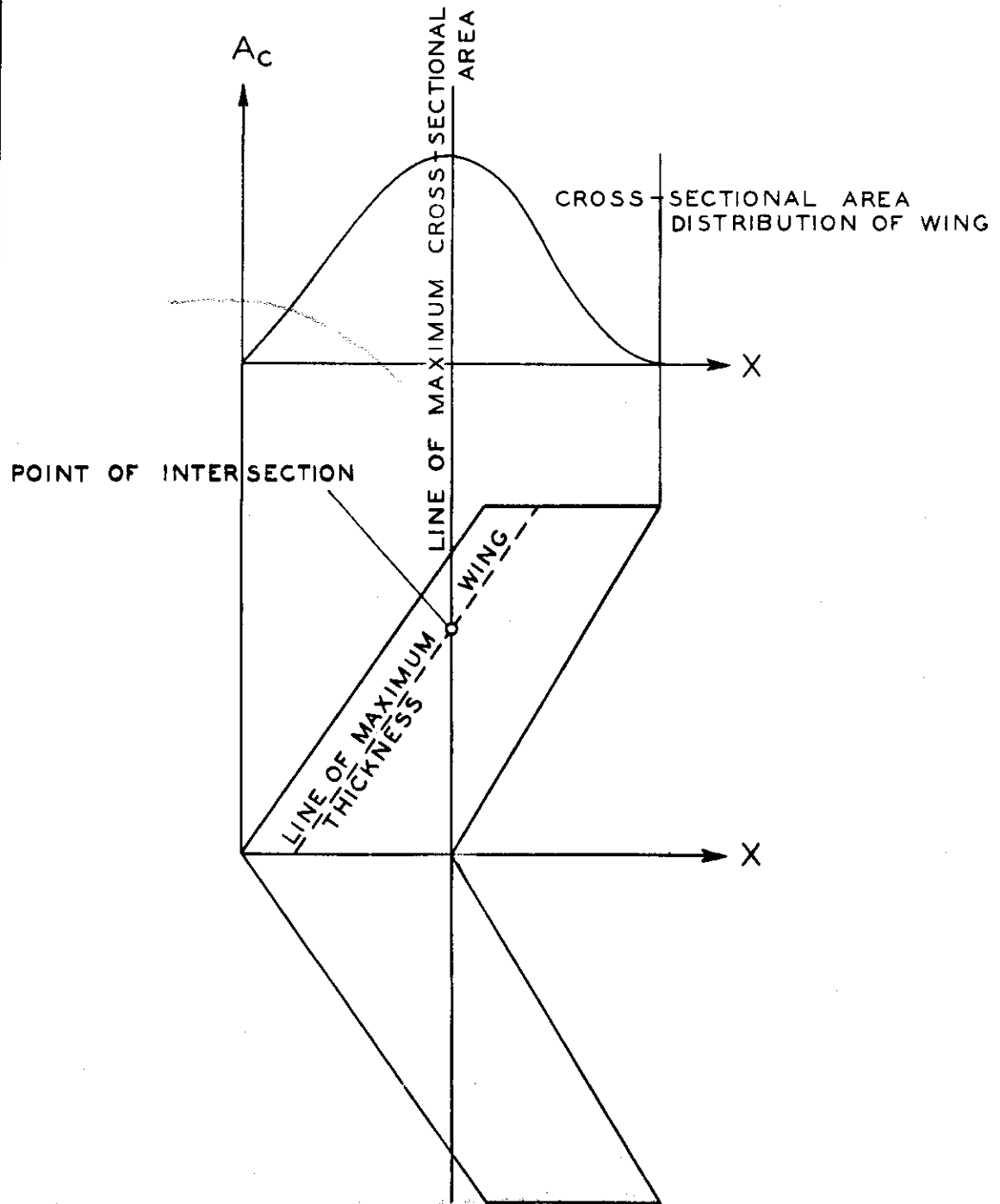


Fig. 43 DIAGRAM OF FRONTAL AREA DISTRIBUTION OF A SWEEPED WING

WADC-TR-55-12

A COMPARISON OF THE SUM OF WING + FUSELAGE DRAG
AND TOTAL MODEL DRAG OF THE F-86E AT $C_L=0^\circ$

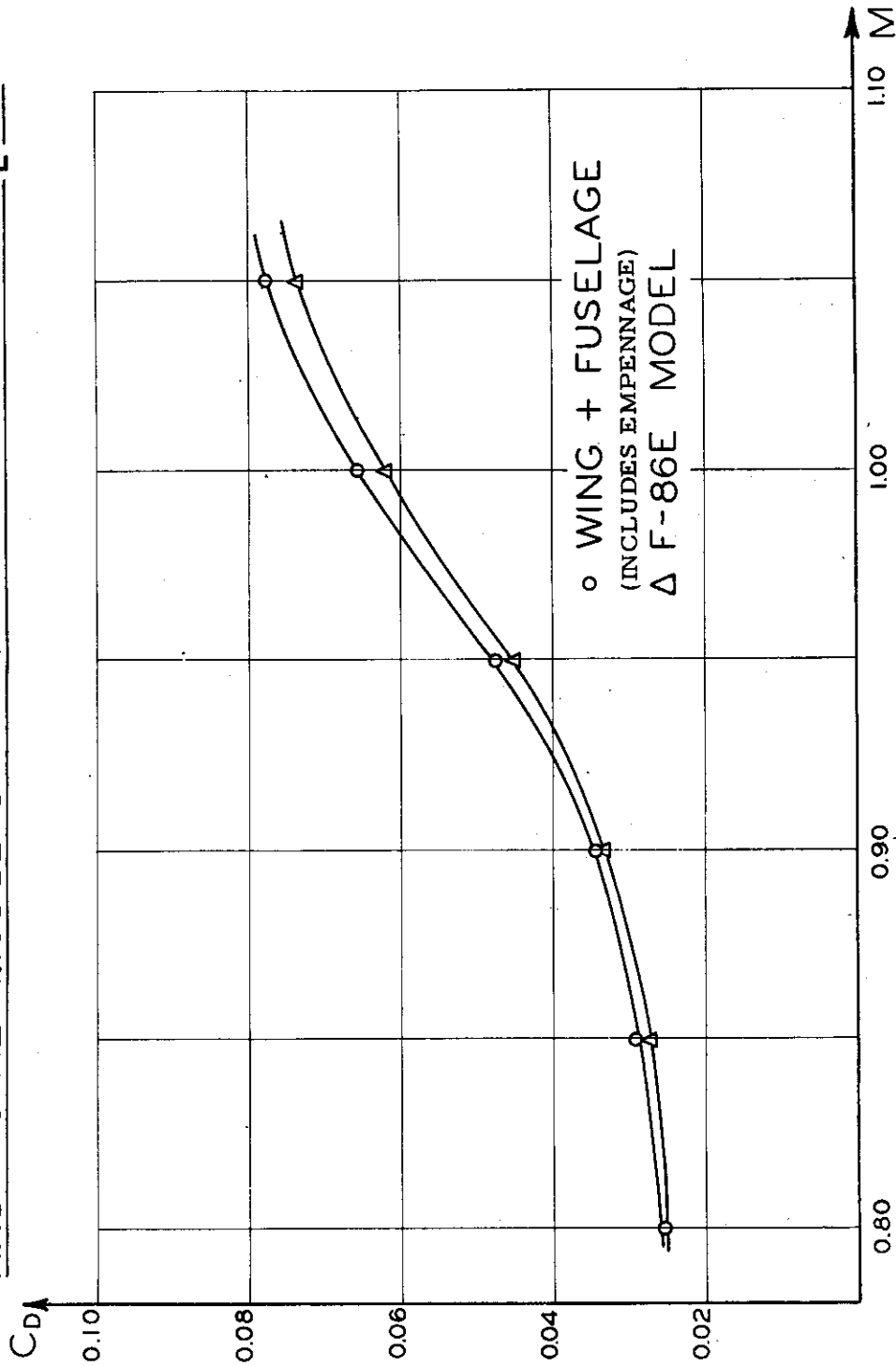
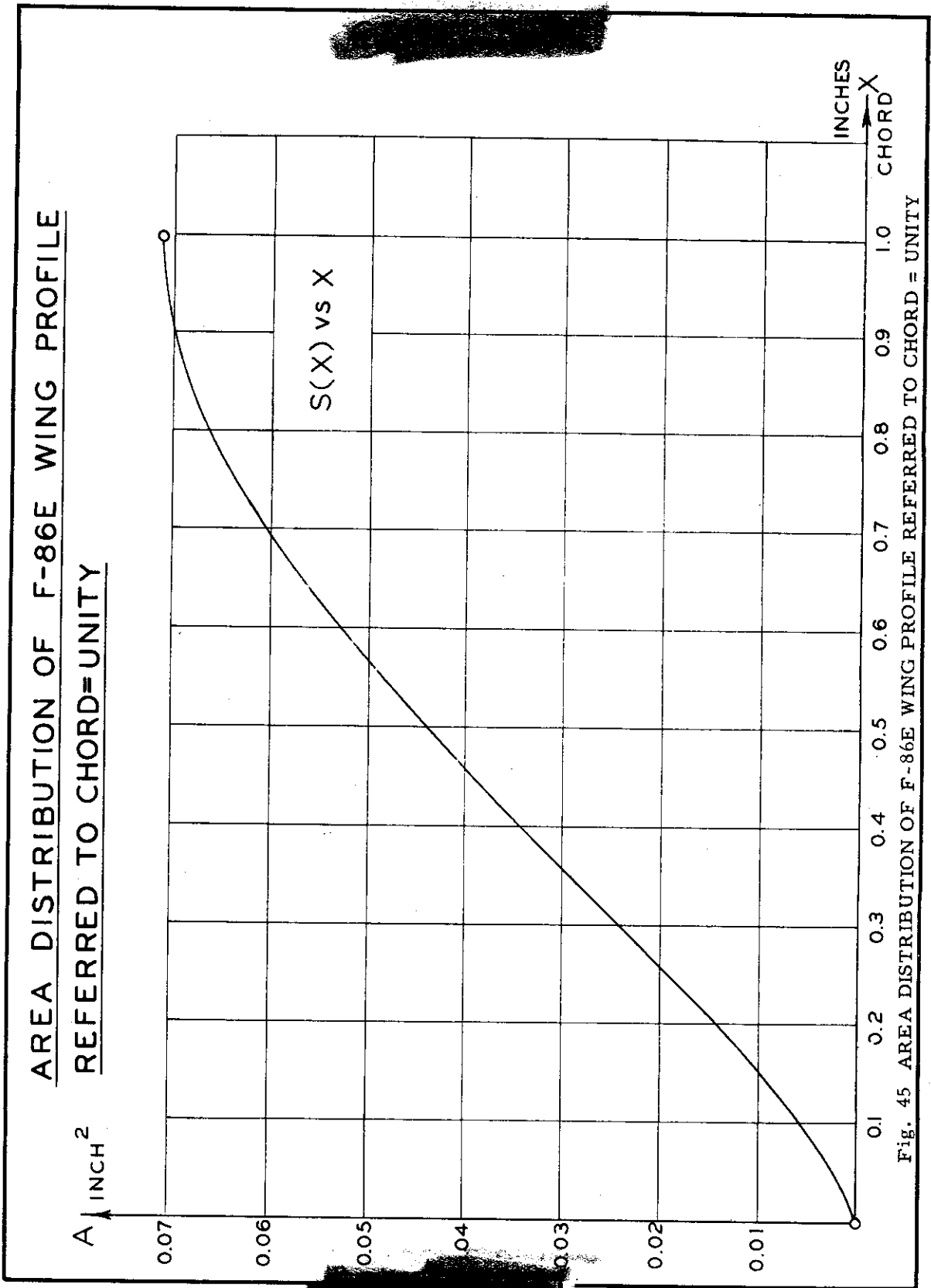


Fig. 44 A COMPARISON OF THE SUM OF WING + FUSELAGE DRAG AND TOTAL MODEL DRAG OF THE F-86E AT $C_L = 0^\circ$



CORRECTION FACTOR FOR AREA INDENTATION

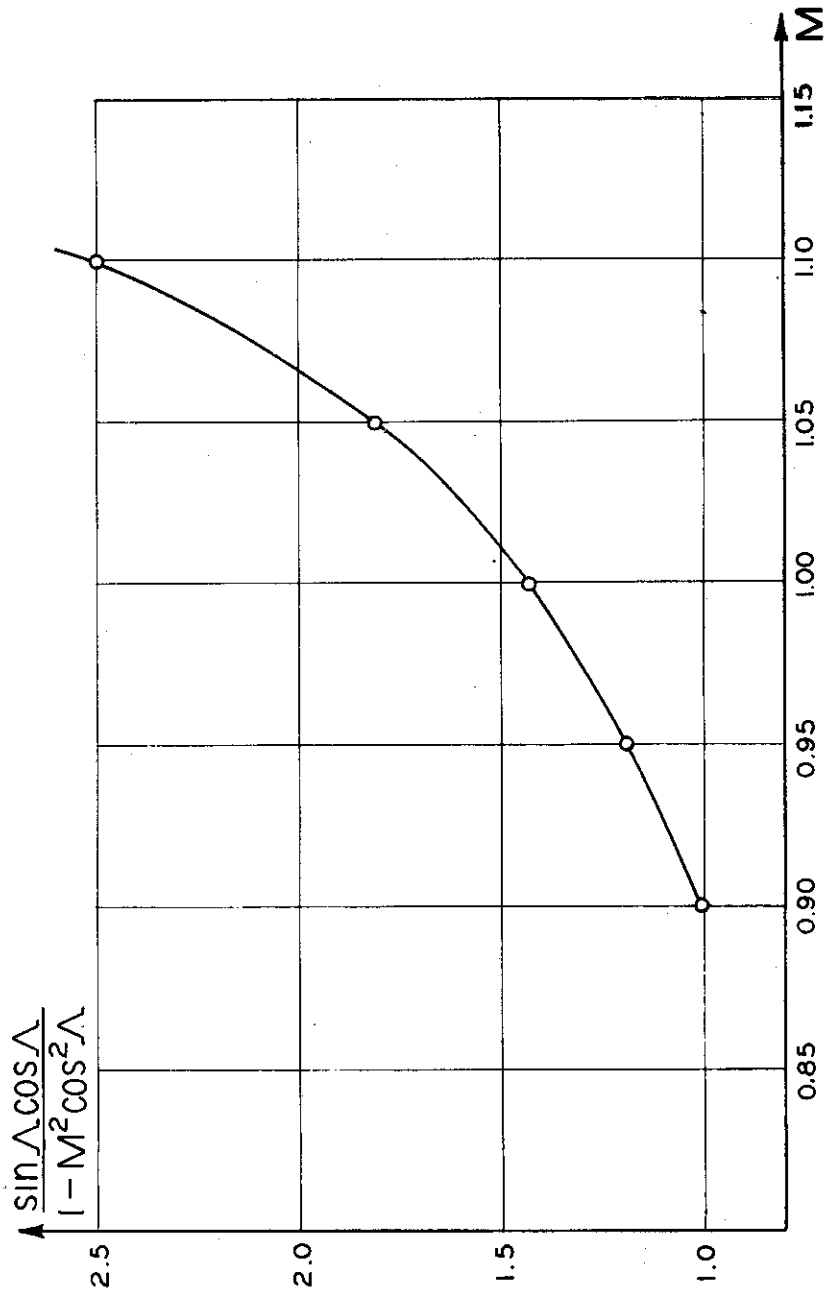


Fig. 46 CORRECTION FACTOR FOR AREA INDENTATION

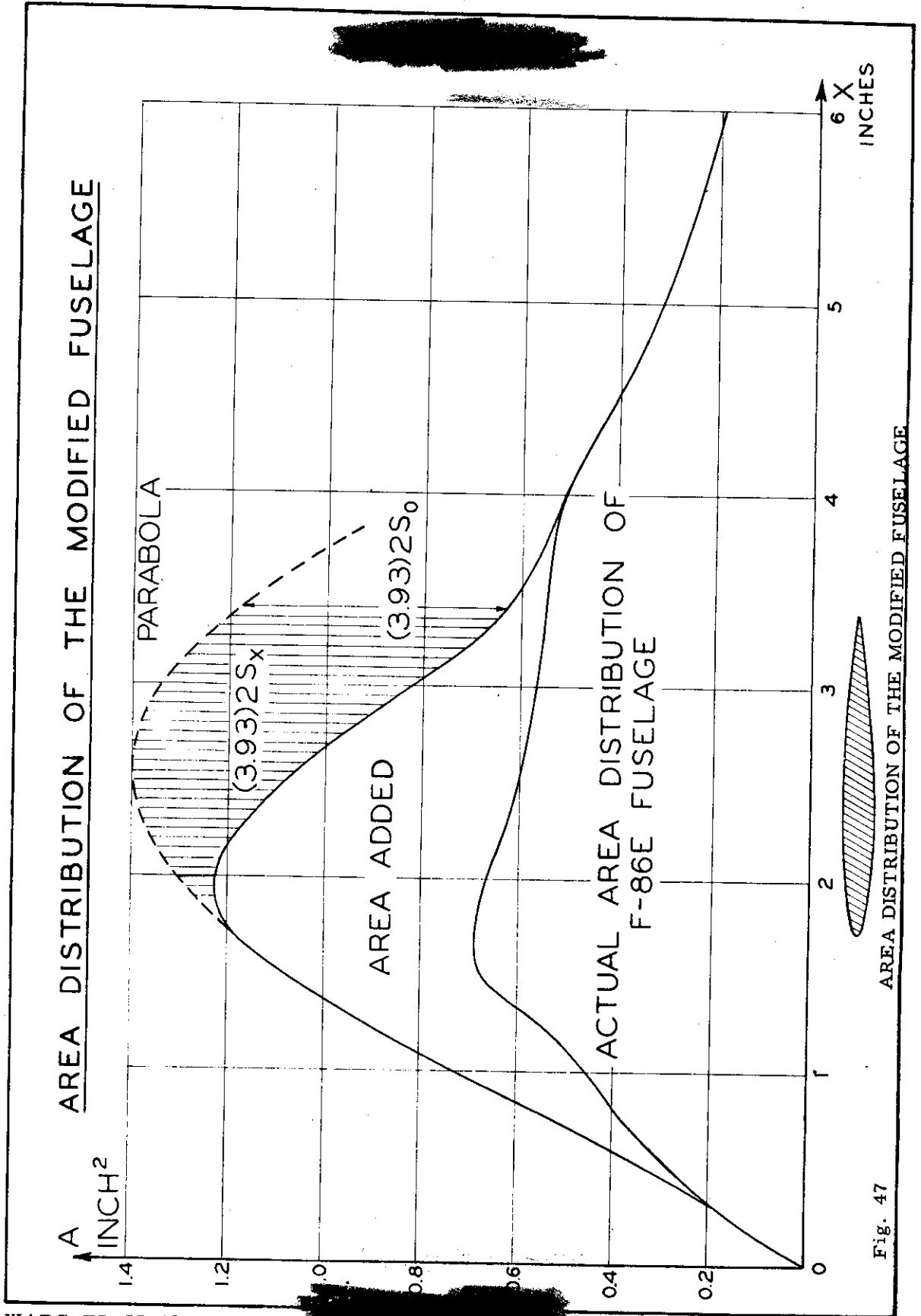
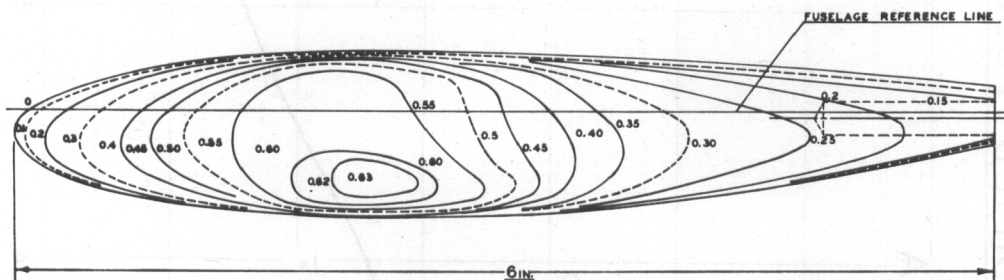


Fig. 47

MODIFIED F-86E MODEL

MODIFIED FUSELAGE
LINES OF CONSTANT WIDTH



SCALE: FULL SIZE

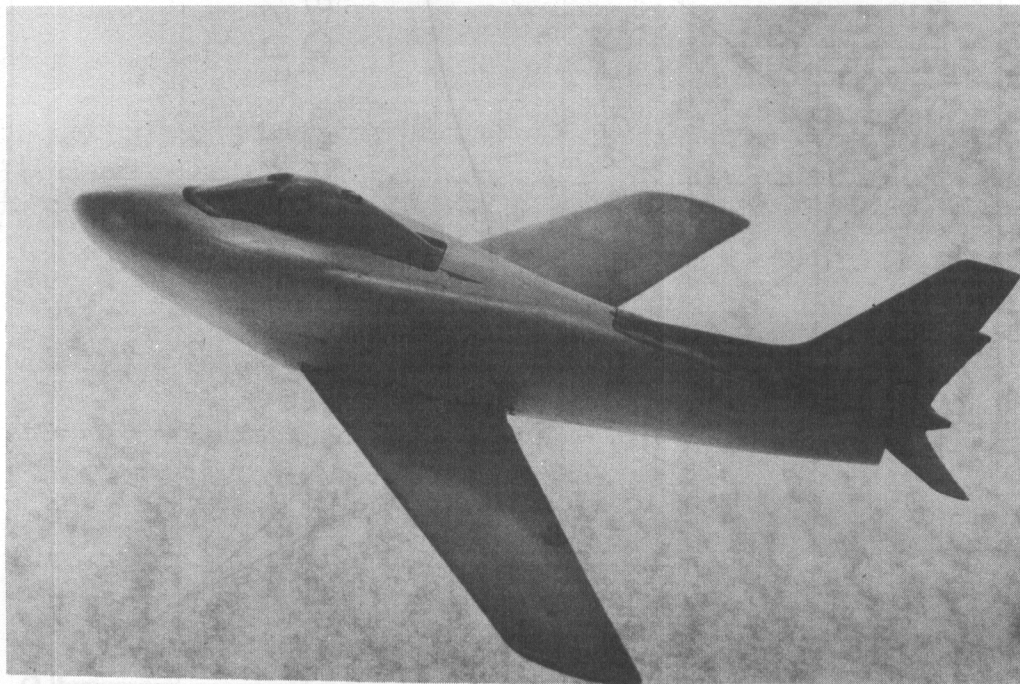


Fig. 48

MODIFIED F-86E MODEL

WADC-TR-55-12

ORIGINAL F-86E MODEL

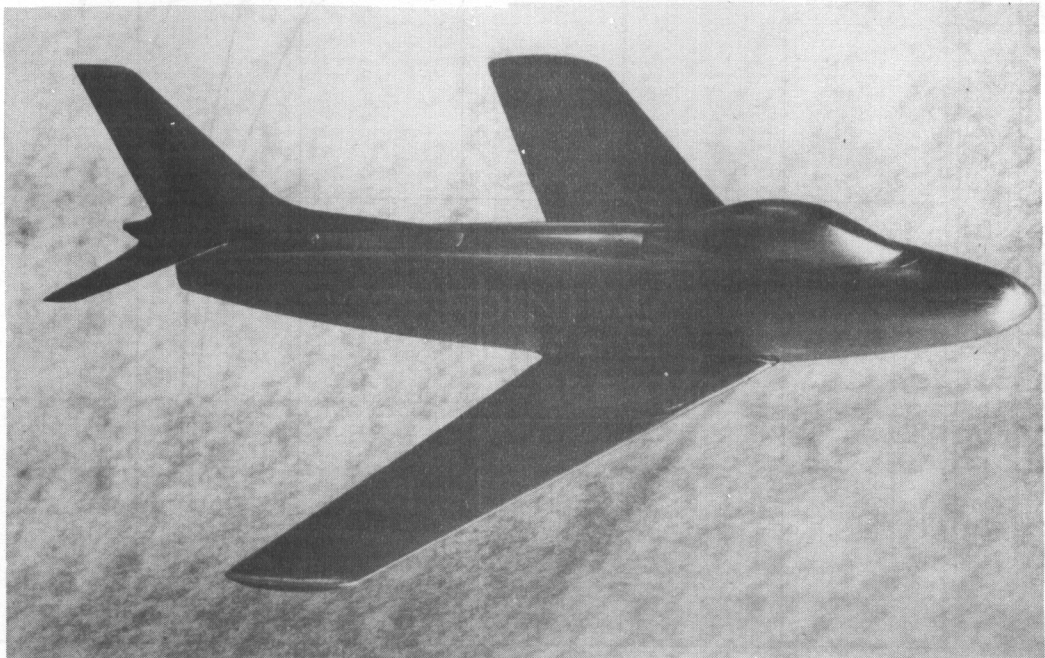
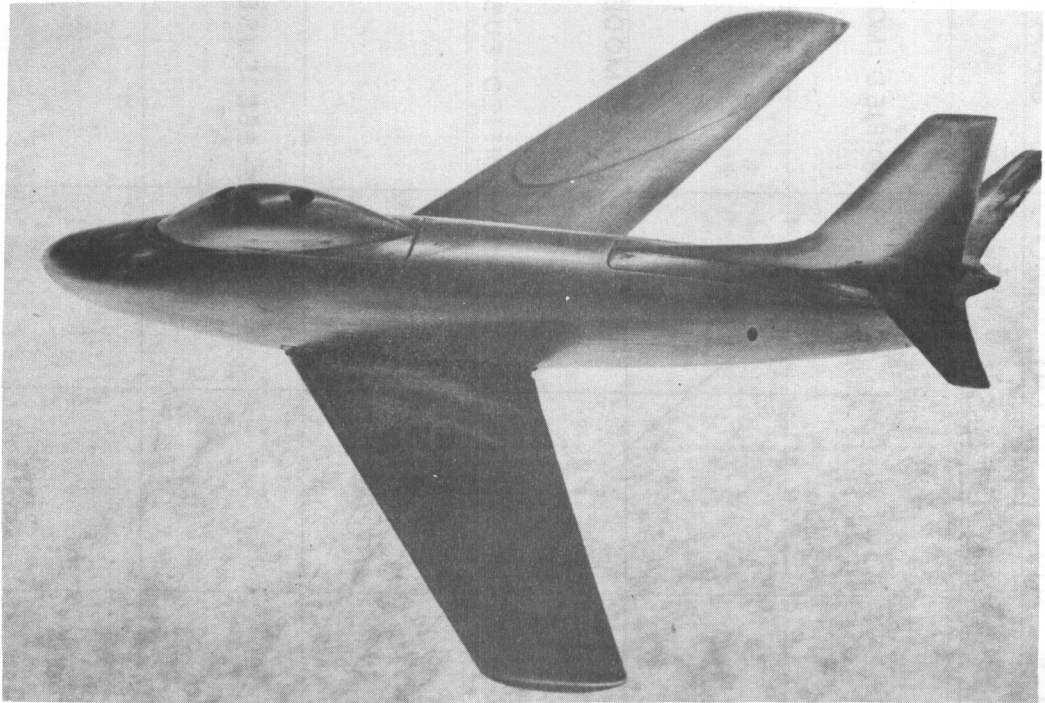


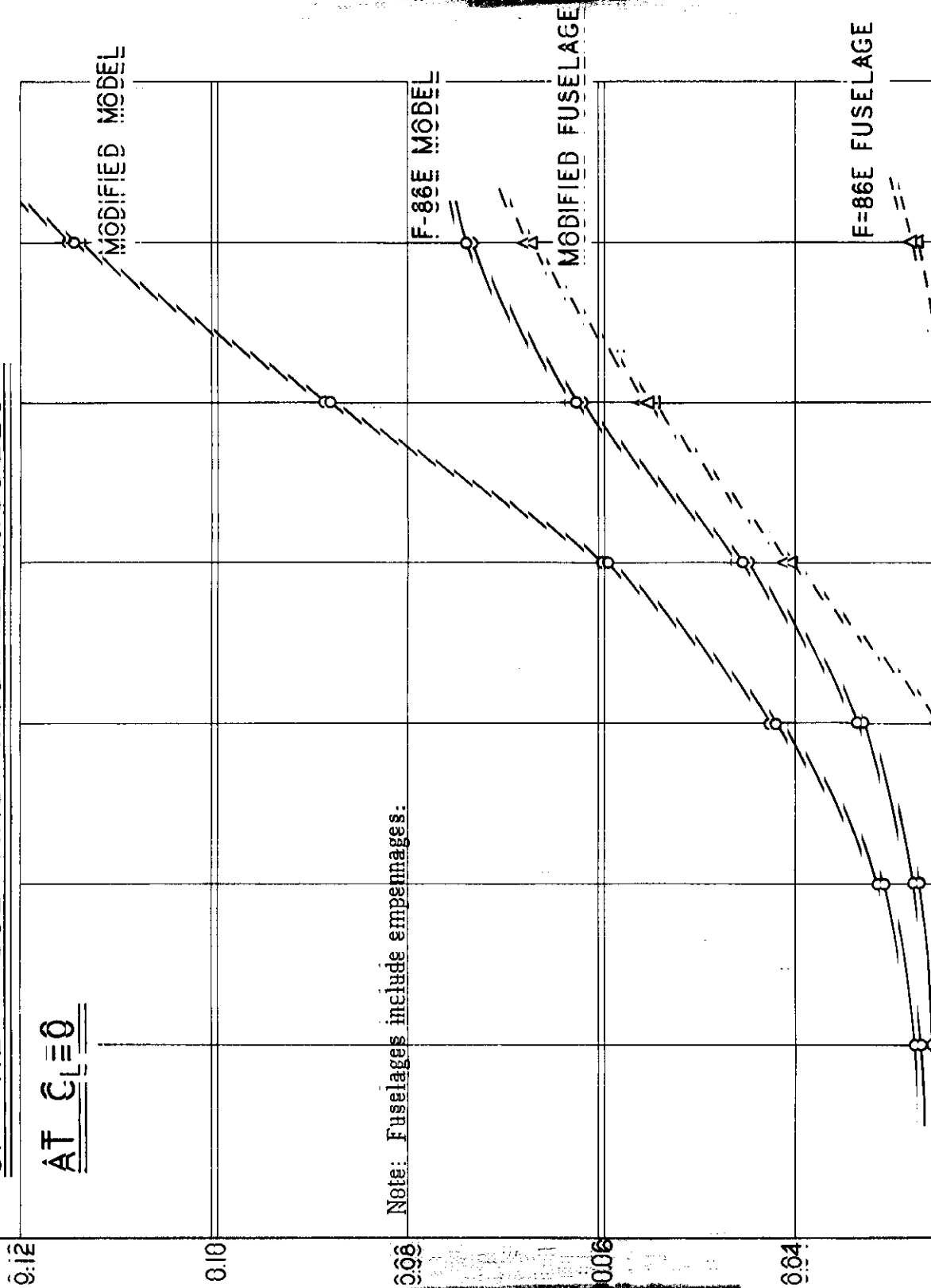
Fig. 49

ORIGINAL F-86E MODEL

WADC-TR-55-12

A COMPARISON OF FUSELAGE AND TOTAL MODEL DRAGS
OF THE F-86E AND MODIFIED MODELS
AT $C_L=0$

C_D



Note: Fuselages include empennages.

A COMPARISON OF THE SUM OF WING + FUSELAGE DRAG AND TOTAL MODEL DRAG OF THE MODIFIED MODEL AT $C_L=0$

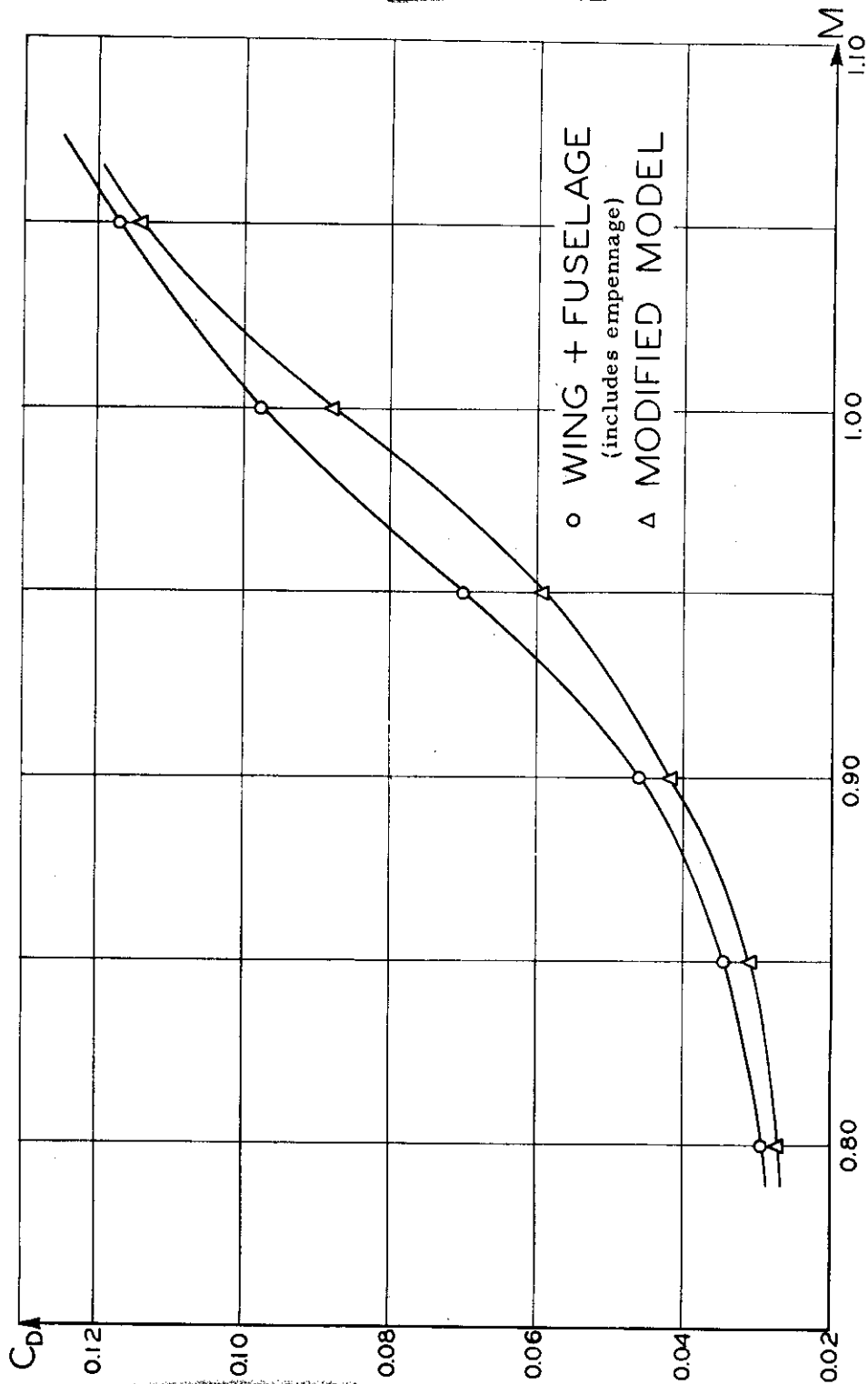


Fig. 51 A COMPARISON OF THE SUM OF WING + FUSELAGE DRAG AND TOTAL MODEL DRAG OF THE MODIFIED MODEL AT $C_L = 0$

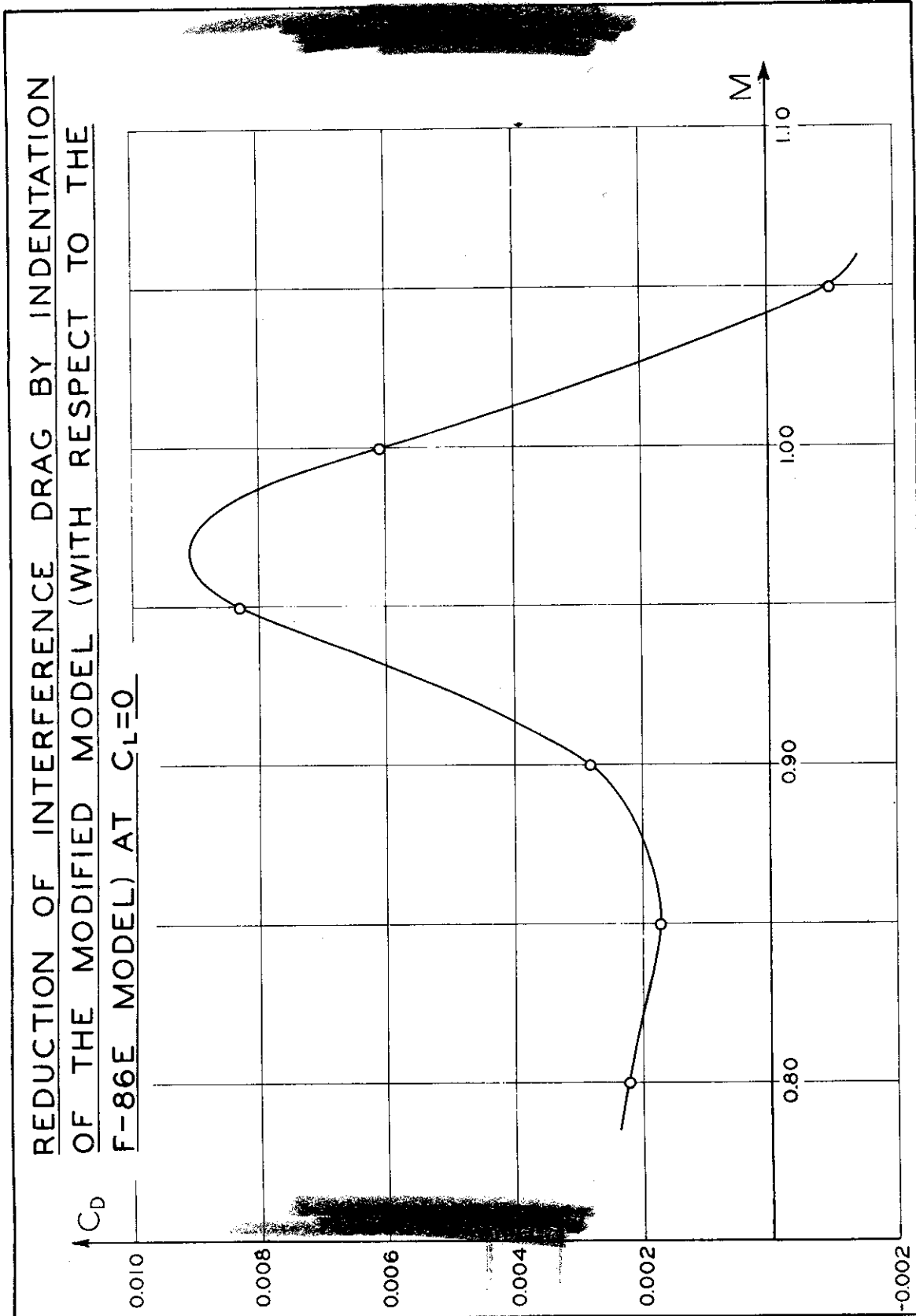


Fig. 52 REDUCTION OF INTERFERENCE DRAG BY INDENTATION OF THE MODIFIED MODEL (WITH RESPECT TO THE F-86E MODEL) AT $C_L = 0$

SCHLIEREN PHOTOGRAPHS OF THE THREE MODELS

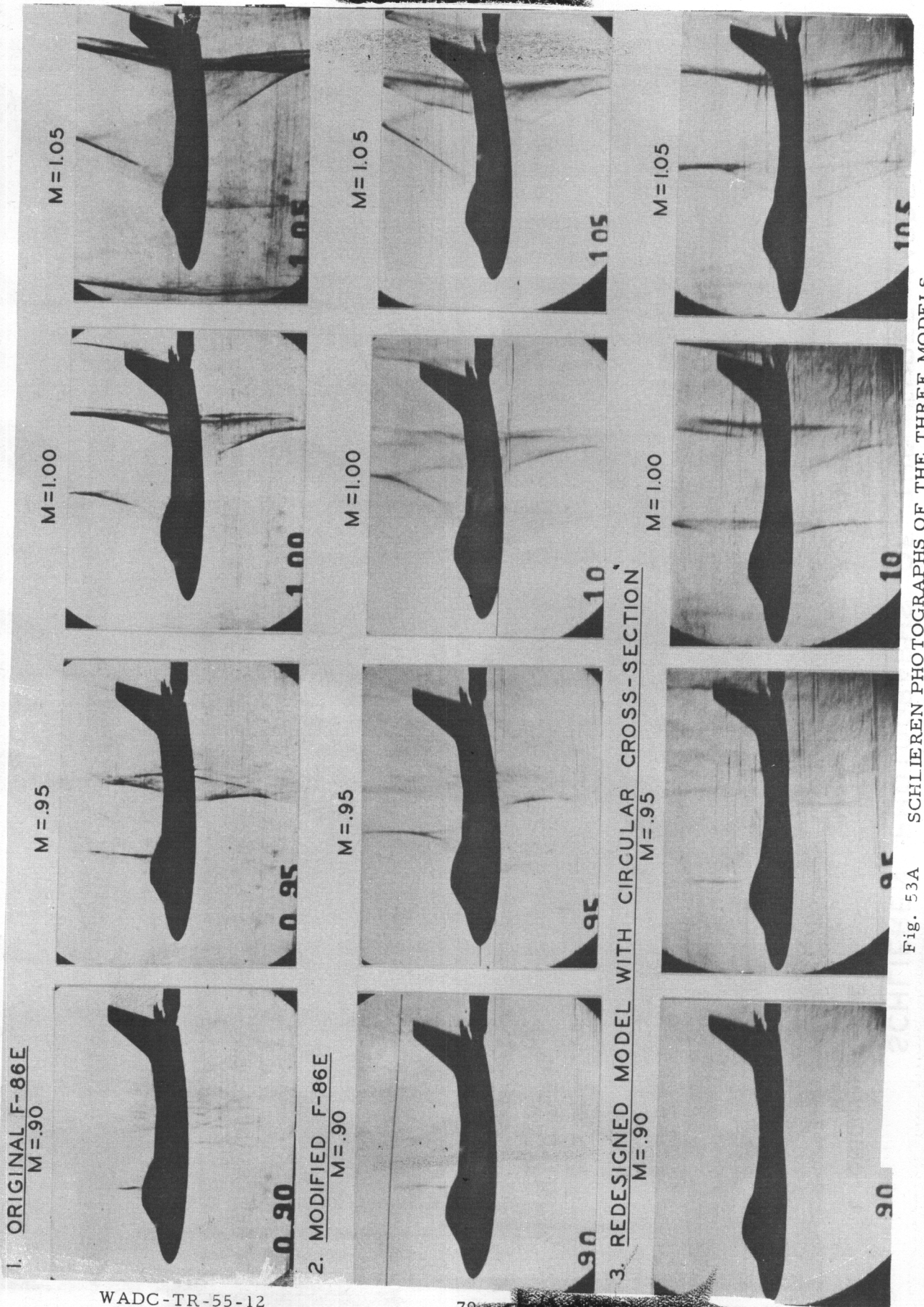


Fig. 53A SCHLIEREN PHOTOGRAPHS OF THE THREE MODELS

SCHLIEREN PHOTOGRAPHS OF THE THREE MODELS

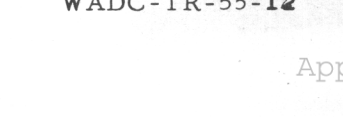
1. ORIGINAL F-86E
M = .90



90

M = .90

1.05



100

M = 1.00

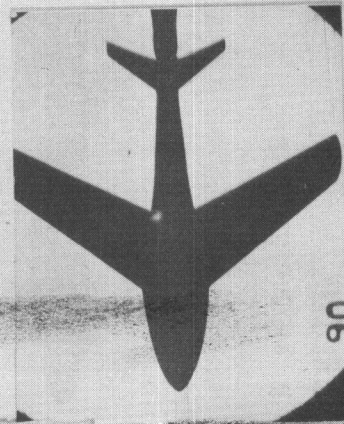
1.05

105

M = 1.05

1.05

2. MODIFIED F-86E
M = .90



90

M = .90

1.05



100

M = 1.00

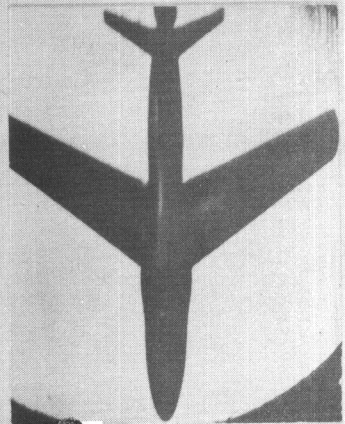
1.05

105

M = 1.05

1.05

3. REDESIGNED MODEL WITH CIRCULAR CROSS-SECTION
M = .95



95

M = .95

1.05



100

M = 1.00

1.05

105

M = 1.05

1.05

Fig. 53B SCHLIEREN PHOTOGRAPHS OF THE THREE MODELS

PITCHING MOMENT FOR MODIFIED MODEL

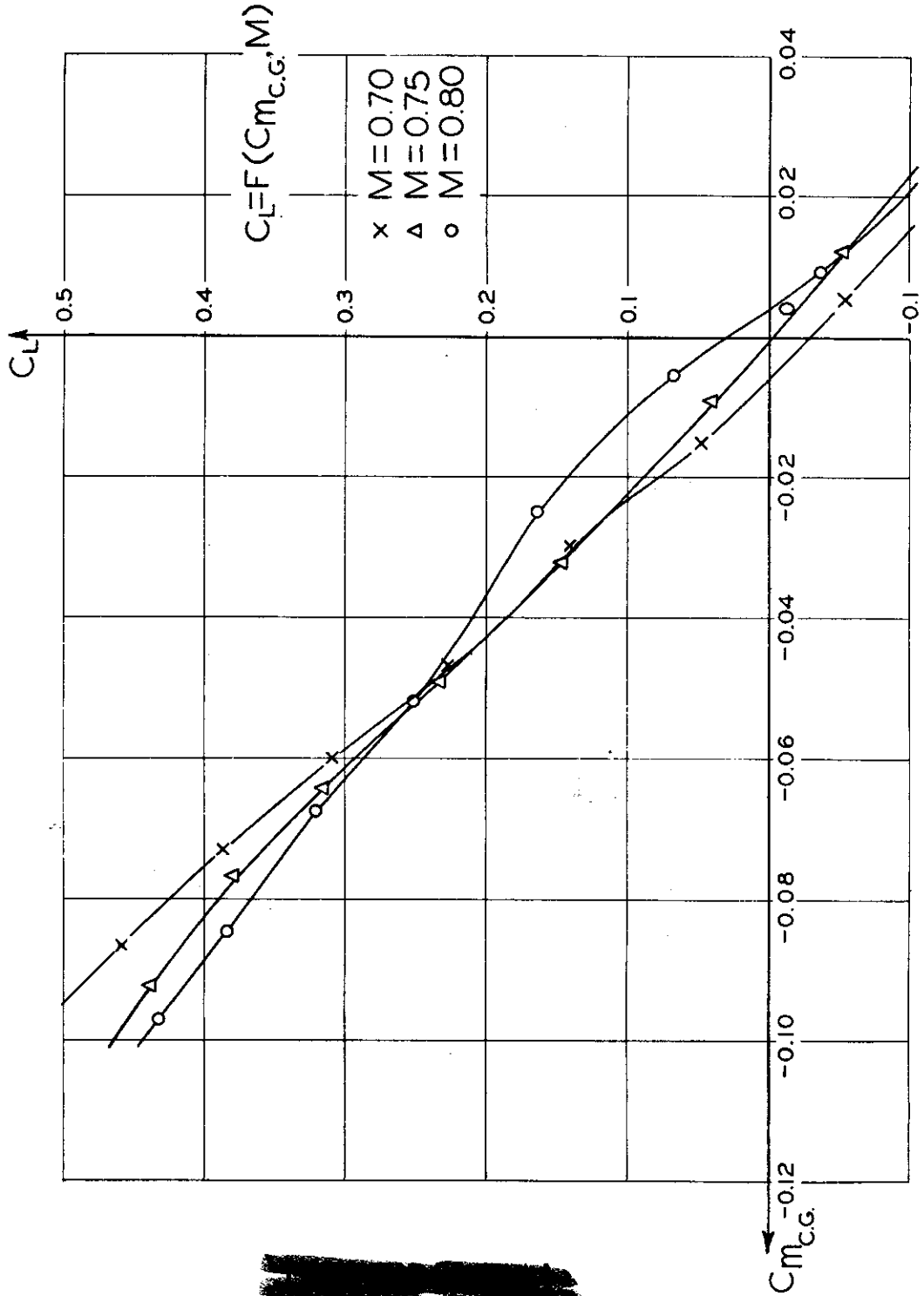


Fig. 54 PITCHING MOMENT VERSUS LIFT COEFFICIENT FOR MODIFIED MODEL

PITCHING MOMENT FOR MODIFIED MODEL

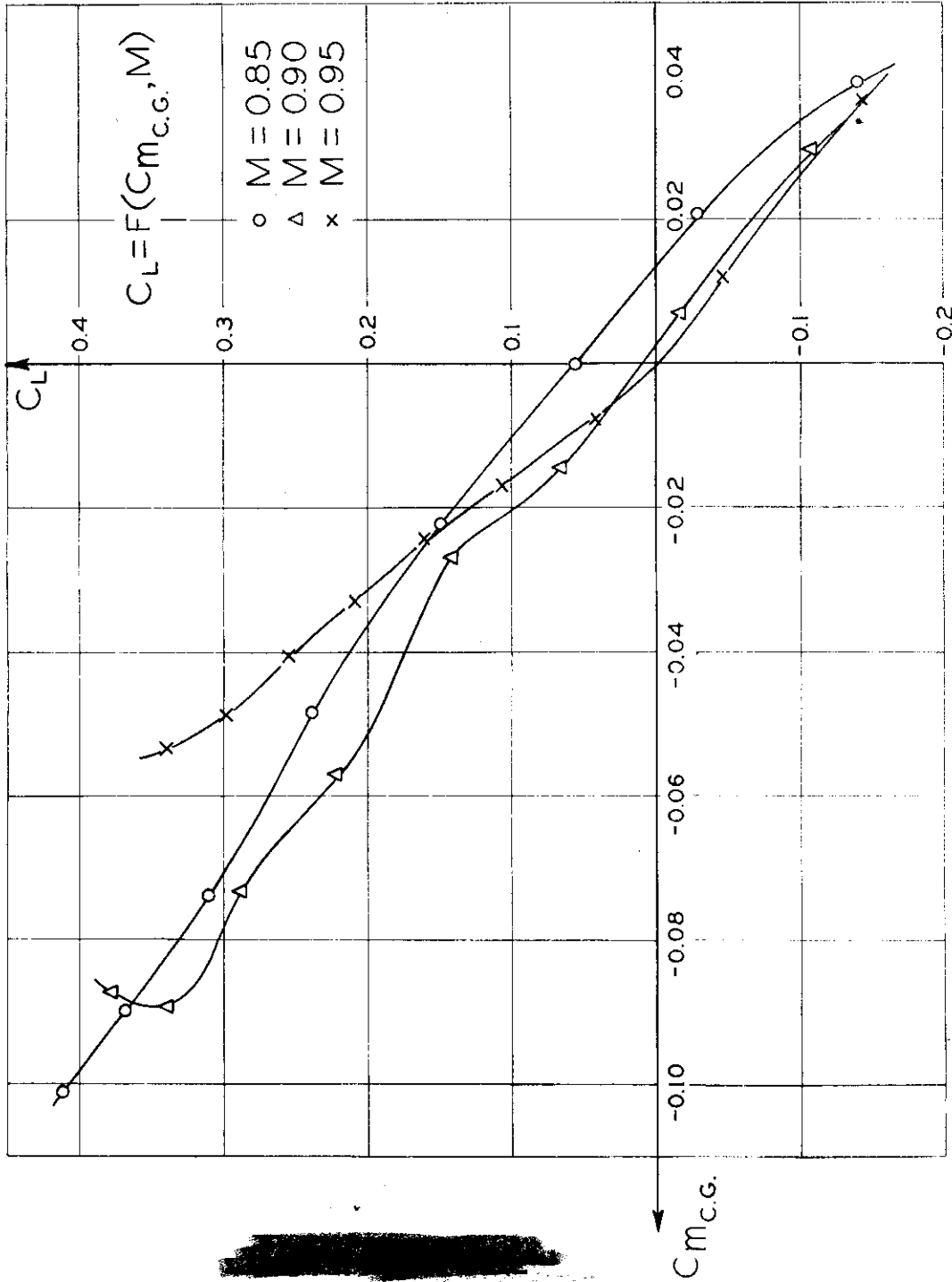


Fig. 55 PITCHING MOMENT VERSUS LIFT COEFFICIENT FOR MODIFIED MODEL

PITCHING MOMENT FOR MODIFIED MODEL

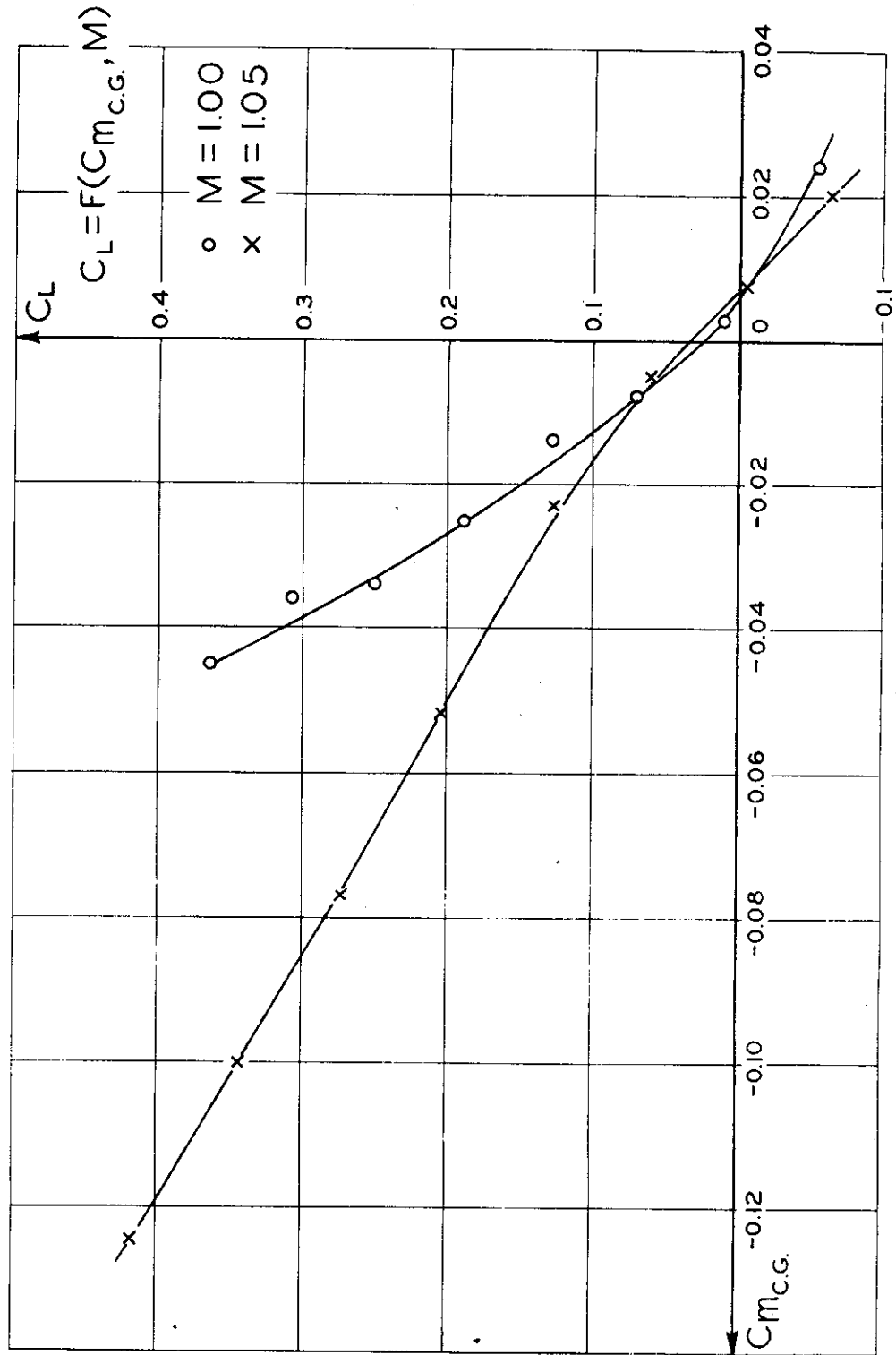


Fig. 56 PITCHING MOMENT VERSUS LIFT COEFFICIENT FOR MODIFIED MODEL

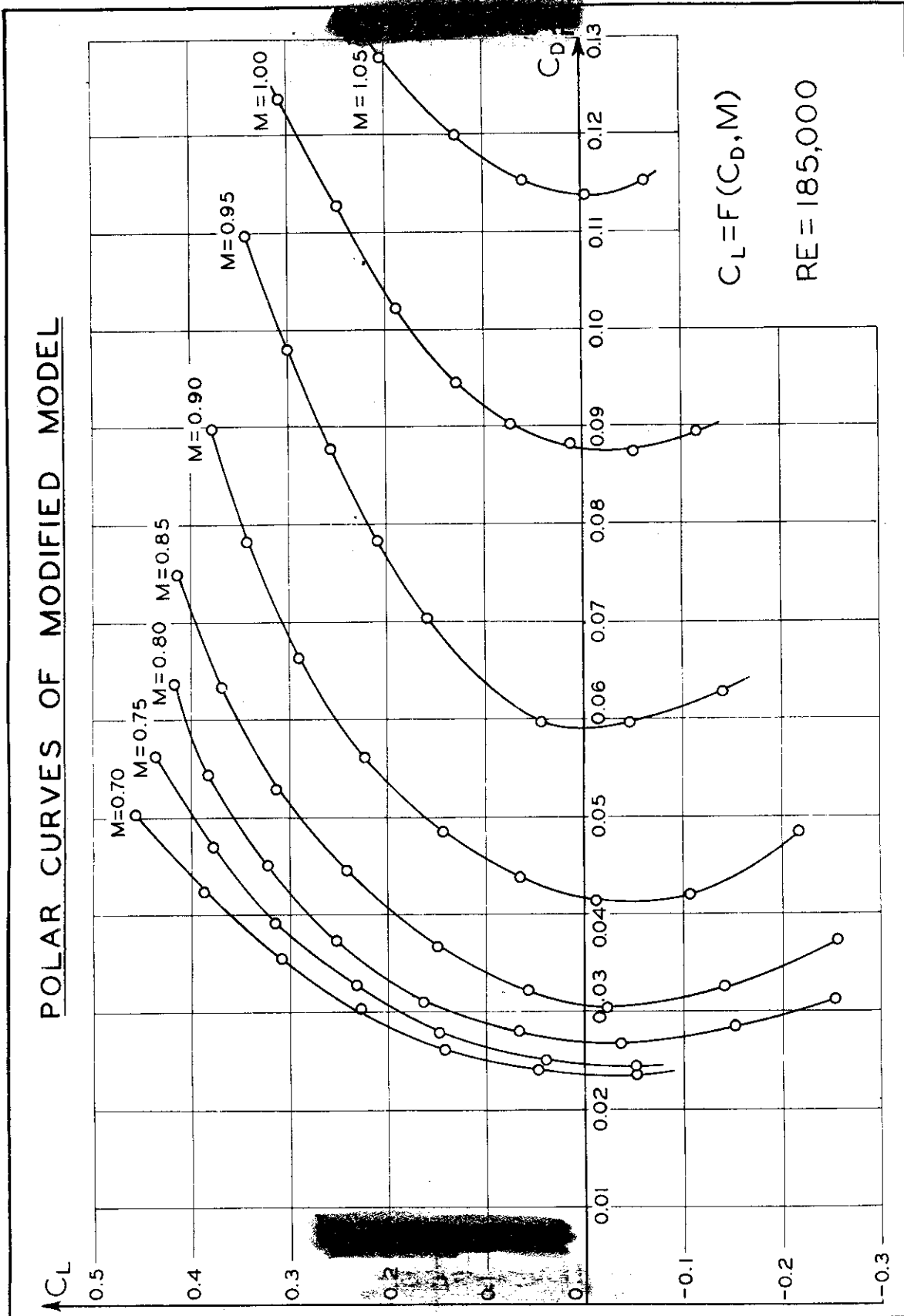


Fig. 57 POLAR CURVES OF MODIFIED MODEL

LIFT COEFFICIENT AS A FUNCTION OF α_{GEO} AND M
FOR THE MODIFIED MODEL

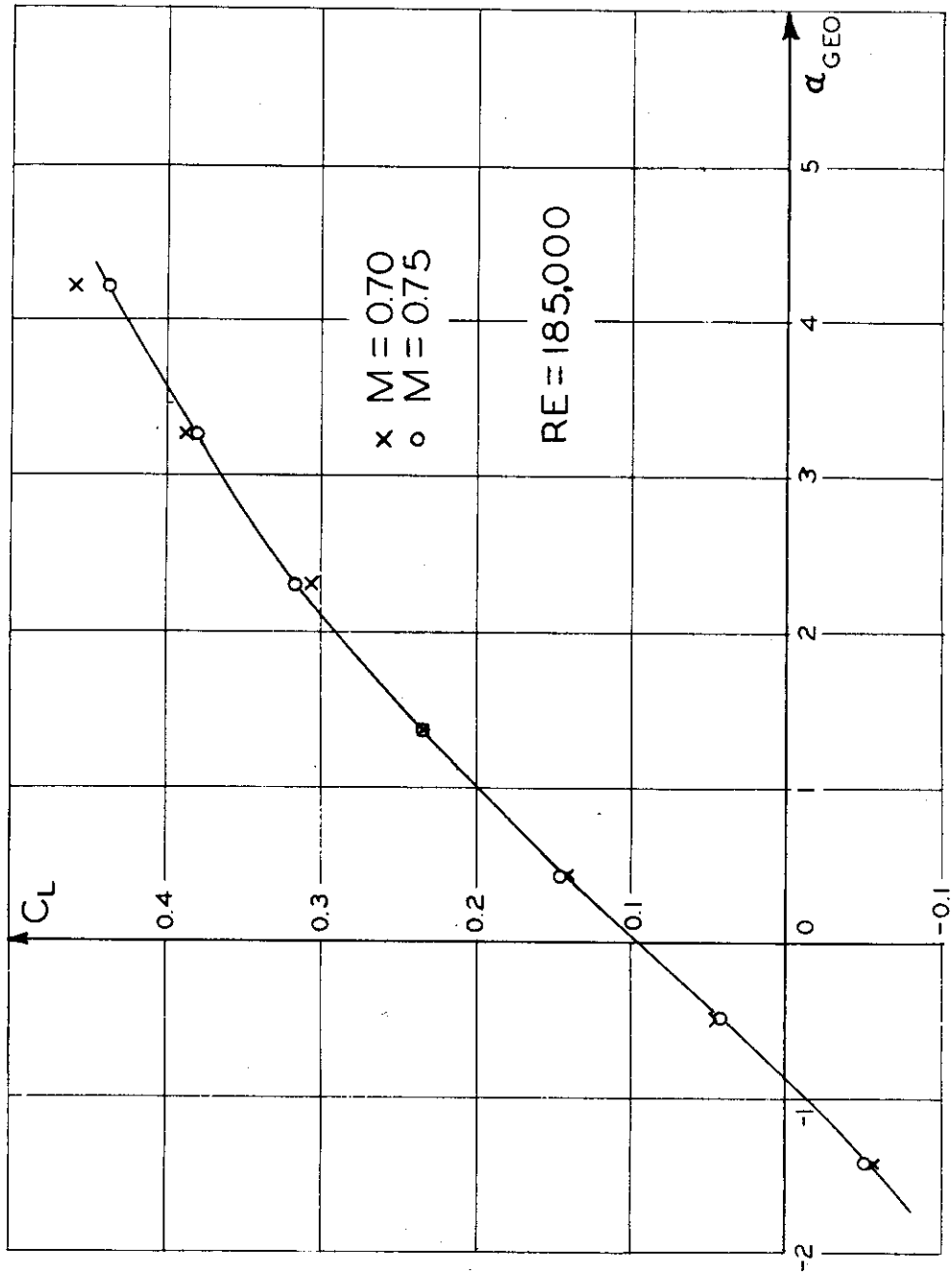


Fig. 58 LIFT COEFFICIENT AS A FUNCTION OF α_{geo} AND M FOR THE MODIFIED MODEL

LIFT COEFFICIENT AS A FUNCTION OF α_{GEO} AND M
FOR THE MODIFIED MODEL

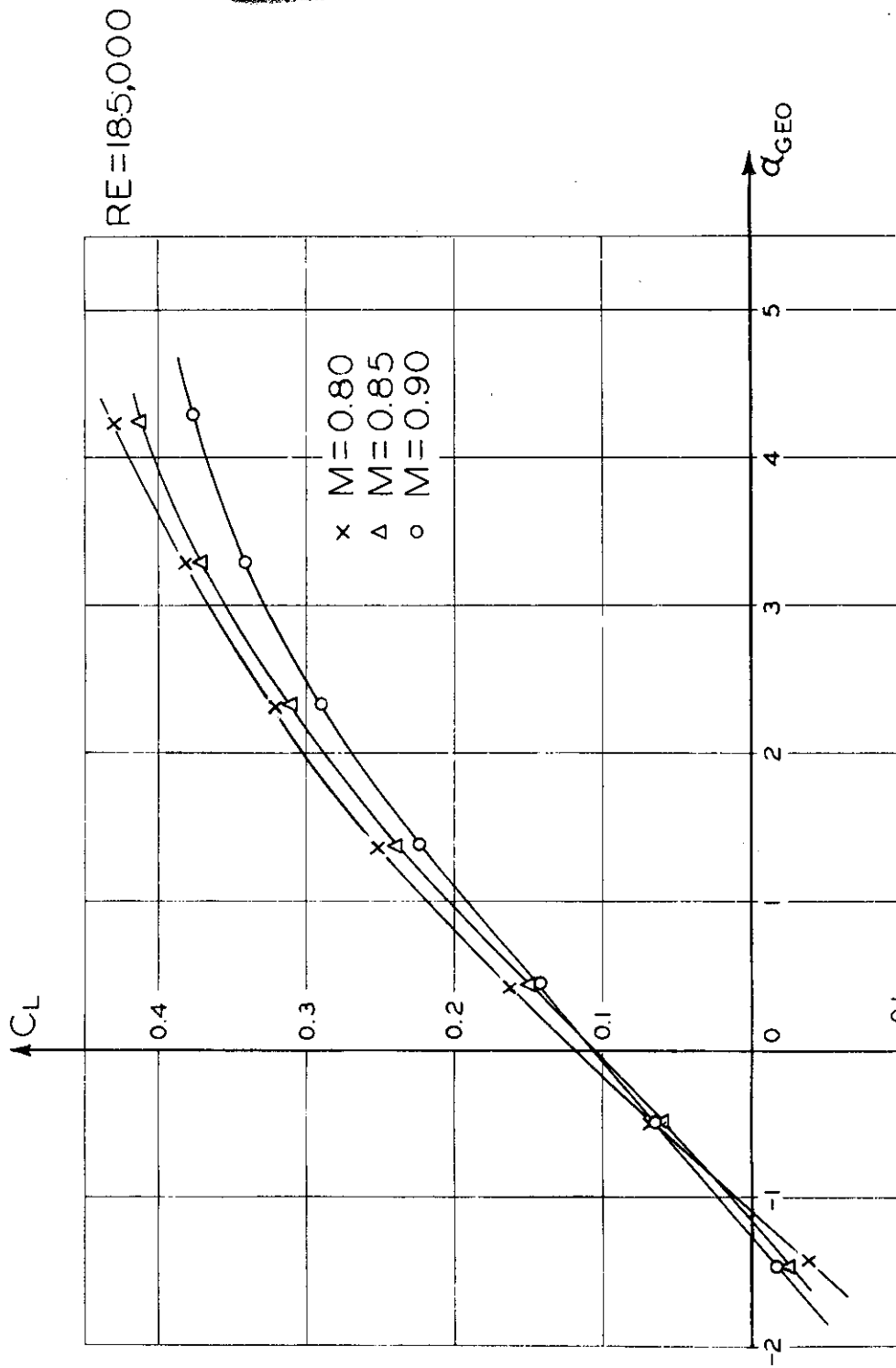


Fig. 59 LIFT COEFFICIENT AS A FUNCTION OF α_{GEO} AND M FOR THE MODIFIED MODEL

LIFT COEFFICIENT AS A FUNCTION OF α_{GEO} AND M
FOR THE MODIFIED MODEL

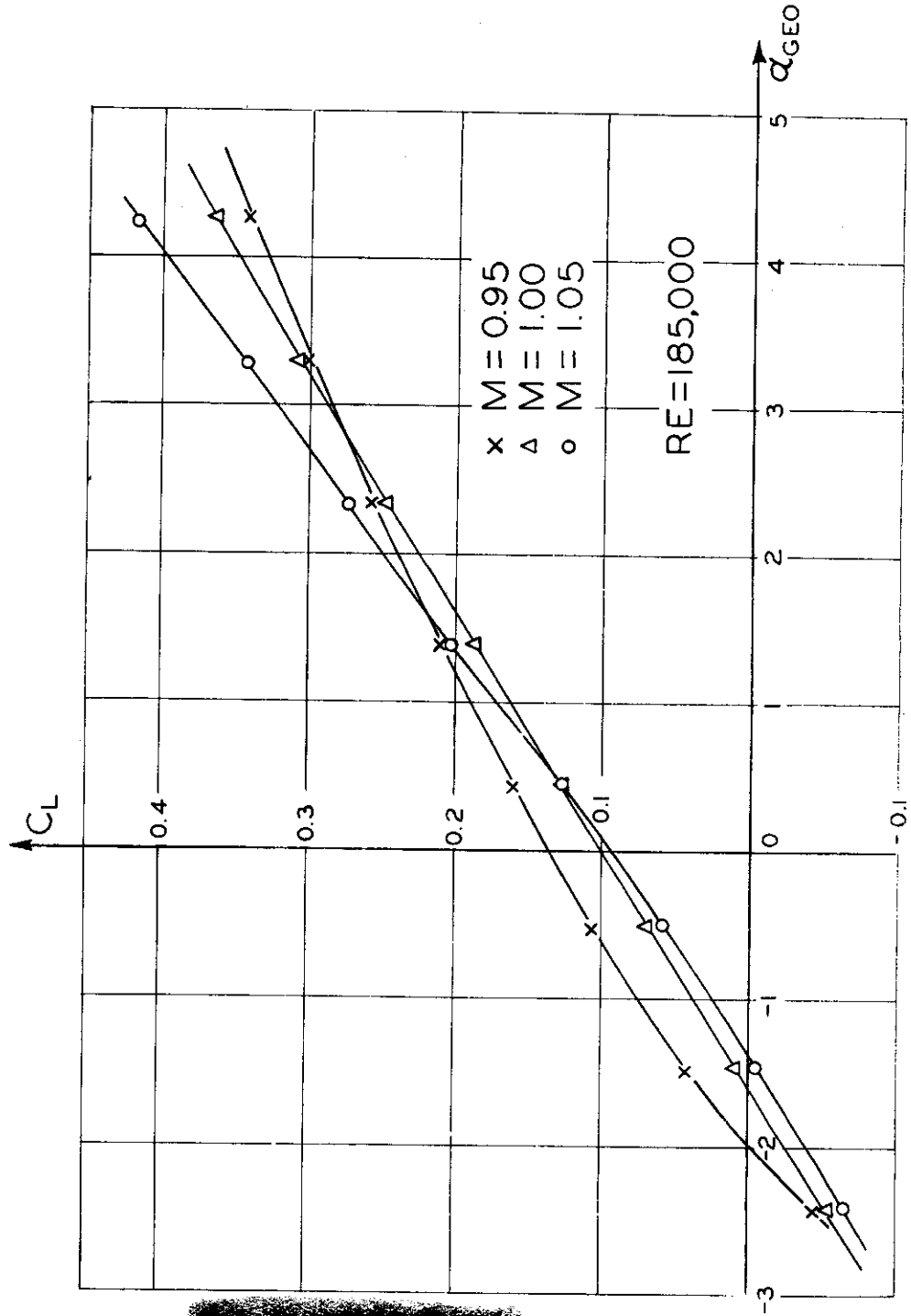


Fig. 60 LIFT COEFFICIENT AS A FUNCTION OF α_{geo} AND M FOR THE MODIFIED MODEL

AREA DISTRIBUTION OF ORIGINAL AND REDESIGNED FUSELAGES

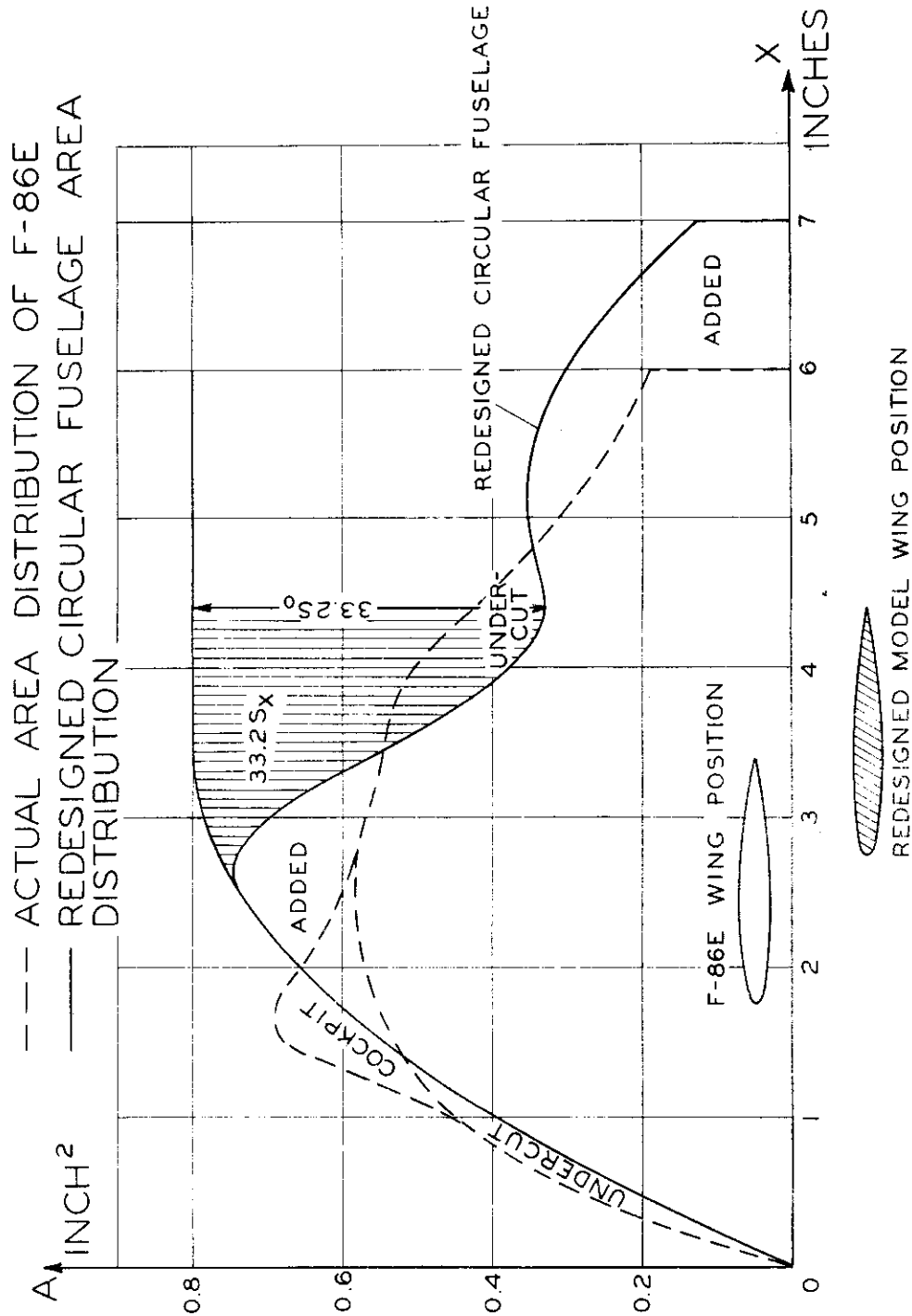


Fig. 61 AREA DISTRIBUTION OF ORIGINAL AND REDESIGNED FUSELAGES

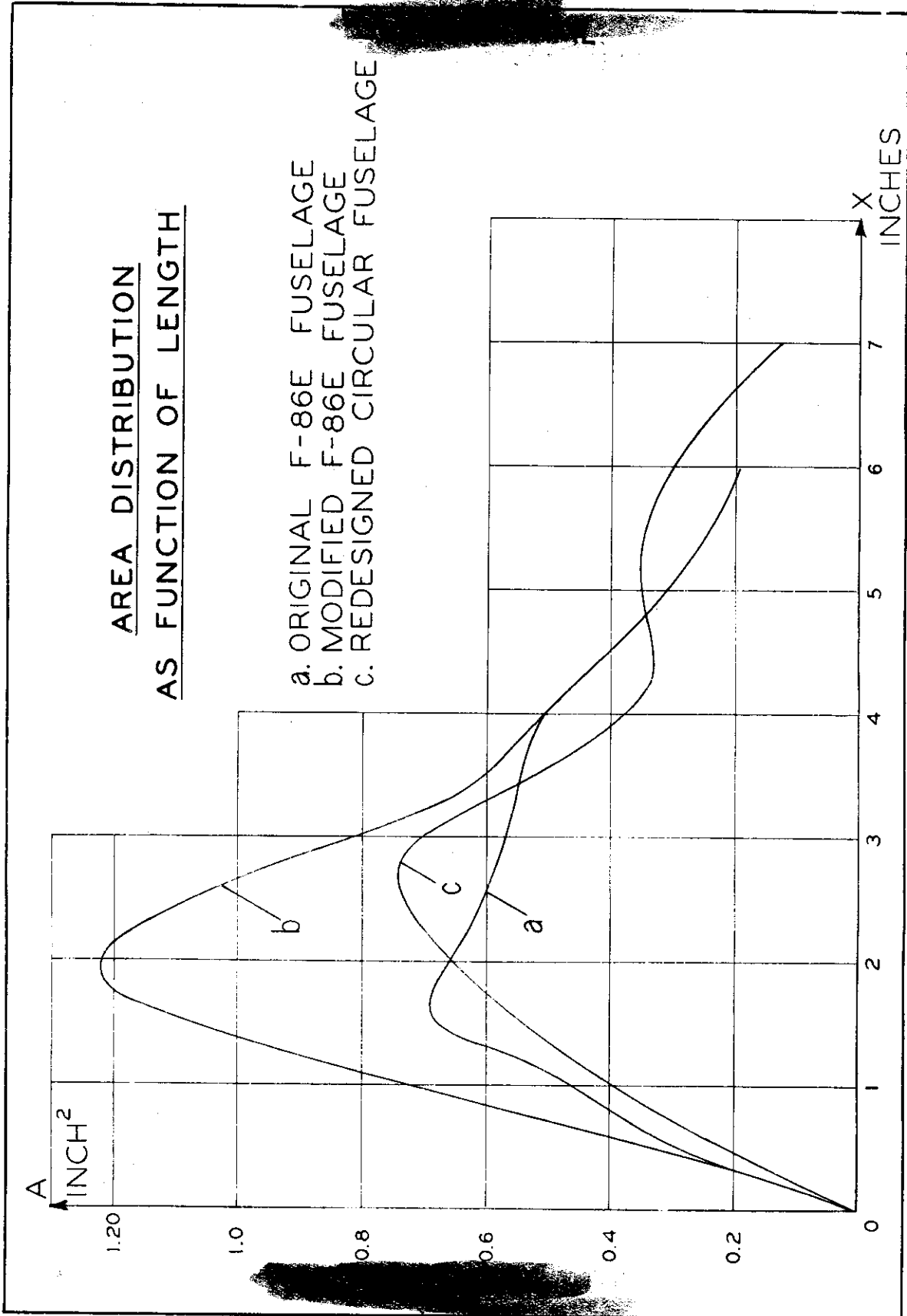


Fig. 62 AREA DISTRIBUTION AS FUNCTION OF LENGTH FOR THE THREE FUSELAGES

DRAG COEFFICIENTS OF THE REDESIGNED AND F-86E FUSELAGES AS A FUNCTION OF M

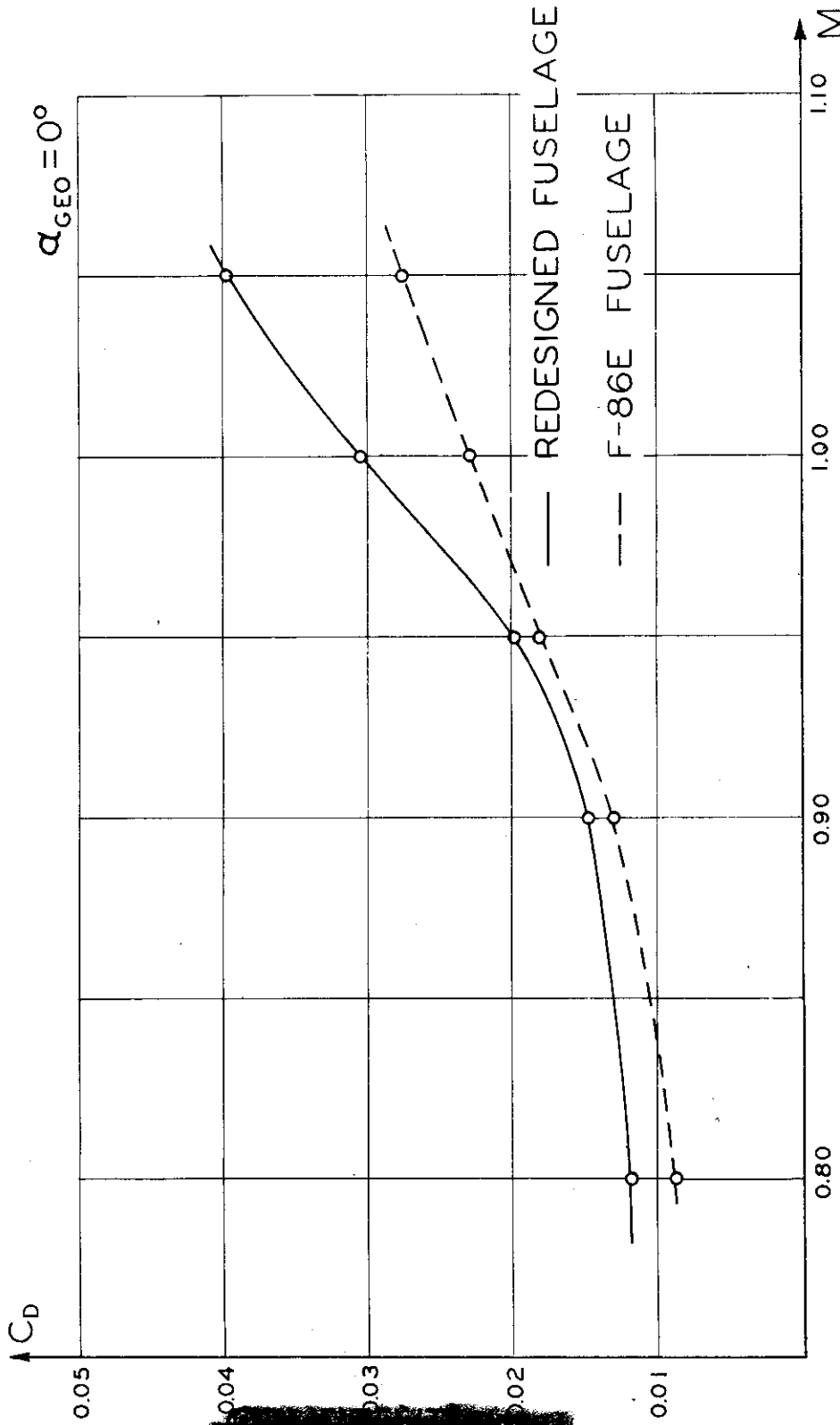


Fig. 63 DRAG COEFFICIENTS OF THE REDESIGNED AND F-86E FUSELAGES AS A FUNCTION OF M

SCHLIEREN PHOTOGRAPHS OF THE REDESIGNED MODEL
WITH AND WITHOUT THE WING

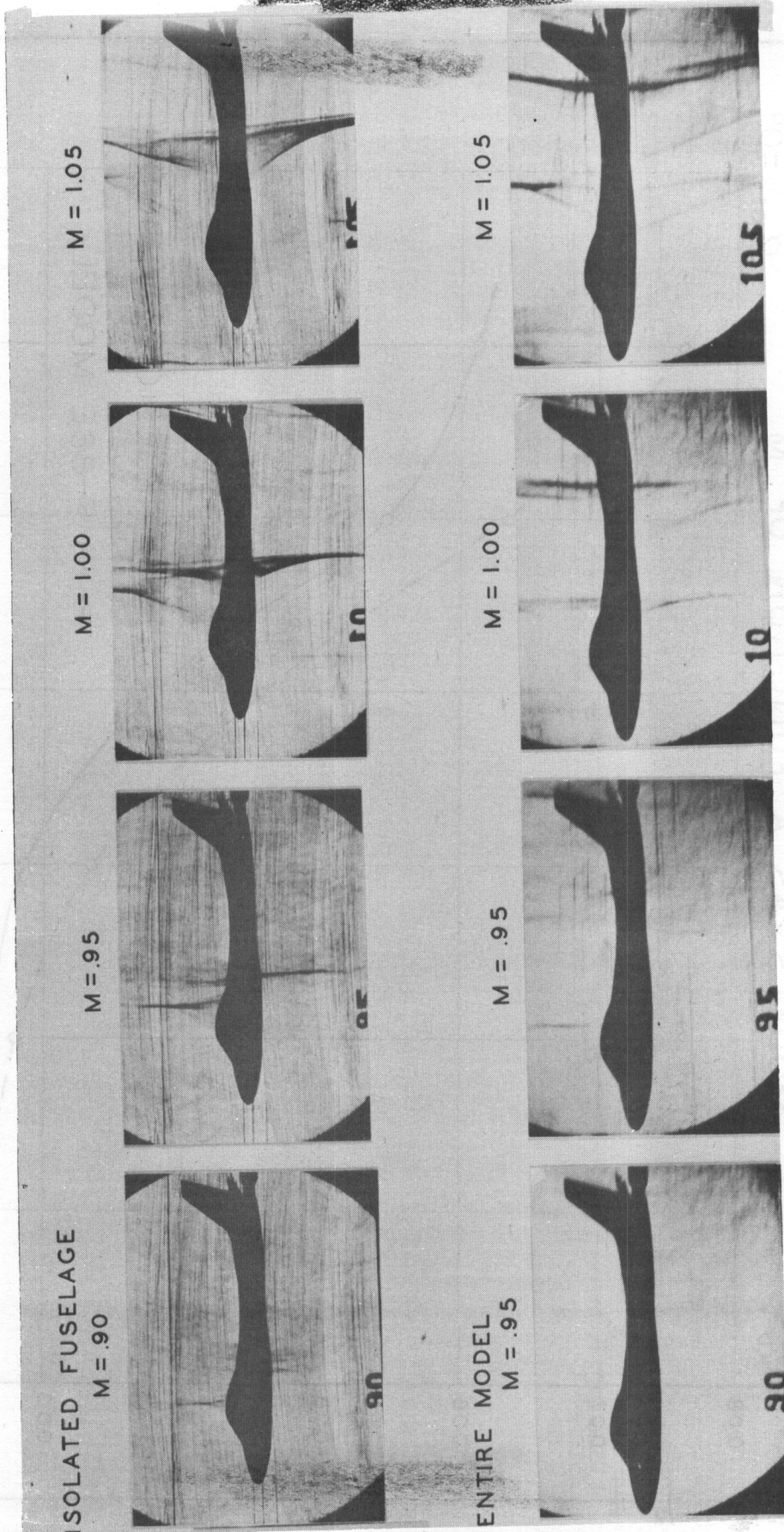


Fig. 64 SCHLIEREN PHOTOGRAPHS OF THE REDESIGNED MODEL WITH AND WITHOUT THE WING

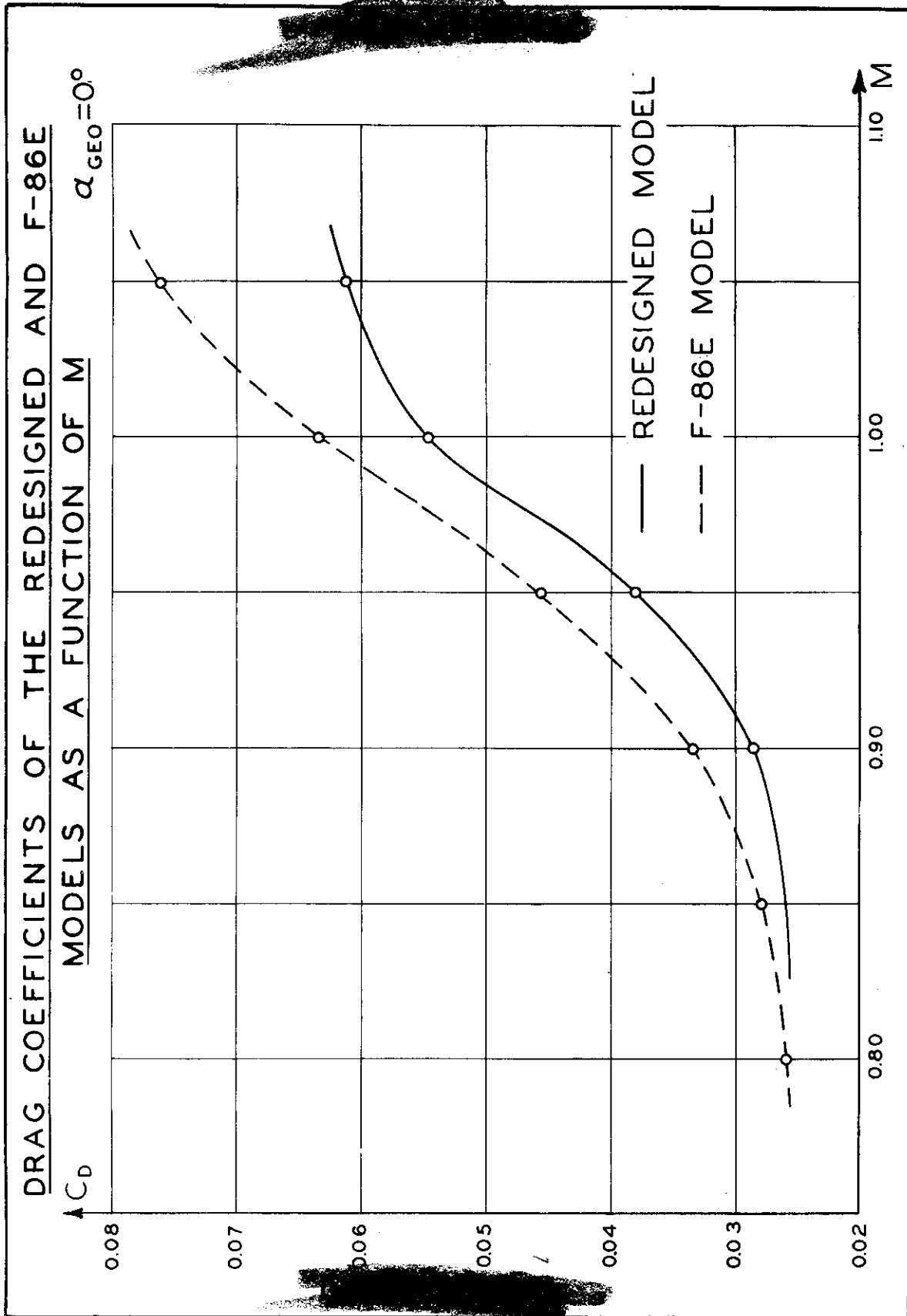


Fig. 65 DRAG COEFFICIENTS OF THE REDESIGNED AND F-86E MODELS AS A FUNCTION OF M

DRAG COEFFICIENTS OF THE REDESIGNED AND F-86E MODELS AS A FUNCTION OF M

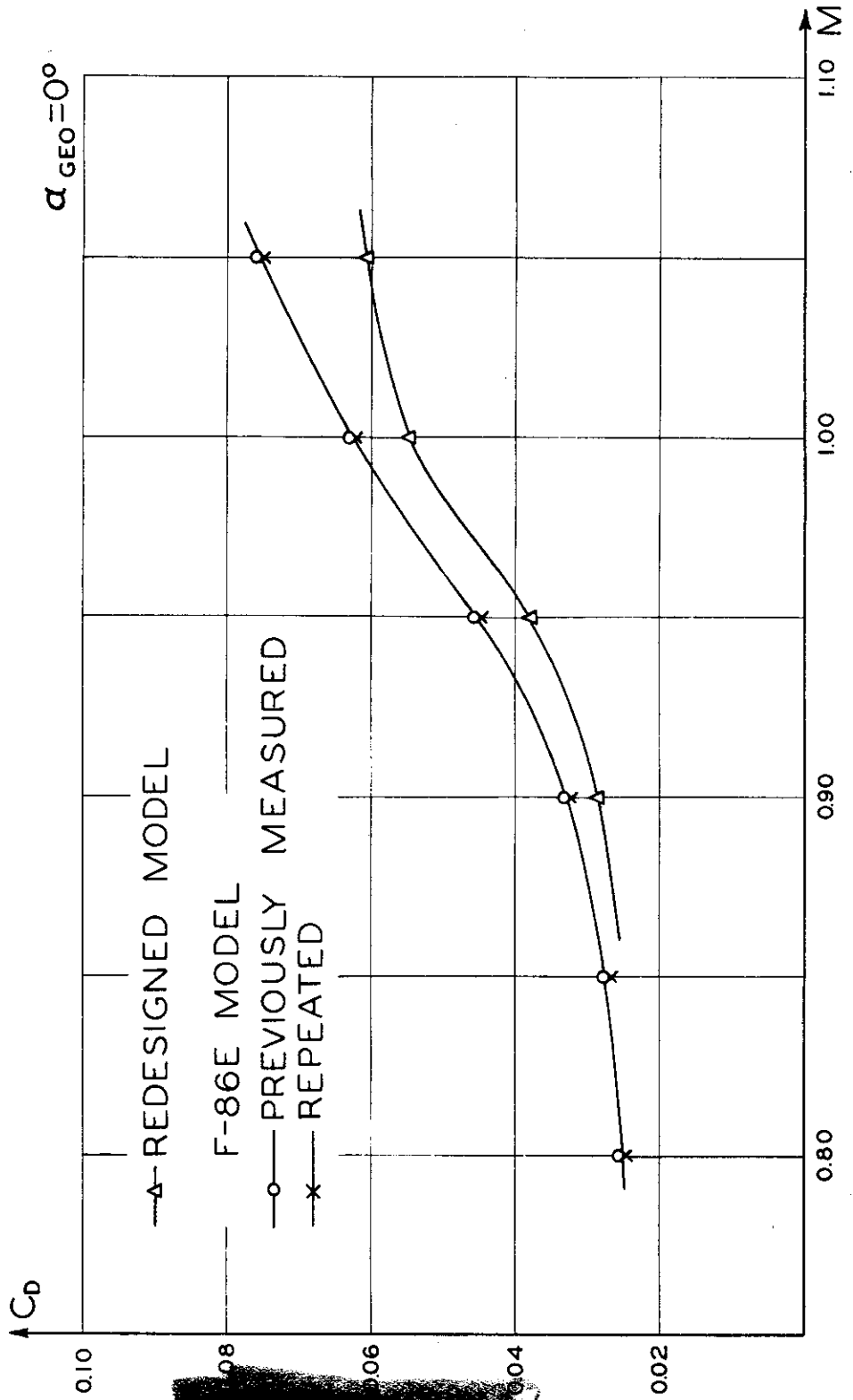


Fig. 66 DRAG COEFFICIENTS OF THE REDESIGNED AND F-86E MODELS AS A FUNCTION OF M

DRAG REDUCTION OF THE REDESIGNED MODEL
WITH RESPECT TO THE F-86E MODEL

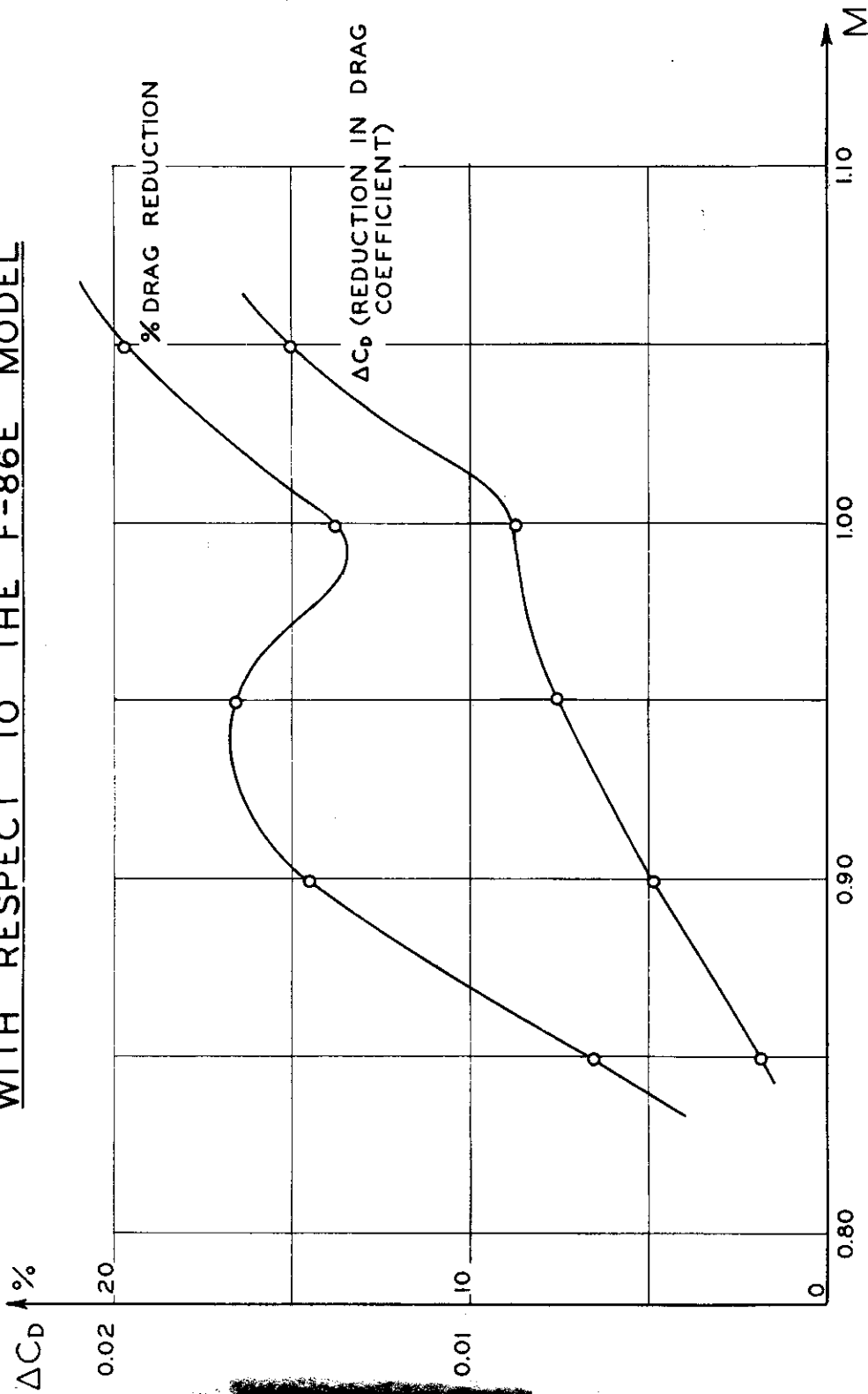


Fig. 67 DRAG REDUCTION OF THE REDESIGNED MODEL WITH RESPECT TO THE F-86E MODEL

A COMPARISON OF THE SUM OF WING + FUSELAGE DRAG AND TOTAL MODEL DRAG OF THE REDESIGNED MODEL AT $\alpha_{GE0}=0^\circ$

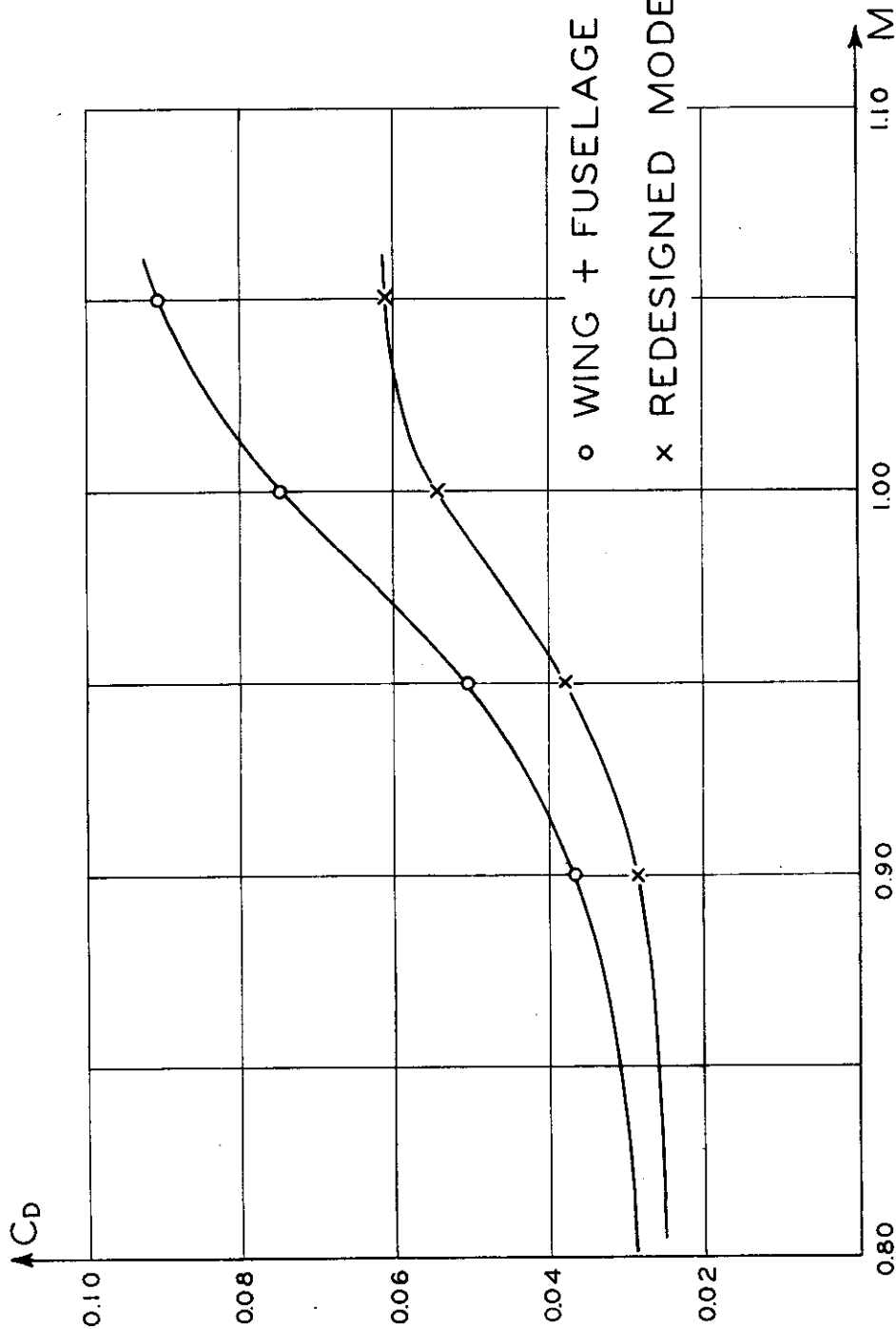


Fig. 68 A COMPARISON OF THE SUM OF WING + FUSELAGE DRAG AND TOTAL MODEL DRAG OF THE REDESIGNED MODEL AT $\alpha_{GE0} = 0^\circ$

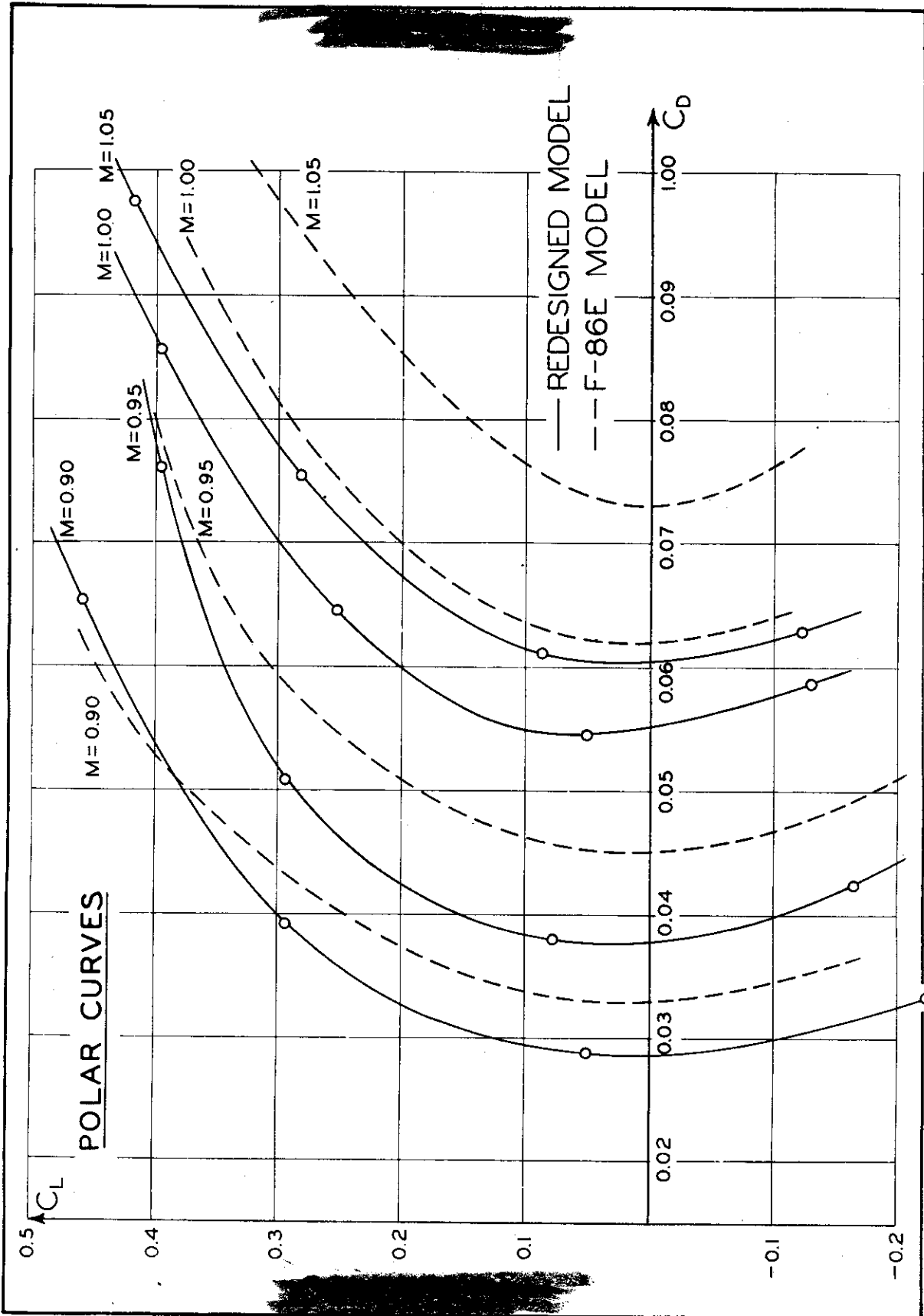


Fig. 69 POLAR CURVE COMPARISON BETWEEN THE F-86E, AND REDESIGNED MODELS

~~CONFIDENTIAL~~

F-86E WITH REDESIGNED FUSELAGE

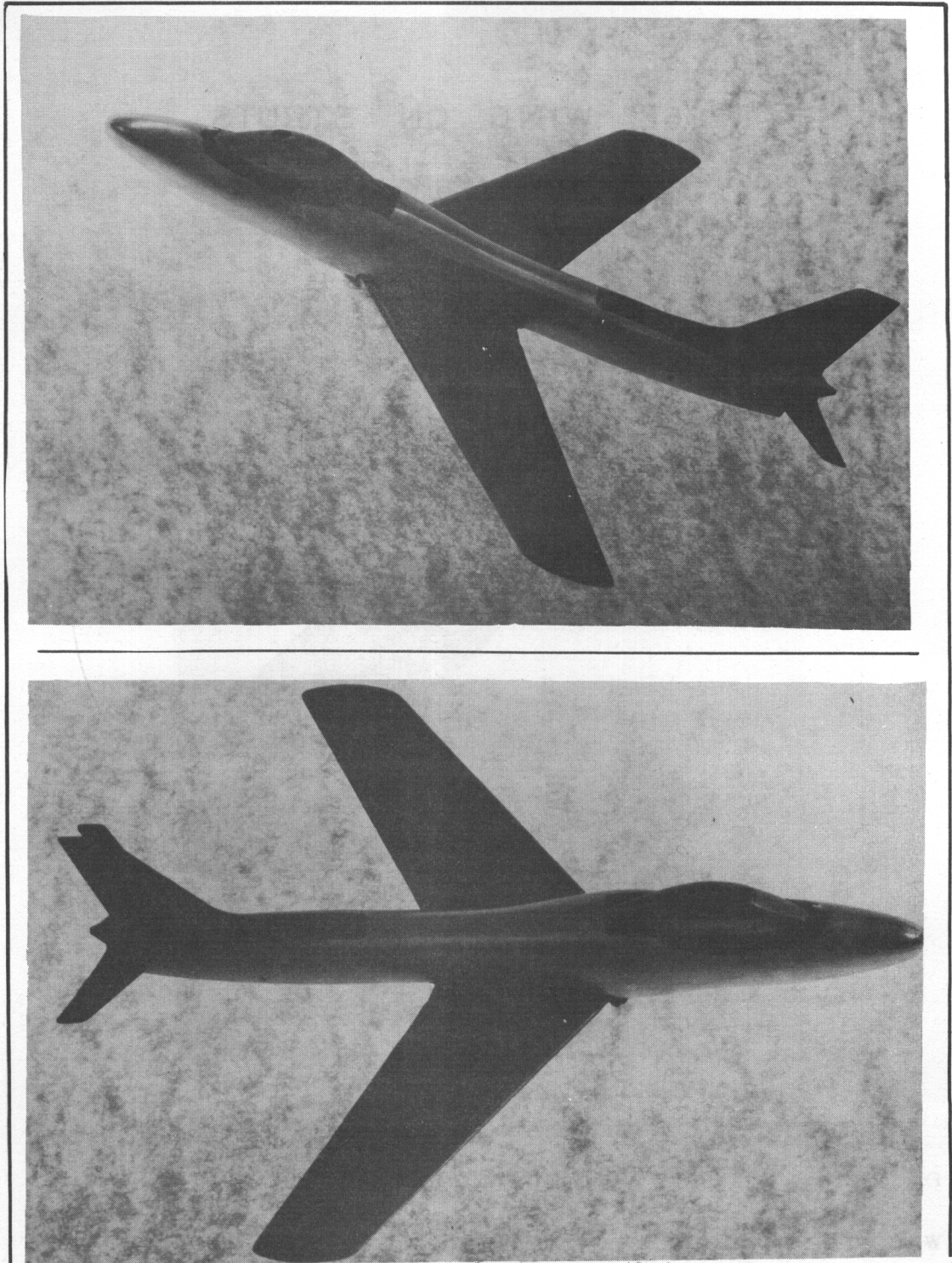


Fig. 70
WADC-TR-55-12

F-86E WITH REDESIGNED FUSELAGE

~~CONFIDENTIAL~~

~~CONFIDENTIAL~~

F-86E WING ON STRUTS

F-86E WING ON STRUTS

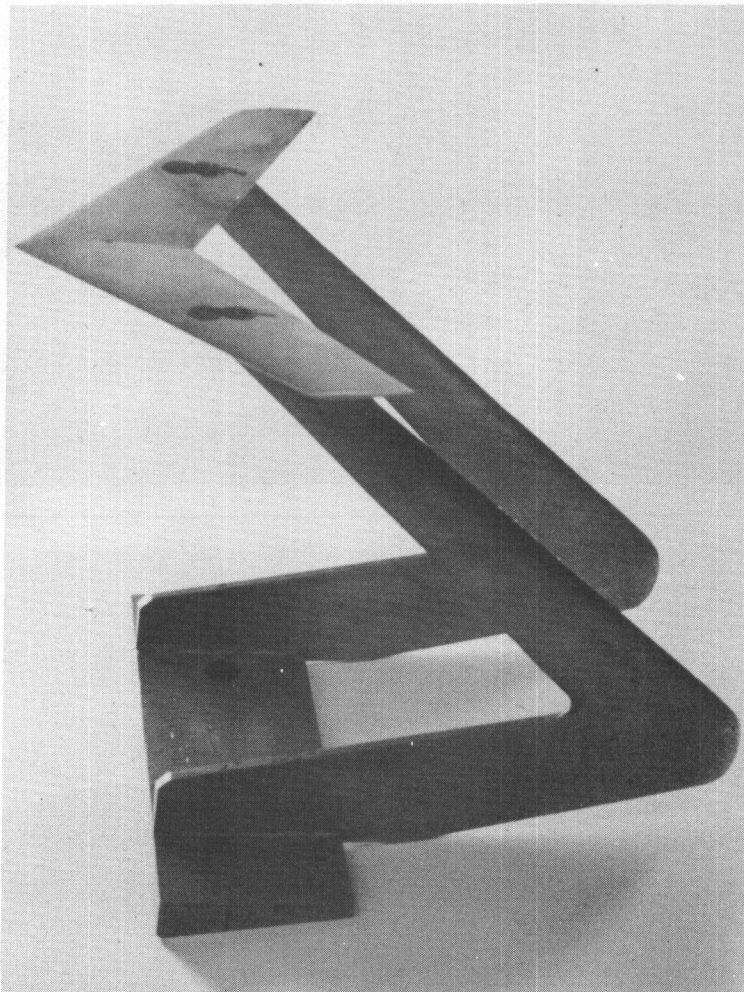


Fig. 71

F-86E WING ON STRUTS

WADC-TR-55-12

98

55WCRR-3786

~~CONFIDENTIAL~~